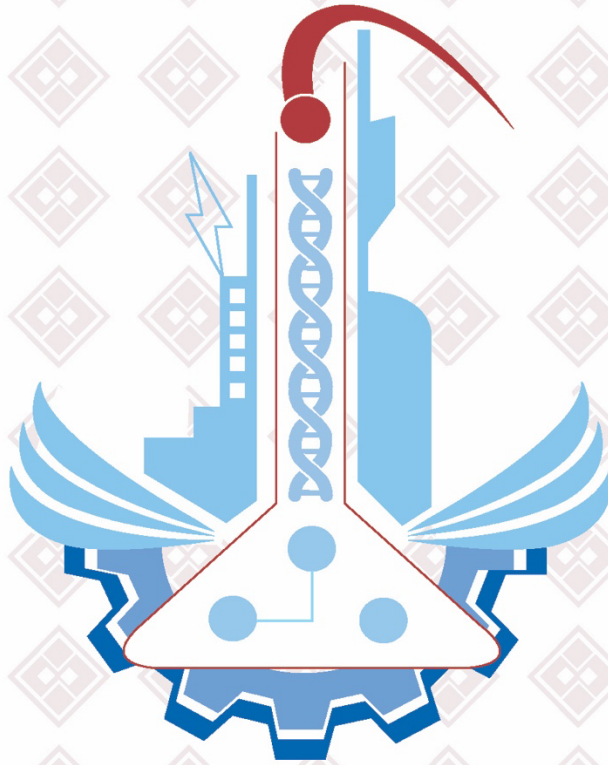


PRINTED ISSN: 1308-9080 / OLINE ISSN: 1308-9099

Volume: 16 / Number: 2 / Year: 2021

TURKISH JOURNAL OF SCIENCE & TECHNOLOGY



TURKISH JOURNAL OF SCIENCE AND TECHNOLOGY (TJST)

Year: 2021 Vol: 16 Number: 2

Address:

Fırat Universitesi
Fen Bilimleri Enstitüsü
23119, Elazig - TURKEY

Tel: 0 424 212 27 07
Fax: 0 424 236 99 55
e-mail: fenbilim@firat.edu.tr

New ISSN

Online: 1308-9099
Printed: 1308-9080

Old ISSN

Online: 1306 – 8555
Printed: 1306 – 8547

Refereed journal. Published twice a year

<https://dergipark.org.tr/tr/pub/tjst>

TURKISH JOURNAL OF SCIENCE & TECHNOLOGY (TJST)
Published by Fırat University

Owner

Prof. Dr. Fahrettin GÖKTAŞ
Rector of Fırat University

Editor in Chef

Assoc. Prof. Dr. Fatih ÖZKAYNAK
Fırat University, Faculty of Technology
Department of Software Engineering

Responsible Director

Assoc. Prof. Dr. Kürşat Esat ALYAMAÇ
Fırat University, Faculty of Engineering
Department of Civil Engineering

Editor

Assoc. Prof. Dr. Emrah YILMAZ
Fırat University, Faculty of Science
Department of Mathematic

ADVISORY BOARD

Eyüp BAĞCI

Fırat University, Department of Biology,
Elazığ-Turkey

Eres SOYLEMEZ

Middle East Technical University,
Department of Engineering Science,
Ankara-Turkey

Coskun BAYRAK

UALR Donaghey Collage of Eng. and
Information Tech. Dept. of Computer
Science, Little Rock, AR, USA

Hikmet GECKİL

Inonu University, Department of Biology,
Malatya-Turkey

Metin CALTA

Fırat University, Fisheries Faculty,
Elazığ-Turkey

Ertan GOKALP

Karadeniz Technical University,
Department of Geodesy and
Photogrametry Engineering, Trabzon-
Turkey

Abdulkadir ŞENGÜR

Fırat University, Department of
Electronics and Computer Education,
Elazığ-Turkey

Hasan EFEOĞLU

Ataturk University, Department of
Electrical-Electronics Engineering,
Erzurum-Turkey

Yanhui GUO

St. Thomas University, School of Science
and Technology, Miami, FL, USA

İbrahim TURKMEN

Balıkesir University, Department of
Geology Engineering, Balıkesir-Turkey

Deniz UNER

Middle East Technical University,
Department of Chemical Engineering,
Ankara-Turkey

M.Polat SAKA

Bahreyn University, Department of Civil
Engineering, Bahrain

Siqing XIA

Tongji Univ, State Key Lab Pollut Control
& Resource Reuse, Coll Environm Sci &
Engn, Shanghai 200092, R China

Zihni DEMIRBAG

Karadeniz Technical University,
Department of Biology, Trabzon-Turkey

Hanifi GULDEMİR

Fırat University, Department of Electronics
and Computer Education, Elazığ-Turkey

Nilgun GULEC

Middle East Technical University,
Department of Geology Engineering,
Ankara-Turkey

Erdogan GUNEL

West Virginia University, Department of
Statistics, Morgantown, USA

Sedigheh GHOFRANI

Islamic Azad University, Electrical
Engineering Department, Tehran South
Branch, Iran

Wang XIBAO

Tianjin University, The School of
Materials Science and Engineering, China

Brain WOERNER

West Virginia University, Department of
Computer Sciences & Electrical
Engineering, Morgantown, WV, USA

A. Kadri CETIN

Fırat University, Department of Biology,
Elazığ-Turkey

Yusuf Kağan KADIOĞLU

Ankara University, Department of Geology
Engineering, Ankara-Turkey

Sezgin BAKIRDERE

Yıldız Technical University, Department of
Chemistry, Ankara-Turkey.

Tuncay OREN

Ottawa Univ, Fac Eng, Inform Technol.
McLeod Inst Sim.t Sci, Ottawa, ON KIN
6N5 Canada

Halil ONDER

Middle East Technical University,
Department of Civil Engineering, Ankara-
Turkey

Nazmi POLAT

Ondokuz Mayıs University, Department of
Biology, Samsun-Turkey

Mustafa DORUCU

Fırat University, Fisheries Faculty,
Elazığ-Turkey

Binod Chandra TRIPATHY

Mathematical Sciences Division, Institute
of Advanced Study Science and Tech.
Paschim Boragaon; Guwahati, India

Eoin CASEY

University College Dublin, Chemical and
Bioprocess Engineering, Dublin, Ireland

Farid EI-TANTAWY

Suez Canal University, Faculty of
Science, Department of Physics, Ismailia,
Egypt

Saleem HASHMI

International College of Technology,
Dublin, Ireland

Sakir ERDOĞDU

Karadeniz Technical University,
Department of Civil Engineering, Trabzon-
Turkey

Serdar SALMAN

Marmara University, Metallurgical and
Materials Engineering, İstanbul-Turkey

Firat University Turkish Journal of Science & Technology (TJST)
16-2, 2021

CONTENTS / İÇİNDEKİLER

1. **Classification of Skin Cancer Images with Convolutional Neural Network Architectures**
Evrişimsel Sinir Ağları Mimarileri ile Cilt Kanseri Görüntülerinin Sınıflandırılması
Muhammed YILDIRIM, Ahmet ÇINAR 187-195
2. **On Generalized Mannheim curves in the Equiform Geometry of the Galilean 4-Space**
4-boyutlu Galileo Uzayının Equiform Geometrisindeki Genelleştirilmiş Mannheim Eğrileri
Sibel TARLA, Handan ÖZTEKİN 197-204
3. **Analysis of The Performance According to Object Density in Static Environments of GA and PSO Algorithms Used in Mobile Robot Path Planning**
Mobil Robot Yol Planlamasında Kullanılan GA ve PSO Algoritmalarının Statik Ortamlardaki Nesne Yoğunluğuna Göre Performansının Analizi
Gürkan GÜRGÖZE, İbrahim TÜRKÖĞLU 205-214
4. **Effect of Nitrogen Source on Growth and Protein and Lipid Amounts of a Freshwater Microalga *Scenedesmus acutus***
*Azot Kaynaklarının *Scenedesmus acutus*' un Gelişim, Protein ve Lipit Miktarına Etkisi*
Ahmet ÇOBAN, Gökçe KENDİRLİOĞLU ŞİMŞEK, A. Kadri ÇETİN 215-220
5. **Special Curves According to Extended Darboux Frame Field in E_1^4**
 E_1^4 de Geniştirilmiş Darboux Çatı Alanına Göre Özel Eğriler
Esra ERDEM, Mihriban ALYAMAÇ KÜLAHÇI, Münevver YILDIRIM YILMAZ 221-230
6. **Detection of Phishing Attacks on Websites with Lasso Regression, Minimum Redundancy Maximum Relevance Method, Machine Learning Methods, and Deep Learning Model**
Kement Regresyon, Minimum Yedeklilik Maksimum Alaka Yöntemi, Makine Öğrenimi Yöntemleri ve Derin Öğrenme Modeli ile Web Sitelerine Yönelik Ortalama Saldırıların Tespiti
Mesut TOĞAÇAR 231-243
7. **Against Digital Extinction: Cyber Peace**
Dijital Yokoluşa Karşı: Siber Barış
Muharrem Tuncay GENÇOĞLU 245-250
8. **Analysis of Mutated RNA-Type Breast Cancer Data with Machine Learning Methods**
Mutasyona Uğramış RNA tipli Göğüs Kanseri Verilerinin Makine Öğrenme Yöntemleri ile Analizi
Rumeysa Hanife KARS 251-260
9. **The Characterizations Of Null Quaternionic Curves In Minkowski 3-Space**
Minkowski 3-Uzayda Null Kuaterniyonik Eğrilerin Karakterizasyonları
Şeyda ÖZEL, Mihriban ALYAMAÇ KÜLAHÇI, Mehmet BEKTAŞ 261-267

10. Investigation of Electrophoretic Mobility of Various Nanofibers in Ethanol or Water

Çeşitli Nanoliflerin Etanol veya Sudaki Elektroforetik Hareketliliğinin İncelenmesi

Sercan DEDE, Filiz LOKUMCU ALTAY

269-274



Classification of Skin Cancer Images with Convolutional Neural Network Architectures

Muhammed YILDIRIM^{1*}, Ahmet ÇINAR

¹ Computer Engineering Department, Engineering Faculty, Firat University, Elazığ, Turkey

² Computer Engineering Department, Engineering Faculty, Firat University, Elazığ, Turkey

*¹ 171129205@firat.edu.tr, ² acinar@firat.edu.tr

(Geliş/Received: 28/01/2021;

Kabul/Accepted: 02/05/2021)

Abstract: The skin, in which our body is completely covered, both provides the heat balance of our body and protects our body against external factors. Skin cancer, which occur as a result of the uncontrolled proliferation of cells on the skin surface, are one of the most common types of cancer in the world. Early detection of skin cancer means early treatment of the disease. With early diagnosis, patients can be cured earlier and mortality rates can be reduced. The hardest part of skin cancer diagnosis is that skin lesions are very similar to each other. Therefore, it is of great importance that skin cancer can be diagnosed and classified as benign or malignant tumor. In this study, Convolutional Neural Network were used to determine whether skin cancer is benign or malignant. Separate results are obtained with Alexnet, Resnet50, Densenet201 and Googlenet. Then the performance rates of the models used have been compared. The highest accuracy rate was achieved with the Resnet50 model with 83.49%. Then, the results were obtained with the proposed hybrid model. In the proposed hybrid model, the accuracy rate was 84.11%. This rate is an important value for early diagnosis and treatment of the disease.

Key words: CNN, Classification, Deep Learning, Image Processing, Skin Cancer.

Evrışimsel Sinir Ağları Mimarileri ile Cilt Kanseri Görüntülerinin Sınıflandırılması

Öz: Vücudumuzun tamamen kaplandığı deri hem vücudumuzun ısı dengesini sağlar hem de vücudumuzu dış etkenlere karşı korur. Cilt yüzeyindeki hücrelerin kontrolsüz çoğalması sonucu ortaya çıkan cilt kanserleri, dünyada en sık görülen kanser türlerinden biridir. Deri kanserlerinin erken teşhisi, hastalığın erken tedavisi anlamına gelir. Erken tanı ile hastalar daha erken tedavi edilebilir ve ölüm oranları azaltılabilir. Cilt kanseri teşhisinin en zor kısmı, cilt lezyonlarının birbirine çok benzemesidir. Bu nedenle cilt kanserinin iyi huylu veya kötü huylu tümör olarak teşhis edilip sınıflandırılabilmesi büyük önem taşımaktadır. Bu çalışmada, Evrışimsel Sinir Ağı ağları, cilt kanserinin iyi huylu veya kötü huylu olup olmadığını belirlemek için kullanılmıştır. Alexnet, Resnet50, Densenet201 ve Googlenet ile ayrı ayrı sonuçlar elde edilmiştir. Daha sonra kullanılan modellerin performans oranları karşılaştırılmıştır. En yüksek doğruluk oranı % 83,49 ile Resnet50 modelinde elde edilmiştir. Daha sonra önerilen hibrit modelle sonuçlar elde edilmiştir. Önerilen hibrit modelde doğruluk oranı %84.11 olmuştur. Bu oran, hastalığın erken teşhis ve tedavisi için önemli bir değerdir.

Anahtar kelimeler: CNN, Sınıflandırma, Derin Öğrenme, Görüntü işleme, Cilt Kanseri.

1. Introduction

The skin, which covers almost all of our body, can deteriorate over time and lead to various types of cancer [1]. Skin cancer have become one of the most common types of cancer in the world [2]. Early diagnosis of these types of cancer is of great importance for the treatment process [3]. When tumor is called, generally 2 different types of tumors are considered. The first of these are benign tumors and the second is malignant tumors [4]. Benign tumors put the person in more visual and functional problems. Malignant tumors can put a person's life at risk [5]. There are many deaths in the world due to malignant tumor.

The reason why the detection of tumors is difficult is that different skin lesions are very similar to each other [6]. Because of this similarity, detection of these tumors becomes very difficult. Dermatoscopy is the most common method used by physicians to detect these cancer tumors [7]. In this method, an examination is made with a device with a very high visual resolution and the relevant region is examined by enlarging. In this process, the professional experience of the doctor and the images obtained from dermatoscopy are of great importance [8].

In this study, CNN models, which are very popular in recent years, are used. After the Alexnet architecture won the large-scale visual recognition (ILSVRC) competition in 2012, CNN models have become increasingly important [9]. With the developing technology, deep learning architectures have started to achieve successful results in large data sets [10]. Since skin cancer is a common and deadly disease, computer-aided systems are of

* Corresponding author: 171129205@firat.edu.tr. ORCID Number of authors: ¹0000-0003-1866-4721, ² 0000-0001-5528-2226

great importance in combating this disease. CNN networks need to be trained with large amounts of data so that this disease can be diagnosed early and the treatment process can be initiated [11]. For the classification of skin cancer data, segmented images of the skin cancer data are used and the models are trained and tested.

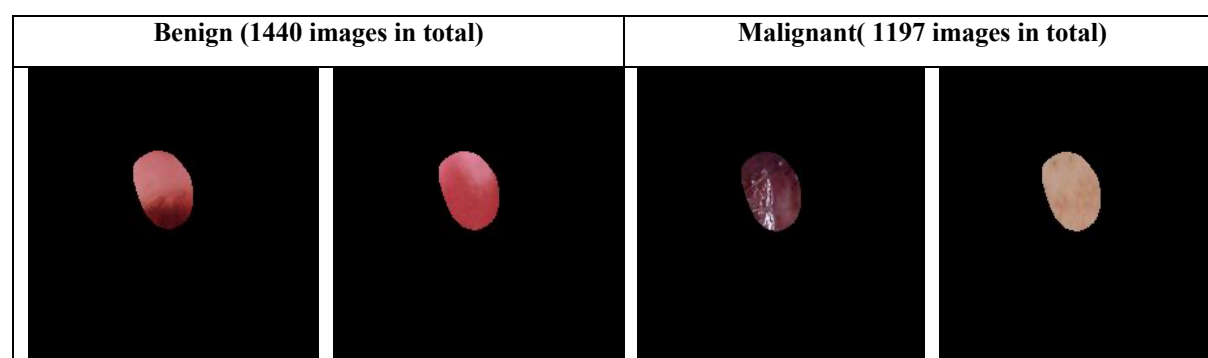
In this paper, Densenet201 architecture [12], Alexnet architecture [13], Googlenet architecture [14] and Resnet50 architecture [15] are used to classify skin cancer data.

The data set used in the rest of the article is examined. Then the architectures used are discussed. After that, the application and the results obtained are shared. Finally, the conclusion section is prepared.

2. Description of the Skin Cancer Dataset

For the classification of skin cancer data, segmented images of the skin cancer dataset [16] on Kaggle's page were used. This data set consists of 2 classes. The first class is the benign class; the second class is the malignant class. While benign class refers to benign tumor, malignant refers to malignant tumor. Although benign type tumors cause more visual and functional problems, malignant type tumors can lead to death. Examples from the data set used in the study and the number of images used are given in table 1.

Table 1. Examples belonging to the benign and malignant class.



3. Models

Cnn architectures Alexnet, Resnet50, Densenet201 and Googlenet are used to classify data belonging to benign and malignant classes. When designing Cnn architectures, we can classify the parameters to be considered as kernel size, batch-size, number of cycles, number of layers, activation function, learning rate, dropout and the size of the data set [17]. The characteristics of the computer used also affect the training and testing time of the model. The architectures and training values used in this study are given in table 2.

Table 2. Training values of models.

Models	MiniBatchSize	MaxEpochs	ValidationFrequency	InitialLearnRate
Alexnet Resnet50 Densenet201 Googlenet	16	5	6	10^{-4}

In deep learning applications, processing all data in the data set at the same time is a costly process in terms of time and memory. Because in every iteration of learning, back propagation is done. This is an important process in terms of time and cost. To solve this problem, it is necessary to divide the data sets into small groups. In this way, giving more than one input piece by piece is called minibatch. In this study, the reason for choosing the minibatch size value 16 is related to the computer used. Since the learning of the network becomes stable after 5

epoch values, the epoch value of 5 was chosen for the architectures used. In order to increase the readability of the accuracy and loss curves, the ValidationFrequency value of 6 was chosen. InitialLearnRate value is 10^{-4} .

3.1. Alexnet

Published by LE Cun in 1988, LeNet architecture is one of the first articles published for deep learning. But when Alexnet won the large-scale visual recognition (ILSVRC) competition in 2012, deep learning architectures began to be heard around the world. The victory of Alexnet architecture in this competition led to the start of a popular era in deep learning. With this architecture, the error rate in pattern recognition has been reduced from 26% to 15%. Relu is used as the activation function in the model. This model is designed to classify 1000 objects. The filters used here are 11 x 11 in size. Alexnet architecture consists of 25 layers in total [18].

3.2. Resnet50

The Resnet50 model was the winner of the ImageNet competition in 2015. The error rate of the Resnet50 architecture in this competition was 3.6%. While the ResNet50 architecture classifies images with an error rate of 3.6%, people can classify the image with an average error rate of 5-10%. This ratio is a great success for the Resnet50 architecture. The Resnet50 architecture is one of the first architectures to use BatchNormalization for the normalization process. Relu is used as the activation function in this architecture. It has a deeper structure than previously designed architectures [19].

3.3. Densenet201

DenseNet201 provides the merged feature maps produced by all previous layers as input to the next layer. In this way, it is aimed to make the training process easier. It is aimed to use the parameters more efficiently in the Densenet201 architecture. This allows access to all feature maps produced in layers prior to the deeper layers in the network. Avaragepooling has been preferred for the pooling process in the Densenet201 architecture. Relu was used as the activation function and Batchnormalization was used for the normalization process [20].

3.4. Googlenet

This model is the winner of the ILSVRC competition held in 2014. The model with an error rate of 5.7% gave successful results in data sets. The Googlenet model, which has a depth of 22 layers, has a 144-layer structure. This model is one of the convolution and CNN architectures that move away from the common layers in an ordered structure. The start-up modules used here have reduced memory and power usage. [21].

3.5. Proposed Hybrid Model

In the proposed hybrid model, features obtained from the Resnet50 and Densenet201 architectures are concatenated. These features are taken from the layer before the softmax layer. Later, these concatenated features were classified in the SVM classifier. A rough representation of the proposed hybrid model is given in figure 1.

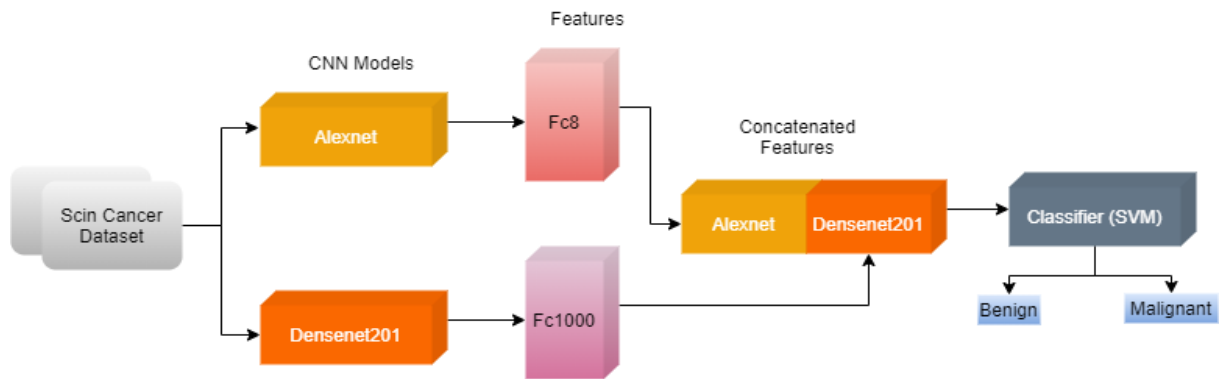


Figure 1. Proposed Hybrid Model.

4. Experimental Results

In this study, CNN architectures are used to classify the skin cancer data set as benign and malignant. CNN architectures used in these paper are the most widely used in recent years. Cnn architectures are widely used, especially in biomedical image processing [23].

Some values must be calculated in order to perform performance evaluation of data classified with CNN architectures [24]. An example of a confusion matrix, which presents a sort of summary of the success of the model used, is given in Table 3. Performance criteria of CNN models are calculated using a Confusion matrix.

Table 3. Confusion matrix obtained in models.

	Benign	Malignant
Benign	TruePositive	FalsePositive
Malignant	FalseNegative	TrueNegative

TP: The benign image is correctly predicted and placed in the benign class.

FN: The image belonging to the class of malignant is guessed incorrectly and placed in the benign class.

FP: Image belonging to the benign class are predicted as malignant.

TN: The malignant image is correctly predicted and placed in the malignant class.

F-Measure value in equation 1, Precision value in equation 2, Specificity value in equation 3, **Sensitivity** value in equation 4, False Positive Rate (FPR) value in equation 5, False Discovery Rate (FDR) value in equation 6, the False Negative Rate (FNR) value is given in equation 7 and the Accuracy value is given in equation 8. Confusion matrix was used to calculate all these values.

$$F - measure = \frac{2 * Precision * Recall}{Precision + Recall} \quad (1), \quad Precision = \frac{TP}{TP + FP} \quad (2), \quad Specificity (TNR) = \frac{TN}{TN + FP} \quad (3)$$

$$Sensitivity (TPR) = \frac{TP}{TP + FN} \quad (4), \quad False Positive Rate (FPR) = \frac{FP}{FP + TN} \quad (5),$$

$$False Discovery Rate (FDR) = \frac{FP}{FP + TP} \quad (6), \quad False Negative Rate (FDR) = \frac{FN}{FN + TP} \quad (7)$$

$$Accuracy = \frac{TP + TN}{TP + TN + FP + FN} \quad (8)$$

Alexnet architecture was first used to classify benign and malignant images of the skin cancer data set. The accuracy and loss curves of the benign and malignant classes obtained using the Alexnet architecture are given in figure 2.

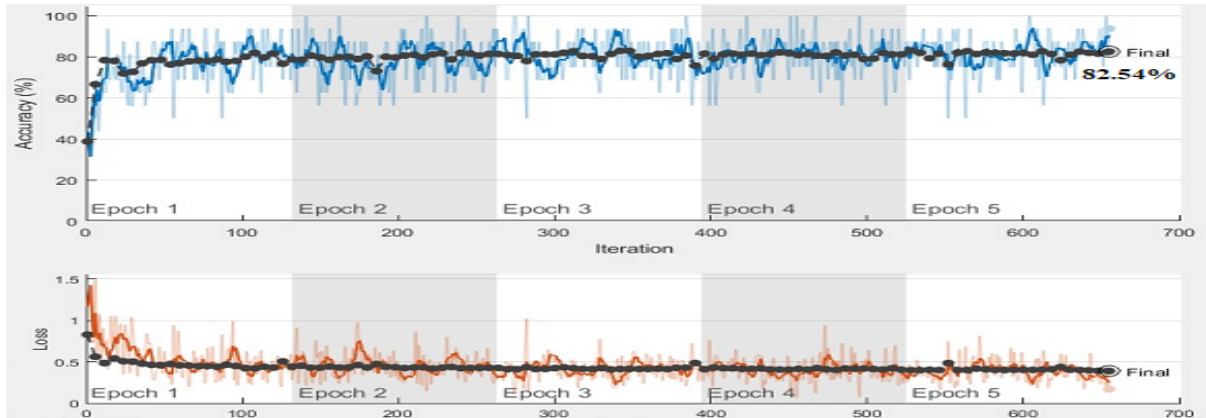


Figure 2. Alexnet's accuracy and loss curves.

The confusion matrix and success rates obtained as a result of the classification process performed by the Alexnet model in the skin cancer dataset are given in table 4. When table 4 is examined, it is seen that 220 out of 288 benign data were placed correctly and 68 were incorrectly placed. Likewise, 215 of 239 malignant data were placed in the correct class, while 24 were placed in the wrong class. The accuracy rate of the model is 82.54%.

Table 4. Alexnet's confusion matrix and success rates achieved.

		Benign		Malignant			
Benign		220		68			
Malignant		24		215			
F-Measure	Precision	Specifity	Sensitivity	FPR	FDR	FNR	Accuracy
82.71%	76.39%	75.97%	90.16%	24.03%	23.61%	9.84%	82.54%

Another model used to classify benign and malignant images belonging to the skin cancer data set is Densenet201. The accuracy and loss curves of the benign and malignant classes obtained using the Densenet201 architecture are given in figure 3.

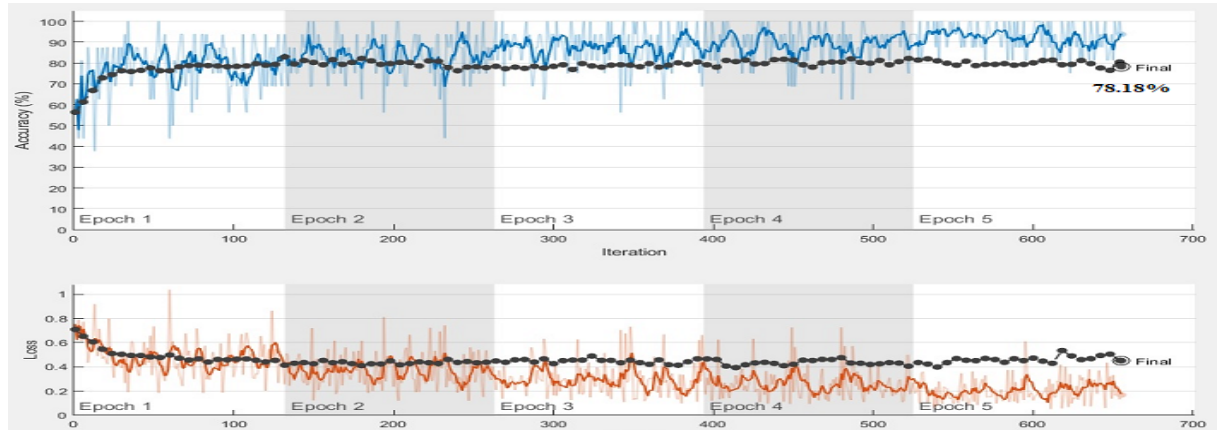


Figure 3. Densenet201's accuracy and loss curves.

The confusion matrix and success rates obtained as a result of the classification process performed by the Densenet201 model in the skin cancer data set are given in table 5. When table 5 is examined, it is seen that 227 of 288 benign data were placed correctly and 61 were placed incorrectly. Likewise, 185 of 239 malignant data were placed in the correct class, while 54 were placed in the wrong class. The accuracy rate of the model is 78.18%

Table 5. Densenet201's confusion matrix and success rates achieved.

		Benign		Malignant			
Benign		227		61			
Malignant		54		185			
F-Measure	Precision	Specifity	Sensitivity	FPR	FDR	FNR	Accuracy
79.79%	78.82	75.20%	80.78%	24.80%	21.18%	19.22%	78.18%

Another model used to classify benign and malignant images belonging to the skin cancer data set is Googlenet. The accuracy and loss curves of the benign and malignant classes obtained using the Googlenet architecture are given in figure 4.

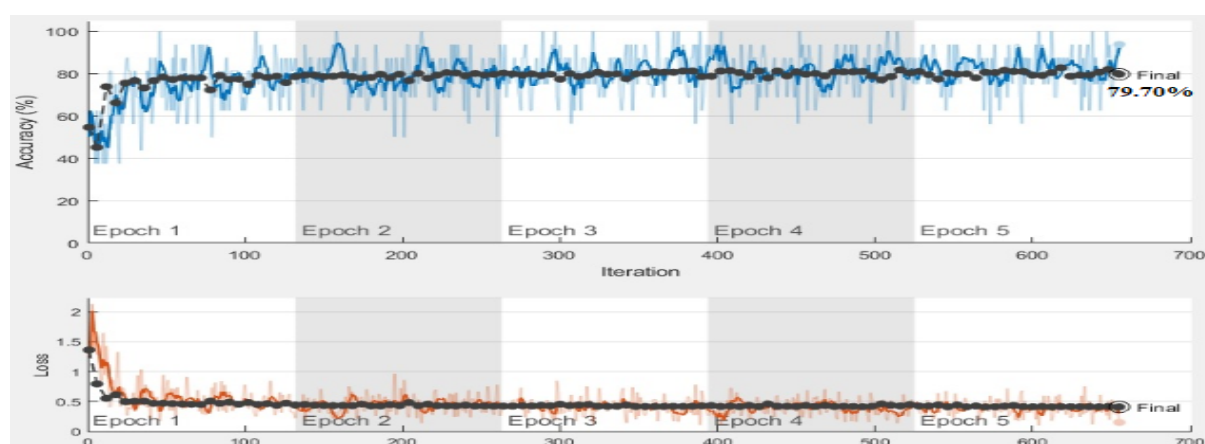


Figure 4. Googlenet's accuracy and loss curves.

The confusion matrix and success rates obtained as a result of the classification process performed by the Googlenet model in the skin cancer data set are given in table 6. When table 6 is examined, it is seen that 204 out of 288 benign data were placed correctly and 84 were placed incorrectly. Likewise, 216 out of 239 malignant data were placed in the correct class, while 23 were placed in the wrong class. The accuracy rate of the model is 79.70%.

Table 6. Googlenet's confusion matrix and success rates achieved.

		Benign		Malignant			
Benign		204	84				
Malignant		23	216				
F-Measure	Precision	Specifity	Sensitivity	FPR	FDR	FNR	Accuracy
79.22%	70.83%	72%	89.87%	28%	29.17%	10.13%	79.70%

Resnet50 is the model that classifies benign and malignant images of the skin cancer data set with the highest accuracy. Accuracy and loss curves of benign and malignant classes obtained using the Resnet50 architecture are given in figure 5.

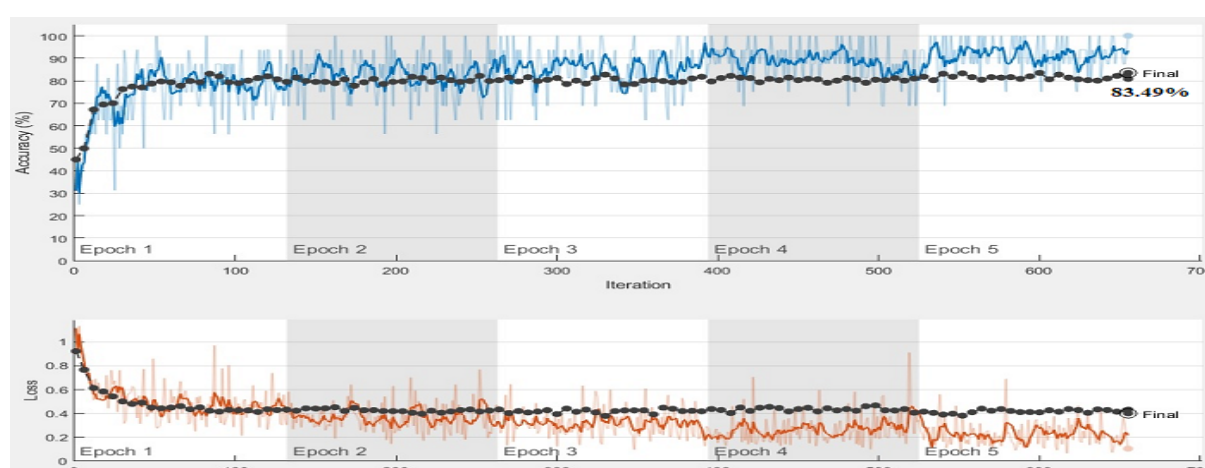


Figure 5. Resnet50's accuracy and loss curves.

The confusion matrix and success rates obtained as a result of the classification process performed by the Resnet50 model in the skin cancer data set are given in table 7. When table 7 is examined, it is seen that 253 of

288 benign data were placed in the correct class and 35 were placed in the wrong class. Likewise, 187 of 239 malignant data were placed in the correct class, while 52 were placed in the wrong class. The accuracy rate of the model is 83.49%.

Table 7. Resnet50’s confusion matrix and success rates achieved.

		Benign		Malignant			
Benign		253		35			
Malignant		52		187			
F-Measure	Precision	Specifity	Sensitivity	FPR	FDR	FNR	Accuracy
85.33%	87.85%	84.23%	82.95%	15.77%	12.15%	17.05%	83.49%

Among the models used in this study, the highest accuracy rate was obtained with the Resnet50 architecture, while the lowest accuracy rate was obtained in the Densenet201 architecture. The accuracy values of the models used are given in table 8.

Table 8. Accuracy values of pre-trained CNN models.

Resnet50	Alexnet	Googlenet	Densenet201
83.49%	82.54%	79.70%	78.18%

When the features obtained from the four pre-trained CNN architectures used in the study were classified in the SVM classifier, the accuracy values in table 9 were obtained.

Table 9. CNN models + SVM classifier.

Resnet50 + SVM	Alexnet + SVM	Googlenet + SVM	Densenet201 + SVM
82.6%	82.8%	81.5%	82.7%

Finally, the confusion matrix obtained in the proposed hybrid model and the performance metrics of the proposed hybrid model are given in table 10.

Table 10. Proposed Hybrid model’s confusion matrix and performance metrics.

		Benign		Malignant			
Benign		1194		246			
Malignant		173		1024			
F-Measure	Precision	Specifity	Sensitivity	FPR	FDR	FNR	Accuracy
85.07%	82.92%	80.63%	87.34%	19.37%	17.18%	12.66%	84.11%

While the proposed hybrid model correctly classified 1194 of 1440 Benign images, it misclassified 246 of them. While the proposed hybrid model correctly classified 1024 out of 1197 Malignant images, 173 were misclassified. The accuracy rate of the model was 84.11%.

5. Conclusion

Skin cancer is one of the most common types of cancer that occurs as a result of uncontrolled proliferation of cells on the skin surface. It is difficult to diagnose because different skin lesions are very similar. Early detection of cancer cells is very important for the treatment process. For this reason, computer aided systems were used to diagnose skin cancer in this study. Resnet50 architecture achieved the highest performance among pre-trained

networks with an accuracy of 83.49%. In the proposed hybrid model, the accuracy value obtained is 84.11%. With the proposed hybrid model, it is aimed to alleviate the workload of the experts and shorten the diagnosis time. Thanks to computer-aided systems, individual mistakes that can be made by experts are prevented. In subsequent studies, it is aimed to increase the success rate of the model by developing different models on the subject.

References

- [1] Kabashima, K., Honda, T., Ginhoux, F., & Egawa, G. (2019). The immunological anatomy of the skin. *Nature Reviews Immunology*, 19(1), 19-30. <https://doi.org/10.1038/s41577-018-0084-5>
- [2] American Cancer Society: Cancer facts and figures, Aug 2018, [online] Available: <https://www.cancer.org/content/dam/cancer-org/research/cancer-factsand-statistics/annual-cancer-facts-and-figures/2018/cancer-facts-and-figures-2018.pdf>.
- [3] N. C. F. Codella et al., "Deep learning ensembles for melanoma recognition in dermoscopy images", *IBM Journal of Research and Development*, vol. 61, pp. 5:1-5:15, 2017.
- [4] Taroni, P., Paganoni, A. M., Ieva, F., Pifferi, A., Quarto, G., Abbate, F., ... & Cubeddu, R. (2017). Non-invasive optical estimate of tissue composition to differentiate malignant from benign breast lesions: A pilot study. *Scientific reports*, 7(1), 1-11. <https://doi.org/10.1038/srep40683>.
- [5] Wylie, J. D., Jenkins, P. A., Beckmann, J. T., Peters, C. L., Aoki, S. K., & Maak, T. G. (2018). Computed tomography scans in patients with young adult hip pain carry a lifetime risk of malignancy. *Arthroscopy: The Journal of Arthroscopic & Related Surgery*, 34(1), 155-163. <https://doi.org/10.1016/j.arthro.2017.08.235>
- [6] Yap, J., Yolland, W., & Tschandl, P. (2018). Multimodal skin lesion classification using deep learning. *Experimental dermatology*, 27(11), 1261-1267. <https://doi.org/10.1111/exd.13777>
- [7] Bottou, L. (2010). Large-scale machine learning with stochastic gradient descent. In *Proceedings of COMPSTAT'2010*(pp. 177-186). Physica-Verlag HD.
- [8] Deng, L., & Yu, D. (2014). Deep learning: methods and applications. *Foundations and Trends® in Signal Processing*, 7(3-4), 197- 387.
- [9] Espinosa, J. E., Velastin, S. A., & Branch, J. W. (2017, November). Vehicle detection using alex net and faster R-CNN deep learning models: a comparative study. In *International Visual Informatics Conference* (pp. 3-15). Springer, Cham. https://doi.org/10.1007/978-3-319-70010-6_1
- [10] Singh, A. K., Ganapathysubramanian, B., Sarkar, S., & Singh, A. (2018). Deep learning for plant stress phenotyping: trends and future perspectives. *Trends in plant science*, 23(10), 883-898. <https://doi.org/10.1016/j.tplants.2018.07.004>
- [11] Yildirim, M., Cinar, A. (2020). A deep learning based hybrid approach for COVID-19 disease detections. *Traitement du Signal*, 37(3): 461-468. <https://doi.org/10.18280/ts.370313>.
- [12] Huang, G., Liu, Z., Van Der Maaten, L., & Weinberger, K. Q. (2017). Densely connected convolutional networks. In *Proceedings of the IEEE conference on computer vision and pattern recognition* (pp. 4700-4708).
- [13] Krizhevsky, A., Sutskever, I., & Hinton, G. E. (2012). Imagenet classification with deep convolutional neural networks. In *Advances in neural information processing systems* (pp. 1097-1105).
- [14] Szegedy, C., Liu, W., Jia, Y., Sermanet, P., Reed, S., Anguelov, D., ... & Rabinovich, A. (2015). Going deeper with convolutions. In *Proceedings of the IEEE conference on computer vision and pattern recognition* (pp. 1-9).
- [15] He, K., Zhang, X., Ren, S., & Sun, J. (2016). Deep residual learning for image recognition. In *Proceedings of the IEEE conference on computer vision and pattern recognition* (pp. 770-778).
- [16] URL-1, <https://www.kaggle.com/naim99/segmented-images-of-the-skin-cancer-dataset>, Last Accessed Date:03.02.2021
- [17] Yildirim, M., Çinar, A. (2019). Classification of white blood cells by deep learning methods for diagnosing disease. *Revue d'Intelligence Artificielle*, Vol. 33, No. 5, pp. 335-340. <https://doi.org/10.18280/ria.330502>.
- [18] Liu, Z. (2020). Soft-shell shrimp recognition based on an improved AlexNet for quality evaluations. *Journal of Food Engineering*, 266, 109698. <https://doi.org/10.1016/j.jfoodeng.2019.109698>
- [19] Zahisham, Z., Lee, C. P., & Lim, K. M. (2020, September). Food Recognition with ResNet-50. In *2020 IEEE 2nd International Conference on Artificial Intelligence in Engineering and Technology (IICAET)* (pp. 1-5). IEEE. doi: 10.1109/IICAET49801.2020.9257825.
- [20] Carcagnì, P., Leo, M., Cuna, A., Mazzeo, P. L., Spagnolo, P., Celeste, G., & Distante, C. (2019, September). Classification of skin lesions by combining multilevel learnings in a DenseNet architecture. In *International Conference on Image Analysis and Processing* (pp. 335-344). Springer, Cham. https://doi.org/10.1007/978-3-030-30642-7_30

- [21] Al-Qizwini, M., Barjasteh, I., Al-Qassab, H., & Radha, H. (2017, June). Deep learning algorithm for autonomous driving using googlenet. In 2017 IEEE Intelligent Vehicles Symposium (IV) (pp. 89-96). IEEE. doi: 10.1109/IVS.2017.7995703.
- [22] Çinar, A., Yıldırım, M. (2020). Detection of tumors on brain MRI images using the hybrid convolutional neural network architecture. Medical Hypotheses, 139: 109684. <https://doi.org/10.1016/j.mehy.2020.109684>
- [23] Çinar, A., Yıldırım, M., & Eroğlu, Y. (2021). Classification of Pneumonia Cell Images Using Improved ResNet50 Model. Traitement du Signal, 38(1), 165-173. <https://doi.org/10.18280/ts.380117>

On Generalized Mannheim curves in the Equiform Geometry of the Galilean 4-Space

Sibel TARLA ^{1*}, Handan ÖZTEKİN ²

^{1,2} Department of Mathematics, Faculty of Science, University of Firat, Elazig, Turkey

^{1*} sibeltarla@gmail.com, ² handanoztekin@gmail.com

(Geliş/Received: 17/02/2021;

Kabul/Accepted: 03/06/2021)

Abstract: In this paper on curve, we give a definition of generalized Mannheim curves that we will depict over the Equiform differential geometry of Galilean 4-space. We show some characterizations of generalized Mannheim curves. A new characterization has been procured among curvatures by employing the Mannheim curve overview

Key words: Manheimm curve, Galilean space, Equiform geometry

4-boyutlu Galileo Uzayının Equiform Geometrisindeki Genelleştirilmiş Mannheim Eğrileri

Öz: Eğri hakkında ki bu makale de, Galileo 4-uzayının Equiform diferansiyel geometrisi üzerinde tanımlayacağımız genelleştirilmiş Mannheim eğrinin bir tanımını veriyoruz. Genelleştirilmiş Mannheim eğrilerin bazı karakterizasyonlarını gösteriyoruz. Mannheim eğrilerine genel bir bakış kullanılarak eğrilikler arasında yeni bir karakterizasyon sağlandı.

Anahtar kelimeler: Mannheim eğri, Galileo uzayı, Equiform geometri

1. Introduction

Although many issues are taken into consideration in differential geometry, curves have an important place for this geometry. Curves have been studied in several spaces and continue to be studied. The topic of curves has been studied in many areas and is still being studied. The characterizations of curves is grand circumstance for curves in curves geometry. The articles concerning Equiform geometry are few. Many scientists studied, joining different perspectives on the curves in Mannheim. Mannheim presented in 1878 for the first time that space curves, whose principal normal are binormal of another curve, are called Mannheim curves [1]. Using the relationships between curvature and torsion of curves, some custom curves can be called. Some researchers attained Mannheim curves by identifying conditions between curvature of the curves [2]. Onder at al. have presented new characterizatons for these curves by examining the Mannheim curves for the spacelike and and timelike conditions [3,4]. Novel characterizations of Mannheim partner curves are granted in Minkowski 3-space by Kahraman and at all [5]. Matsuda and Yorozu had given some characterizations and examples of generalized Mannheim curve [6]. Orbay and Kasap gave [7] novel characterizations of Mannheim partner curves in Euclidean 3-space. Indeed, Mannheim curves for discrepant spaces appear to be able to be depicted Mannheim curves, so new qualifications for these curves have been offered to the literature [8-15]. Mannheim curve have an important place in place in differential geometry and new studies are still being added to the literature on Mannheim curves [16-21]. The Mannheim-B curve is among the new topics presented to the literature [22]. Differential geometry has a large are, and curves are an open area in differential geometry.

In this paper, we introduce a definition of generalized Mannheim curves in the Equiform differential geometry of Galilean 4-space. In this space, new characterizations for the generalized Mannheim curves are obtained. We also give properties of Mannheim curves for the space we work.

2. Preliminaries

Here, we have given some basic information about curves in 4D Galilean space, necessary for our study [23]. The Galilean scalar product between any two points is expressed in Affine coordinates as follows.

$$\mathbb{P}_i = (\mathbb{P}_{i1}, \mathbb{P}_{i2}, \mathbb{P}_{i3}, \mathbb{P}_{i4}), \quad i = 1, 2, \quad (2.1)$$

is designated by

* Corresponding author: sibeltarla@gmail.com. ORCID Number of authors: ^{1*} 0000-0002-8479-0892, ² 0000-0002-5846-1825

$$l(\mathbb{P}_1, \mathbb{P}_2) = \begin{cases} |\mathbb{P}_{21} - \mathbb{P}_{11}|, & \text{if } \mathbb{P}_{21} \neq \mathbb{P}_{11}, \\ ((\mathbb{P}_{22} - \mathbb{P}_{12})^2 + (\mathbb{P}_{23} - \mathbb{P}_{13})^2 + (\mathbb{P}_{24} - \mathbb{P}_{14})^2)^{1/2}, & \text{if } \mathbb{P}_{21} = \mathbb{P}_{11}. \end{cases} \quad (2.2)$$

The Galilean cross product in G_4 for the vectors $\vec{\mathbb{p}} = (\mathbb{p}_1, \mathbb{p}_2, \mathbb{p}_3, \mathbb{p}_4)$, $\vec{\mathbb{r}} = (r_1, r_2, r_3, r_4)$, $\vec{\mathbb{q}} = (q_1, q_2, q_3, q_4)$, is depicted by

$$\vec{\mathbb{p}} \wedge \vec{\mathbb{r}} \wedge \vec{\mathbb{q}} = - \begin{vmatrix} 0 & e_2 & e_3 & e_4 \\ \mathbb{p}_1 & \mathbb{p}_2 & \mathbb{p}_3 & \mathbb{p}_4 \\ r_1 & r_2 & r_3 & r_4 \\ q_1 & q_2 & q_3 & q_4 \end{vmatrix}, \quad (2.3)$$

where $e_m, 1 \leq m \leq 4$, are the standard basis vectors.

The scalar product of any two vectors $\vec{a} = (a_1, a_2, a_3, a_4)$ and $\vec{b} = (b_1, b_2, b_3, b_4)$ in G_4 is designated by

$$\langle \vec{a}, \vec{b} \rangle_{G_4} = \begin{cases} a_1 b_1, & \text{if } a_1 \neq 0 \text{ or } b_1 \neq 0, \\ a_1 b_1 + a_2 b_2 + a_3 b_3, & \text{if } a_1 = 0 \text{ or } b_1 = 0. \end{cases} \quad (2.4)$$

The norm of vector \vec{u} is depicted by

$$\|\vec{u}\|_{G_4} = \sqrt{|\langle \vec{u}, \vec{u} \rangle_{G_4}|}. \quad (2.5)$$

Let $\alpha: I \subset \mathcal{R} \rightarrow G_4$, $\alpha(s) = (s, \mathbf{y}(s), \mathbf{z}(s), \mathbf{w}(s))$ be a curve parametrized by arclength s . The $t(s)$ tangent vector of α , is depicted by

$$t(s) = \alpha'(s) = (1, \mathbf{y}'(s), \mathbf{z}'(s), \mathbf{w}'(s)). \quad (2.6)$$

Since $t(s)$ is a unit vector, we can phrase

$$\langle \vec{t}, \vec{t} \rangle_{G_4} = 1 \quad (2.7)$$

Differentiating (2.7) in respect of s , we have

$$\langle t', t \rangle_{G_4} = 0. \quad (2.8)$$

The k_1 real-valued function with the help of the derivative of the tangent vector function,

$$k_1(s) = \|t'(s)\| = \sqrt{(\mathbf{y}''(s))^2 + (\mathbf{z}''(s))^2 + (\mathbf{w}''(s))^2} \quad (2.9)$$

is stated the as first curvature of the curve α . We assume that $k_1(s) \neq 0$, for all $s \in I$. The $n(s)$ principal vector is defined by

$$n(s) = \frac{t'(s)}{k_1(s)}, \quad (2.10)$$

in other words

$$n(s) = \frac{1}{k_1(s)} (0, \mathbf{y}''(s), \mathbf{z}''(s), \mathbf{w}''(s)). \quad (2.11)$$

definition the k_2 second curvature function that is depicted by

$$k_2(s) = \|n'(s)\|_{G_4}. \quad (2.12)$$

The $b(s)$ binormal vector field is

$$b(s) = \frac{1}{k_2(s)} \left(0, \left(\frac{y''(s)}{k_1(s)} \right)', \left(\frac{z''(s)}{k_1(s)} \right)', \left(\frac{w''(s)}{k_1(s)} \right)' \right). \quad (2.13)$$

The $e(s)$ fourth unit vector is defined by

$$e(s) = \mu t(s) \wedge n(s) \wedge b(s). \quad (2.14)$$

The k_3 third curvature of the curve α is depicted by

$$k_3(s) = \langle b', e \rangle_{G_4}. \quad (2.15)$$

Here, as well known, the set $\{t, n, b, e, k_1, k_2, k_3\}$ is Frenet apparatus of the curve α . Thus the Frenet equations of the curve in G_4 are given by [15]

$$\begin{aligned} t'(s) &= k_1(s)n(s), \\ n'(s) &= k_2(s)b(s), \\ b'(s) &= -k_2(s)n(s) + k_3(s)e(s), \\ e'(s) &= -k_3(s)b(s). \end{aligned} \quad (2.17)$$

3. Frenet Formulas in Equiform Geometry of Galilean 4-Space

Here, we confer it in our study in Equiform differential geometry of curves in [24]. Let's take $\alpha: I \subset \mathcal{R} \rightarrow G_4$ as with arc-length parameter s . The equiform parameter of the curve $\alpha(s)$ expressed as

$$\varrho = \int \frac{ds}{\rho}, \quad (3.1)$$

where $\rho = \frac{1}{k_1}$ is radius of curvature of our curve. We can write the above equation as

$$\frac{ds}{d\varrho} = \rho. \quad (3.2)$$

assuming that h is homothety with the center in the origin and the coefficient λ . Also, we take

$$\tilde{s} = \lambda s \text{ and } \tilde{\rho} = \lambda \rho, \quad (3.3)$$

where \tilde{s} and $\tilde{\rho}$ are the arc-length parameter of $\tilde{\alpha}$ and the radius of curvature of this curve, respectively. So ϱ is an equiform invariant parameter of α .

The curvatures k_1, k_2, k_3 of the curve α are not invariants of the homothety group, because from (2.17), we can write

$$\tilde{k}_1 = \frac{1}{\lambda} k_1, \quad \tilde{k}_2 = \frac{1}{\lambda} k_2, \quad \tilde{k}_3 = \frac{1}{\lambda} k_3.$$

Now, if we get

$$\mathfrak{t} = \frac{d\alpha}{d\varrho} \quad (3.4)$$

and using (3.2), we have

$$\mathfrak{t} = \rho t. \quad (3.5)$$

Also, we define the vectors $\mathfrak{m}, \mathfrak{b}, \mathfrak{e}$ by

$$\mathfrak{m} = \rho n, \quad \mathfrak{b} = \rho b, \quad \mathfrak{e} = \rho e \quad (3.6)$$

Thus, the frenet formula for the $\mathfrak{t}, \mathfrak{m}, \mathfrak{b}, \mathfrak{e}$ vectors in respect of ϱ are follows

$$\begin{aligned} \mathfrak{t}' &= \dot{\rho} \mathfrak{t} + \mathfrak{m}, \\ \mathfrak{m}' &= \dot{\rho} \mathfrak{m} + \frac{k_2}{k_1} \mathfrak{b} \\ \mathfrak{b}' &= -\frac{k_2}{k_1} \mathfrak{m} + \dot{\rho} \mathfrak{b} + \frac{k_3}{k_1} \mathfrak{e}, \\ \mathfrak{e}' &= -\frac{k_3}{k_1} \mathfrak{b} + \dot{\rho} \mathfrak{e}. \end{aligned}$$

Definition 3.1. The function $\mathbb{k}_m: I \rightarrow R, m = 1,2,3$, is depicted as

$$\mathbb{k}_1 = \dot{\rho}, \quad \mathbb{k}_2 = \frac{k_2}{k_1}, \quad \mathbb{k}_3 = \frac{k_3}{k_1} \quad (3.7)$$

is named the m^{th} equiform curvature of the curve. In addition, the formula in Equiform geometry of G_4 with similar logic, it is expressed as follows

$$\begin{aligned} \mathfrak{t}' &= \mathbb{k}_1 \mathfrak{t} + \mathfrak{m}, \\ \mathfrak{m}' &= \mathbb{k}_1 \mathfrak{m} + \mathbb{k}_2 \mathfrak{b} \\ \mathfrak{b}' &= -\mathbb{k}_2 \mathfrak{m} + \mathbb{k}_1 \mathfrak{b} + \mathbb{k}_3 \mathfrak{e}, \\ \mathfrak{e}' &= -\mathbb{k}_3 \mathfrak{b} + \mathbb{k}_1 \mathfrak{e}. \end{aligned} \quad (3.8)$$

[24].

4. Generalized Mannheim curves in Equiform Geometry of Galilean 4-Space

Current porsion, we designate the generalized Mannheim curve with respect to Equiform differential geometry of G_4 .

Definition 4.1. Let's take as a special Frenet curve C in Equiform differential geometry of G_4 . In the Equiform differential geometry of G_4 , there is a special Frenet curve \hat{C} such that the first normal line at each point of C is included in the plane generated by the second and third normal lines of \hat{C} at corresponding point under \emptyset . Where $\emptyset: C \mapsto \hat{C}$ is a bijection. As a consequence, the curve \hat{C} is named the generalized Mannheim mate curve of C under this circumstance.

Hereafter, a privative Frenet curve C in Equiform differential geometry of G_4 is parametrized by parameter ϱ , that is, C is dedicated by $x: L \ni \varrho \mapsto x(\varrho) \in G_4$. When C is a generalized Mannheim curve in G_4 and, because of descript, a generalized Mannheim mate curve \hat{C} is denoted as the map $\hat{x}: L \rightarrow G_4$ such that

$$\hat{x} = x(\varrho) + \alpha(\varrho)e_2(\varrho), \quad \varrho \in L, \quad (4.1)$$

is written. Where α is a smooth function on L . We remark that the parameter ϱ generally is not an arc-length parameter of \hat{C} . Let $\hat{\varrho}$ be the arc-length of \hat{C} defined by

$$\hat{\varrho} = \int_0^s \left\| \frac{d\hat{x}(\varrho)}{d\varrho} \right\| d\varrho.$$

We can count a smooth function $F: L \rightarrow \hat{L}$ given by $F(\varrho) = \hat{\varrho}$. We remark that $\hat{\varrho}$ is the parameter of \hat{C} , and the bijection $\emptyset: C \rightarrow \hat{C}$ is defined by $\emptyset(x(\varrho)) = \hat{x}(F(\varrho))$. From the definition of the Mannheim curve, corresponding point under a bijection \emptyset for each $\varrho \in L$ the vector $e_2(\varrho)$ is grant by linear combination of $\hat{e}_3(F(\varrho))$ and $\hat{e}_4(F(\varrho))$, that is, we can set $e_2(\varrho) = g(\varrho) \hat{e}_3(F(\varrho)) + h(\varrho) \hat{e}_4(F(\varrho))$ for some smooth functions g and h on L . According to this definition, Differentiating (4.1) according to equiform invariant parameter ϱ and using the equations (3.8), we have

$$F'(\varrho)\hat{e}_1(F(\varrho)) = e_1(\varrho) + \alpha'(\varrho)e_2(\varrho) + \alpha(\varrho)(\mathbb{k}_1(\varrho)e_2(\varrho) + \mathbb{k}_2(\varrho)e_3(\varrho))$$

$$F'(\varrho)\hat{e}_1(F(\varrho)) = e_1(\varrho) + (\alpha'(\varrho) + \alpha(\varrho)\mathbb{k}_1(\varrho))e_2(\varrho) + \alpha(\varrho)\mathbb{k}_2(\varrho)e_3(\varrho) \quad (4.2)$$

if we inner product both sides of this equation by $e_2(\varrho)$ and considering the following equality

$$\langle \hat{e}_1(F(\varrho)), g(\varrho)\hat{e}_3(F(\varrho)) + h(\varrho)\hat{e}_4(F(\varrho)) \rangle = 0,$$

we obtain

$$0 = (\alpha'(\varrho) + \alpha(\varrho)\mathbb{k}_1(\varrho))\rho^2, \rho \neq 0$$

from this equation we get

$$\alpha(\varrho) = e^{-\mathbb{k}_1\varrho}c \quad (4.3)$$

where $c \in R$. Thus we have

$$F'(\varrho)\hat{e}_1(F(\varrho)) = e_1(\varrho) + e^{-\mathbb{k}_1\varrho}c\mathbb{k}_2(\varrho)e_3(\varrho),$$

that is,

$$\hat{e}_1(F(\varrho)) = \frac{e_1(\varrho)}{F'(\varrho)} + \frac{e^{-\mathbb{k}_1\varrho}c\mathbb{k}_2(\varrho)e_3(\varrho)}{F'(\varrho)},$$

where $\|F'(\varrho)\| = \sqrt{1 + (e^{-\mathbb{k}_1\varrho}c\mathbb{k}_2(\varrho))^2}$ for $\varrho \in L$. If we take the differential of the above equality according to ϱ , we have

$$\begin{aligned} F'(\varrho)\hat{e}_1'(F(\varrho)) &= \left(\frac{1}{F'(\varrho)}\right)' e_1(\varrho) + \frac{1}{F'(\varrho)} e_1'(\varrho) \\ &\quad + \left(\frac{1}{F'(\varrho)}\right)' e^{-\mathbb{k}_1\varrho}c\mathbb{k}_2(\varrho)e_3(\varrho) \\ &\quad + \frac{1}{F'(\varrho)} (-\mathbb{k}_1 e^{-\mathbb{k}_1\varrho}c\mathbb{k}_2(\varrho)e_3(\varrho) + e^{-\mathbb{k}_1\varrho}c\mathbb{k}_2(\varrho)e_3'(\varrho)), \\ F'(\varrho)(\mathbb{k}_1(\varrho)\hat{e}_1(\varrho) + \hat{e}_2(\varrho)) &= \left(\frac{1}{F'(\varrho)}\right)' e_1(\varrho) \\ &\quad + \frac{1}{F'(\varrho)} (\mathbb{k}_1(\varrho)e_1(\varrho) + e_2(\varrho)) \\ &\quad + \left(\frac{1}{F'(\varrho)}\right)' e^{-\mathbb{k}_1\varrho}c\mathbb{k}_2(\varrho)e_3(\varrho) \\ &\quad + \frac{1}{F'(\varrho)} (-\mathbb{k}_1 e^{-\mathbb{k}_1\varrho}c\mathbb{k}_2(\varrho)e_3(\varrho)) \\ &\quad + \frac{1}{F'(\varrho)} e^{-\mathbb{k}_1\varrho}c\mathbb{k}_2(\varrho)(-\mathbb{k}_2(\varrho)e_2(\varrho) + \mathbb{k}_1(\varrho)e_3(\varrho) + \mathbb{k}_3(\varrho)e_4(\varrho)), \end{aligned}$$

If we inner product both sides of this equation by $e_2(\varrho)$ and using the $e_2(\varrho) = g(\varrho)\hat{e}_3(F(\varrho)) + h(\varrho)\hat{e}_4(F(\varrho))$ equality

$$\frac{e^{\mathbb{k}_1\varrho}}{(\mathbb{k}_2)^2} = \text{const.}$$

In this way, we have following theorem from the explanations:

Theorem 4.1. Let's take a Frenet curve C in equiform differential geometry of G_4 . If the curve α is a generalized Mannheim curve, from here, the following equality is satisfied the relationship between the curve functions \mathbb{k}_1 and \mathbb{k}_2 of C .

$$\frac{e^{\mathbb{k}_1\varrho}}{(\mathbb{k}_2)^2} = \text{const.}, \varrho \in L. \quad (4.4)$$

Let $\hat{\varrho}$ be the arc-length of \hat{C} . Also, $\hat{\varrho}$ we know it is defined by

$$\hat{\varrho} = \int_0^s \left\| \frac{d\hat{x}(\varrho)}{d\varrho} \right\| d\varrho$$

for $\varrho \in L$. We can take into consideration a smooth function $F : L \rightarrow \hat{L}$ given by $F(\varrho) = \hat{\varrho}$. Considering the following equality

$$\|F'(\varrho)\| = \sqrt{1 + (e^{-\mathbb{k}_1 \varrho} c \mathbb{k}_2)^2},$$

from (4.4) equality

$$\|F'(\varrho)\| = \sqrt{1 + \frac{1}{(\mathbb{k}_2)^2}}$$

for $\varrho \in L$.

The description of \hat{C} by arc-length parameter $\hat{\varrho}$ is denoted by $\hat{x}(\hat{\varrho})$, here we use the same letter “ \hat{x} ” for simplicity. Then we can simply write

$$\hat{x}(\hat{\varrho}) = \hat{x}(F(\varrho)) = x(\varrho) + \alpha(\varrho)e_2(\varrho)$$

for curve \hat{C} . By receiving the derivative of this equation with respect to ϱ ,

$$\frac{d\hat{x}(\hat{\varrho})}{d\varrho} = \frac{d\hat{x}(\hat{\varrho})}{d\hat{\varrho}} F'(\varrho) = F'(\varrho) \hat{e}_1(F(\varrho))$$

and

$$F'(\varrho) \hat{e}_1(F(\varrho)) = e_1(\varrho) + e^{-\mathbb{k}_1 \varrho} c \mathbb{k}_2 e_3(\varrho)$$

Thus we have

$$\hat{e}_1(F(\varrho)) = \frac{1}{\sqrt{1 + \frac{1}{(\mathbb{k}_2)^2}}} e_1(\varrho) + \frac{e^{-\mathbb{k}_1 \varrho} c \mathbb{k}_2}{\sqrt{1 + \frac{1}{(\mathbb{k}_2)^2}}} e_3(\varrho)$$

for $\varrho \in L$. We differentiate of the above equality according to ϱ , then we have

$$\begin{aligned} F'(\varrho) \left(\hat{\mathbb{k}}_1(F(\hat{\varrho})) \hat{e}_1(F(\varrho)) + \hat{e}_2(F(\varrho)) \right) &= \frac{\mathbb{k}_1}{\sqrt{1 + \frac{1}{(\mathbb{k}_2)^2}}} e_1(\varrho) \\ &+ \left(\frac{1}{\sqrt{1 + \frac{1}{(\mathbb{k}_2)^2}}} - \frac{1}{\sqrt{1 + \frac{1}{(\mathbb{k}_2)^2}}} e^{-\mathbb{k}_1 \varrho} c \mathbb{k}_2^2 \right) e_2(\varrho) \\ &+ \left(\frac{-\mathbb{k}_1 e^{-\mathbb{k}_1 \varrho} c \mathbb{k}_2}{\sqrt{1 + \frac{1}{(\mathbb{k}_2)^2}}} + \frac{\mathbb{k}_1 e^{-\mathbb{k}_1 \varrho} c \mathbb{k}_2}{\sqrt{1 + \frac{1}{(\mathbb{k}_2)^2}}} \right) e_3(\varrho) \end{aligned}$$

$$+ \frac{e^{-\mathbb{k}_1 \varrho} c \mathbb{k}_2 \mathbb{k}_3}{\sqrt{1 + \frac{1}{(\mathbb{k}_2)^2}}} e_4(\varrho),$$

considering $1 - e^{-\mathbb{k}_1 \varrho} c (\mathbb{k}_2(\varrho))^2 = 0$ equality, from the above equation, coefficient of $e_3(\varrho)$ is zero. Thus, for each $\varrho \in L$, the vector $\hat{e}_1(F(\varrho))$ is granted by linear combination of $e_1(\varrho)$ and $e_3(\varrho)$. And, as above, the vector $\hat{e}_2(F(\varrho))$ is given by linear combination of $e_1(\varrho)$, $e_3(\varrho)$ and $e_4(\varrho)$.

Since the curve \hat{C} is a special Frenet curve in Equiform differential geometry of G_4 , the vector $e_2(\varrho)$ is grant by linear combination of $\hat{e}_3(F(\varrho))$ and $\hat{e}_4(F(\varrho))$.

With the above description, we have following theorem:

Theorem 4.2. Let C be a special Frenet curve in Equiform differential geometry of G_4 whose curvature functions $\mathbb{k}_1 = \text{constant}$ and $\mathbb{k}_2 = \text{constant}$ are constant functions and satisfy the equality: $1 - e^{-\mathbb{k}_1 \varrho} c (\mathbb{k}_2(\varrho))^2 = 0, \varrho \in L$. If the curve \hat{C} given by $\hat{x}(\hat{\varrho}) = x(\varrho) + \alpha(\varrho)e_2(\varrho), \varrho \in L$ is a private Frenet curve, then C is a generalized Mannheim curve and \hat{C} is the generalized Mannheim mate curve of C .

Theorem 4.3. Let's take the curve C defined by

$$x(\varrho) = (\varrho, \alpha \int (\int \mathfrak{h}(\varrho) \sin \varrho d\varrho) d\varrho, \alpha \int (\int \mathfrak{h}(\varrho) \cos \varrho d\varrho) d\varrho, \alpha \int (\int \mathfrak{h}(\varrho) \mathfrak{g}(\varrho) d\varrho) d\varrho), s \in I,$$

where α is a positive constant number, \mathfrak{g} and \mathfrak{h} are any smooth functions: $I \rightarrow R$, and F defined by

$$\mathfrak{h}(\varrho) = \frac{\ln c(1 + \mathfrak{g}(\varrho)^2)^{-3} (\mathfrak{g}(\varrho)(\mathfrak{g}(\varrho))')^2}{\alpha \sqrt{1 + \mathfrak{g}(\varrho)^2}}$$

for $\varrho \in I$. Then the curvatures \mathbb{k}_1 and \mathbb{k}_2 of the curve C satisfy the equality

$$1 - e^{-\mathbb{k}_1 \varrho} c (\mathbb{k}_2(\varrho))^2 = 0,$$

for each $\varrho \in I$.

Proof. First we have to find \mathbb{k}_1 and \mathbb{k}_2 . Given the definitions of curvatures,

$$\mathbb{k}_1 = \|e'_2(\varrho)\| = \alpha \mathfrak{h}(\varrho) \sqrt{1 + \mathfrak{g}^2(\varrho)}$$

is obtained. Similarly,

$$\mathbb{k}_2 = \langle e'_2(\varrho), e_3(\varrho) \rangle = -(1 + \mathfrak{g}(\varrho)^2)^{-\frac{3}{2}} \mathfrak{g}(\varrho)(\mathfrak{g}(\varrho))'.$$

If we substitute these equations in the condition of Mannheim curve,

$$c = \frac{e^{-\alpha \mathfrak{h}(\varrho) \sqrt{1 + \mathfrak{g}^2(\varrho)}}}{-(1 + \mathfrak{g}(\varrho)^2)^{-\frac{3}{2}} \mathfrak{g}(\varrho)(\mathfrak{g}(\varrho))'}$$

is obtained. If we leave $\mathfrak{h}(\varrho)$ alone in the last equation, it is

$$\mathfrak{h}(\varrho) = \frac{\ln c(1 + \mathfrak{g}(\varrho)^2)^{-3} (\mathfrak{g}(\varrho)(\mathfrak{g}(\varrho))')^2}{\alpha \sqrt{1 + \mathfrak{g}(\varrho)^2}}.$$

So briefly, considering the formula of curvature calculations in Equiform differential geometry of G_4 the proof is can be done easily.

5. Conclusion

In this study, we defined the Mannheim curve for the Equiform differential geometry. We have obtained a new characterizations between the curvatures of the Mannheim curve. A new case is obtained if the curvatures are not zero. We gave the application of the Mannheim curve with a general example.

References

- [1] Mannheim, A.; Paris C. R. 1878; 86, 1254-1256.
- [2] Liu, H. L.; Wang, F. Mannheim partner curves in 3-space, J. Geom, 2008, 88, 120-126
- [3] Onder , M., Uğurlu, H.H., Kazaz, M., Mannheim offsets of spacelike ruled surfaces in minkowski 3-space. arXiv:0906.4660v3.[math.DG]
- [4] Onder , M., Uğurlu, H.H., Kazaz, M., Mannheim offsets of timelike ruled surfaces in minkowski 3-space. arXiv:0906.2077v4.[math.DG]
- [5] Kahraman, T., Önder, M., Kazaz, M., Uğurlu, H.H., Some characterizations of Mannheim partner curves in Minkowski 3-space, arXiv:1108.4570 [math.DG]
- [6] Matsuda, H., and Yorozu,S., On generalized Mannheim curves in Euclidean 4-space, Nihonkai Math.J. Vol.20,2009,33-56.
- [7] Kaymaz, F.,Aksoyak, F.,K., Some Special Curves and Mannheim Curves in Three Dimensional Euclidean Space, Mathematical Sciences and Applications E-Notes, 2017,5(1) 34-39.
- [8] Orbay, K., and Kasap, E., On Mannheim partner curves in E^3 , International Journal of Physical Sciences. 4(5), 2009, 261-264
- [9] Bektaş, Ö., Senyurt, S., On Dual Spacelike Mannheim Partner Curves in ID_1^3 , Ordu Univ. J. Sci. Tech., 2011, Vol:1, No:1, 1-14.
- [10] Ersoy, S., Tosun, M., Matsuda, H.,Generalized Mannheim curves in Minkowski Space-Time E_1^4 ,Mathematical Problems in Engineering, Volume 2011(2011), Article ID 539378,19 pages, doi./10.1155/2011/539378.
- [11] Kızıltuğ,S.,Yaylı, Y., On the quaternionic Mannheim curves of a W(k)-type in Euclidean space, Kuwait J. Sci. 2015; 42(2), pp. 128-140.
- [12] Öztekin, H., Ergüt, M., Null mannheim curves in the minkowski 3-space E_1^3 , Turk J Math 35 ,2011 ,107 – 114. Tübitak doi:10.3906/mat-0907-105.
- [13] Yoon, DW., Mannheim Curves in an n-dimensional Lorentz Manifold, International journal of Pure and Applied Mathematics, Vol. 96 No. 2 ,2014, 165-174.
- [14] Öğrenmiş, A., O., Öztekin, H., Ergüt, M., Some Properties of Mannheim Curves in Galilean and Pseudo - Galilean space, arXiv:1111.0424v1 [math.DG] 2 Nov 2011, 2000 AMS Classification: 53A35; 53B30.
- [15] Şenyurt, S., Çalışkan, A., Smarandache Curves of Mannheim Curve Couple according to Frenet Frame, Turkish Journal of Science and Technology, 2017, 5(1), 122-136.
- [16] Honda, S., Takahashi, M., Bertrand and Mannheim Curves of Framed Curves in the 3-dimensional Euclidean Space, Turkish Journal of Mathematics, 2020, 44, 883-889.
- [17] Camci, Ç., On a New Type Mannheim Curve, arXiv:2101.02021[math.GM].
- [18] Wang, Y., Chang, Y., Mannheim Curves and Spherical Curves, International Journal of Geometric Method in Modern Physics, 2020, 17(7), 2050101.
- [19] Aslan, K,N., İlarıslan, K., Some Characterizations of Generalized Null Mannheim Curves in Semi-Euclidean Space, Journal of Geometry and symmetry in Physics , 2020, 55, 1-20
- [20] Onder, M., Construction of Curve Pairs and their Applications, Proceedings of the National Academy of Sciences India Section A-Physical Sciences, 2021, 91(1), 21-28.
- [21] Liu, H., Liu, Y., Curves in three dimensional Riemannian Space Forms, Journal of Geometry, 2021, 112(1), 8.
- [22] İlarıslan, K., Ucum, A., Nesovic, E., Mannheim B-Curve Couples in Minkowski 3-Space, Tamkang Journal of Mathematics, 2020, 51(3), 219-232.
- [23] Süha Yılmaz, Construction of the Frenet-Serret Frame of a Curve in 4D Galilean Space and Some Applications, Int. Jour. of the Phys. Sci. Vol: 5,No:8, 2010,1284-1289.
- [24] Aydın, M.E.and Ergüt, M., The Equiform Differential Geometry of Curves in 4-dimensional Galilean Space G_4 , Stud. Univ. Babeş-Bolyai Math. 58,2013, No. 3, 399–406.

Analysis of The Performance According to Object Density in Static Environments of GA and PSO Algorithms Used in Mobile Robot Path Planning

Gürkan GÜRGÖZE^{1*}, İbrahim TÜRKOĞLU²

¹ Department of Software Engineering, Institute of Science, Fırat University, Elazığ, Turkey

² Department of Software Engineering, Faculty of Technology, Fırat University, Elazığ, Turkey

*¹ gurkangurgoze@gmail.com, ² iturkoglu@firat.edu.tr

(Geliş/Received: 17/02/2021;

Kabul/Accepted: 26/06/2021)

Abstract: In the movement of autonomous mobile robots in static or dynamic environments, one of the important issues sought for a solution is to reach the target with the shortest and safest path without collision. For this purpose, there are many algorithms. The solutions brought by these algorithms differ according to the dynamics of the environment. However, as is known, the real world environment is complex. As the environment gets more complex, more environment knowledge is required for the performance of the algorithms. Complex mobile robotic systems equipped with sensors are required to obtain environmental information. This causes more energy consumption, processing load and the formation of heavy structures. In order to solve these problems, there are algorithms that perform path planning without the need for all environment information. Two of these are the Genetic Algorithm (GA) and the Particle Swarm Optimization (PSO) algorithm. In the literature review, it is seen that these algorithms are effective in the selection and use of sensors according to the nature of the environment. However, in this respect, it was seen that their performances in static environments with different object densities were not analysed and compared. Therefore, in this study, the performance of both algorithms was compared according to the object density in the environment. Distance, time, curvature, and processing speed analyses were performed in MATLAB / Simulink environment according to different density environment scenarios.

Key words: Particle Swarm Optimization (PSO), Path Planning, Genetic Algorithm(GA), Object Detection.

Mobil Robot Yol Planlamasında Kullanılan GA ve PSO Algoritmalarının Statik Ortamlardaki Nesne Yoğunluğuna Göre Performansının Analizi

Öz: Otonom mobil robotların statik veya dinamik çevrelerdeki hareketinde çözüm aranan önemli konulardan biri de çarpışmadan hedefe en kısa ve en güvenli yol ile ulaşmasıdır. Bu amaçla birçok algoritma mevcuttur. Bu algoritmaların getirdiği çözümler ortamın dinamiklerine göre farklılıklar göstermektedir. Ancak bilindiği gibi gerçek dünya ortamı karmaşıktır. Ortam karmaşıklıklaştıkça algoritmaların performansının iyi olması için daha fazla ortam bilgisi gerekmektedir. Ortam bilgisini almak için ise sensörlerle donatılmış karmaşık mobil robot sistemler gerekmektedir. Bu da daha fazla enerji tüketimi, işlem yükü ve ağır yapıların oluşması sorunlarına neden olmaktadır. Bu sorunların çözümü için tüm ortam bilgisine ihtiyaç duymadan yol planlama gerçekleştiren algoritmalar mevcuttur. Bunlardan ikisi Genetik Algoritma (GA) ve Parçacık Sürü Optimizasyonu (PSO) algoritmasıdır. Literatür taramasında bu algoritmaların ortamın yapısına göre sensör seçimi ve kullanımında etkili olduğu görülmektedir. Fakat bu minvalde farklı nesne yoğunluklarına sahip statik ortamlardaki performanslarının analiz edilmediği ve karşılaştırılmadığı görülmüştür. Bu nedenle bu çalışmada her iki algoritmanın ortamdaki nesne yoğunluğuna göre performanslarının karşılaştırılması yapıldı. Farklı yoğunluktaki ortam senaryolarına göre mesafe, süre, kavis, işlem hızı analizleri MATLAB/Simulink ortamında gerçekleştirildi.

Anahtar kelimeler: Parçacık Sürü Optimizasyonu (PSO), Yol Planlama, Genetik Algoritma (GA), Nesne Tespiti

1. Introduction

One of the most important issues in the movement of autonomous mobile robots is to reach the target with the shortest and safest way without colliding. For this purpose, there are many path planning algorithms based on probabilistic, potential space and artificial intelligence [1-2]. The solutions provided by these algorithms differ according to the dynamics of the environment and the availability of environment information. Mobile robots move in environments with static or dynamic objects. Only the mobile robot is mobile in a static environment. In dynamic environment, it is present in moving objects together with the mobile robot. At the same time, according to the information of the movement environment, road planning is divided into two as general and local road planning. In general path planning, the mobile robot has knowledge about the motion environment before starting

* Corresponding author: gurkangurgoze@gmail.com. ORCID Number of authors: ¹ 0000-0002-2831-498X, ² 0000-0003-4938-4167

to move. Based on this information, a map and route planning is done offline. Then the action begins. There is no parameter that can disrupt the existing road plan during the movement. In local route planning, on the other hand, the mobile robot moves in an environment with little or no knowledge. The mobile robot detects objects in the environment and avoids them and obtains a dynamic route plan to the destination. Map information is updated according to the static or dynamism of the objects in the environment. Such algorithms are also called online path planning algorithms [3].

Mobile robots receive environmental information through sensors such as cameras, LIDAR, ultrasonic sensors, laser, GPS mounted on them. This causes mobile robots to become complex and heavy systems. However, as is known, the real world environment is complex. As the environment gets more complex, more environment knowledge is required for the performance of algorithms to be better [4]. This causes more energy consumption, processing load and the formation of heavy structures. In order to solve these problems, algorithms that perform path planning with limited environment information are required without the need for all environment information. Generally, such path planning is performed by artificial intelligence-based algorithms. In this way, the ability to make decisions like a human is gained. For this purpose, meta-heuristic algorithms, inspired by the behaviour of living things in nature, have been developed. Two of these are the Genetic Algorithm (GA) and the Particle Swarm Optimization (PSO) algorithm [2-5]. GA performs operations by taking samples in very complex environments. This ensures high processing speed. The PSO algorithm, on the other hand, performs meta-heuristic progress according to the information of the particles randomly distributed in the environment. The optimum results are not always obtained from these algorithms. However, the most ideal result can be achieved. In particular, optimization features based on incomplete data have spread their hybrid use with other algorithms [6].

There are many studies on PSO and GA. Ibraheem et al. (2018), with PSO and improved bat algorithm, Hassani et al. (2018) presented a hybrid path planning algorithm with PSO and firefly algorithm [7, 8]. Li et al. (2010) proposed an improved PSO path planning algorithm by increasing the capacity of the PSO algorithm to get out of local minimums [9]. Davoodi et al. (2015) tested problems such as distance and time in route planning with the energy-oriented PSO algorithm [10]. Das et al. (2016) proposed an improved PSO algorithm based on robot rotation and time, focused on reducing energy consumption [11]. Purcaru et al. (2013) presented a hybrid path planning algorithm for static environments from PSO and Gravitational Search Algorithm (GSA) [12]. Roberge et al. (2013) developed a GA and PSO-based hybrid path planning algorithm for autonomous movement in real environment in unmanned aerial vehicles [13]. Shivgan et al. (2020) developed energy optimized path planning to reduce the number of turns of the drone using a genetic algorithm. Souza et al. (2020) developed a hybrid path planning algorithm for unmanned aerial vehicles consisting of GA and Ray Casting algorithm [14]. Tao et al. (2020) developed a path planning and obstacle avoidance algorithm for unmanned aerial vehicles based on an advanced genetic algorithm [15]. Abhishek et al. (2020) presented a hybrid algorithm consisting of PSO and GA for 3D path planning in drones [16]. Yan et al. (2019) developed a hybrid multipurpose route planning model consisting of PSO and waypoint guidance in real-time applications in unmanned water vehicles [17]. Jianwei Ma et al. (2020) developed a hybrid path planning algorithm for a straighter path formation based on GA with Bezier optimization [1].

As can be seen in the studies examined, PSO and GA are among the algorithms widely used in path planning, especially due to their adaptation to the environment and optimization properties. Defining the properties of these algorithms well provide the correct approaches in planning the task and action. At the same time, it enables the mobile robot to make the sensor planning more accurately according to the structure of the environment. This will enable us to obtain mobile robot motion planning that responds faster and prevents the use of unnecessary sensors. At this point, the density of the obstacles in the environment in road planning is one of the factors that significantly affect the performance. Because the curves, lengths and degrees of safety of the roads they put forward will differ [1, 18, 19].

In this study, the performance of PSO and GA in static environments was compared according to object density in the environment. Objects in the environment were detected according to the image information. Distance, time, curvature, processing speed and safe path analyses were performed in MATLAB/Simulink environment according to different intensity environment scenarios.

When we look at the other parts of the article, in the second part, there is the material and method part that contains information about PSO, GA and mobile robot system used in the study. In the third part, simulation results in environments with different barrier density are analysed.

2. Materials and Methods

2.1 Genetic algorithm (GA)

It is an optimization algorithm based on population, genetic and random selection, presented by John Holland in 1975. In particular, it provides the most ideal solution for difficult and complex situations. It has the goal of reaching the best solution by mutation. The processing speed is high by sampling the data it uses. Whether it is ideal or not, it always produces a solution. All solutions are available on chromosomes. The process begins with the formation of the chromosome population. The proper value of each chromosome is determined. Then, according to this fitness value, cross-over, mutation of genes and selection steps are performed. This process is carried out recursively as shown in Figure 1. Meanwhile, the solution definition is expressed as the fitness value. With each iteration, this value is replaced by the value of the best fitting chromosome. Thus, orientation towards the best result is achieved. Chromosomes are randomly selected during the selection phase. Next generation is produced by crossing the chromosomes belonging to the best solution. It realizes the definition of the solution obtained by crossover by the sequence of bits or the exchange of genes [5, 13-15, 20].

In the study, the orbits produced for the path are randomly generated as the first population. Then the suitability values are determined. The sample set suitable for these values is selected. From the chosen coordinate parents, the solution suitable for the fitness function is obtained from the parents of children. Child solutions are mutated by adding, deleting and changing the new waypoint. This process is repeated for each point to be reached until the target is reached.

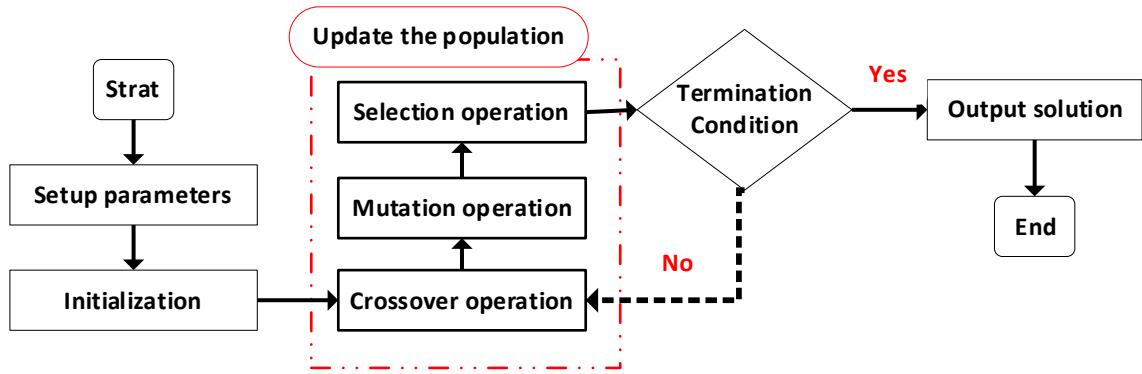


Figure 1. The flowchart of Genetic Algorithm (GA).

2.2 Particle swarm optimization (PSO)

Particle driver optimization (PSO) is a meta heuristic algorithm proposed by Eberhart and James Kennedy in 1995, inspired by the swarm behavior of birds and fish. Generates solutions from randomly generated individuals like GA. Especially, individuals' communication with each other reduces the processing burden. Uses the fitness function for the solution. First, the random particle swarm is created. Every particle has its speed and position. The best solutions (p_{best}) of the particles and the best solutions (q_{best}) of all particles are determined. The best value parameter is updated each time. Points are created with the best solutions until the goal is reached. The algorithm is mathematically expressed as follows.

$$V_{t+1} = w.V_t + crand(p_{best} - X_t) + crand(q_{best} - X_t) \quad (1)$$

V_t particle velocity, X_t particle position, best solution of p_{best} particle, best solution in q_{best} group, rand random variable, c constant [13, 19, 22-24].

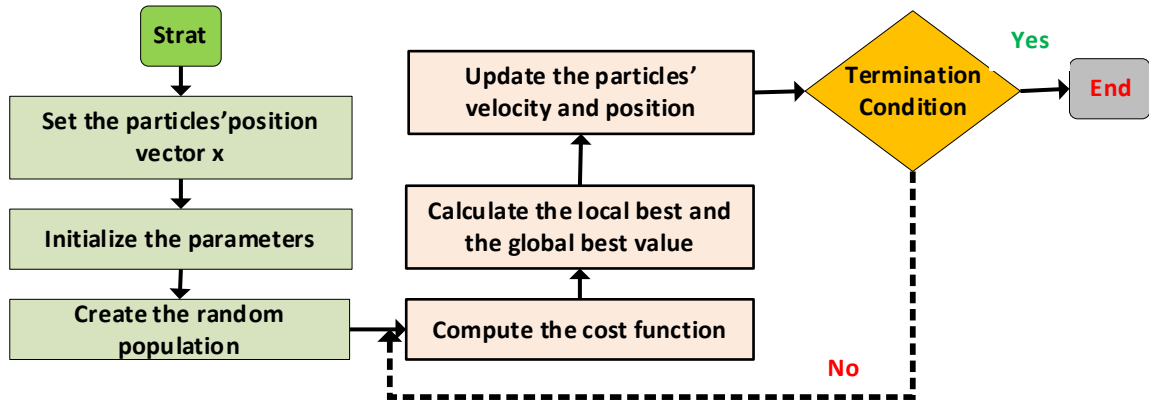


Figure 2. The flowchart of Particle Swarm Optimization (PSO).

2.3 Mobile robot system model

The mobile robot system generally consists of kinematics, dynamic analysis, path planning, speed and position control components. PSO and GA were used for road planning in line with the goal of our article. In this study, a study was carried out according to the object density in the static environment. In this article, the purpose of establishing the mobile robot system model is to determine the safe travels at certain speeds and transportation times of the routes obtained by road planning algorithms in a simulation environment. For this purpose, predetermined environment maps were used.

Kinematic analysis allows us to obtain the position and orientation information of the mobile robot in the environment. Thus, the information about where it is and where it will go is obtained. A mobile robot needs to meet the following coordinate information according to linear velocity V and orientation angle (θ). With kinematic modeling, general, local position information and orientation angle are obtained according to the signals measured from incremental encoders connected to the motor. The encoders generate a digital PWM signal based on the amount of rotation on the wheels of the robots. The obtained position information is compared with the reference motion waypoints and the deviation rate is obtained and necessary signal generation is obtained from the controllers (PID, Fuzzy, etc.). According to the control laws, the movement of the mobile robot is realized by PID speed control. PID gains were obtained by Ziegler-Nichols method for high stability [25].

$$\begin{aligned}
 V &= V_x = \frac{(V_R + V_L)}{2} = \frac{(r \cdot \omega_R + r \cdot \omega_L)}{2} \\
 \dot{x} &= v \cdot \cos \theta \\
 \dot{y} &= v \cdot \sin \theta
 \end{aligned} \tag{2}$$

Dynamic analysis is a mathematical model of the mobile robot system. Since the motion is realized by DC motors, it is usually sufficient to create a DC motor model. The mathematical model of the DC motor is obtained as a transfer function according to Kirchoff's and Newton's laws.

According to Kirchoff's laws;

$$\sum V = V_{in} - V_R - V_L - EMF = 0 \tag{3}$$

According to Newton's law;

$$T_m = T_L + T_s + T_a$$

Transfer function;

$$G_s(s) = \frac{w(s)}{V(s)} = \frac{K}{(Ls + R_a)(J_m s + b_m) + K^2} \tag{4}$$

R_a is armature resistance, K_t inductance constant, L armature inductance, T_L load torque, J_m motor inertia, and b_m motor internal friction [25, 26].

In order for the mobile robot to proceed without deviating from the road, a position control algorithm is required. It provides speed-based control by taking into account the difference between the current position and the target position. Pure Pursuit, Kalman, Kinematic Model, Markov etc. position algorithms are available [25].

The speed control algorithm is required to realize the speed that the position control algorithm obtains for the advance. For this, PID, Fuzzy, Fuzzy-PID, visual based etc. controllers are used. The aim is to bring the speed of the mobile robot closer to the speed required for the desired position. It does this by taking into account the targeted speed difference achieved during the movement.

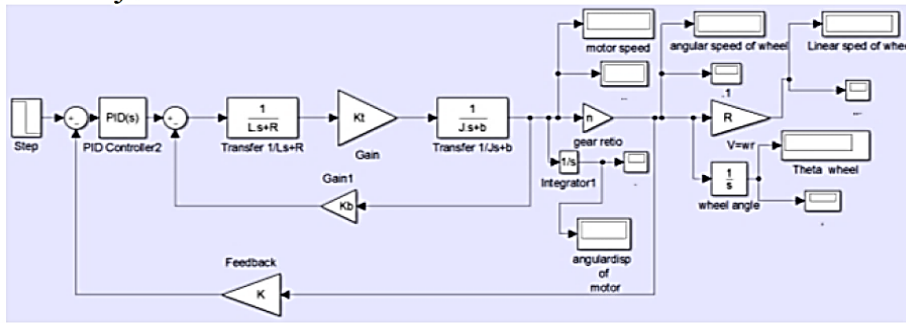


Figure 3. Mobile robot DC motor model [26].

3. Experimental Result and Discussion

Required DC motor parameters for simulation $K_t=0,062$ Nm/A, $K_e=0,062$ Vs/rad, $J_m=0,0551$ Kg/m², $b_m=0,188$ Nms/rad, $R_a=0.56$ Ohm, $L_a=0,97$ mH, $b_z=0,7$ Nms/rad, $K_{tac}=1,8$ Volt.s/rad [26]. PID was used for speed control in the mobile robot simulation model. PID gain values were determined as $K_p=20$, $K_i=5$ and $K_d=25$. Mobile robot dimensions are width = 0.1 m, length = 0.1 m.

Pure Pursuit algorithm was used to follow the obtained path. The parameters required for the algorithm were determined as look ahead distance (m) -0.2, maximum angular velocity (rad / s) -3, linear velocity (m / s) -0.6.

PSO parameters: Number of handle points = 5, maximum number of iterations = 100, population size (swarm size) = 150, inertia weight damping ratio = 0.98, personal learning coefficient $c_1=1.5$, global learning coefficient $c_2=1.57$

GA parameters: No of points that represent a candidate path, excluding the source =3, minimum generation size= 10, swarm size =150.

Starting and target points were determined as $[x, y] = [0.5 \ 0.1]$ and $[x, y] = [4 \ 4.9]$.

In order to be used in road planning, 5 object-dense environment maps in Figure 4 were used. Algorithms were run 5 times.

In this study, for a successful comparison of both algorithms, the mobile robot model and parameters, environment structure, maps and object densities, population numbers, position control algorithms, speed control structure and gains are taken common.

Best results used in this article:

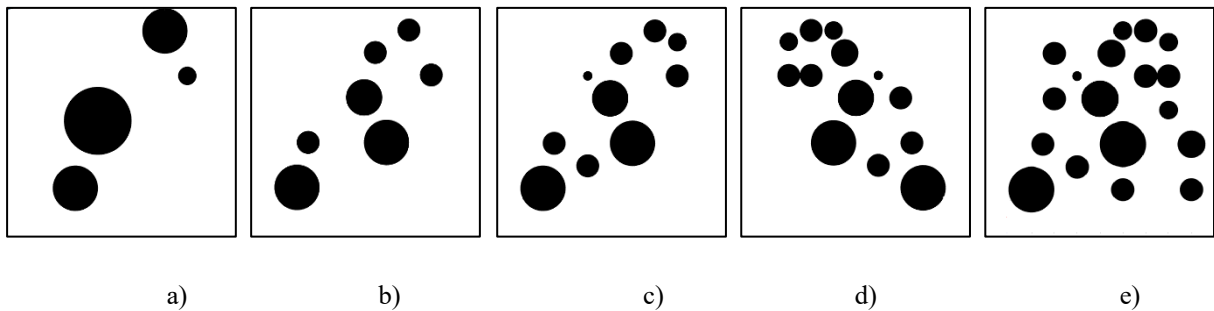


Figure 4. Five different object density maps: Towards more objects from less objects a) Map 1, b) Map 2, c) Map 3, d) Map 4, e) Map 5

Path planning created with PSO:

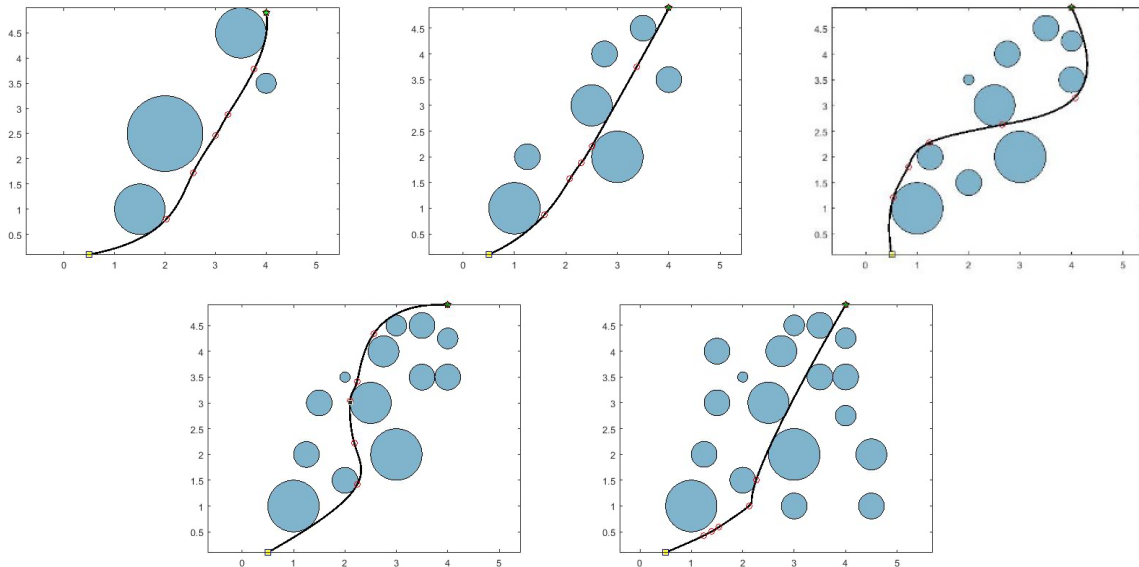


Figure 5. Path planning according to object density by PSO

Path planning created with GA:

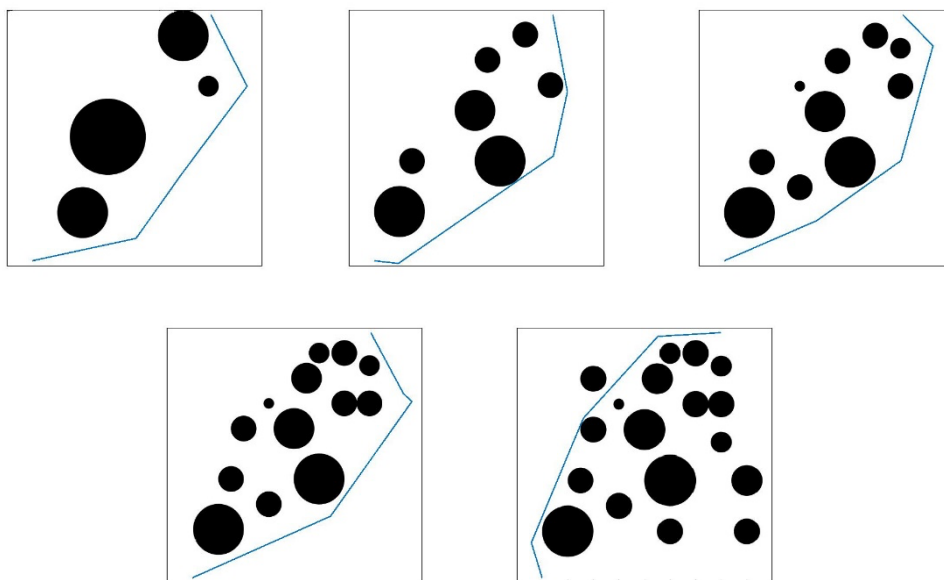


Figure 6. Path planning according to object density by GA

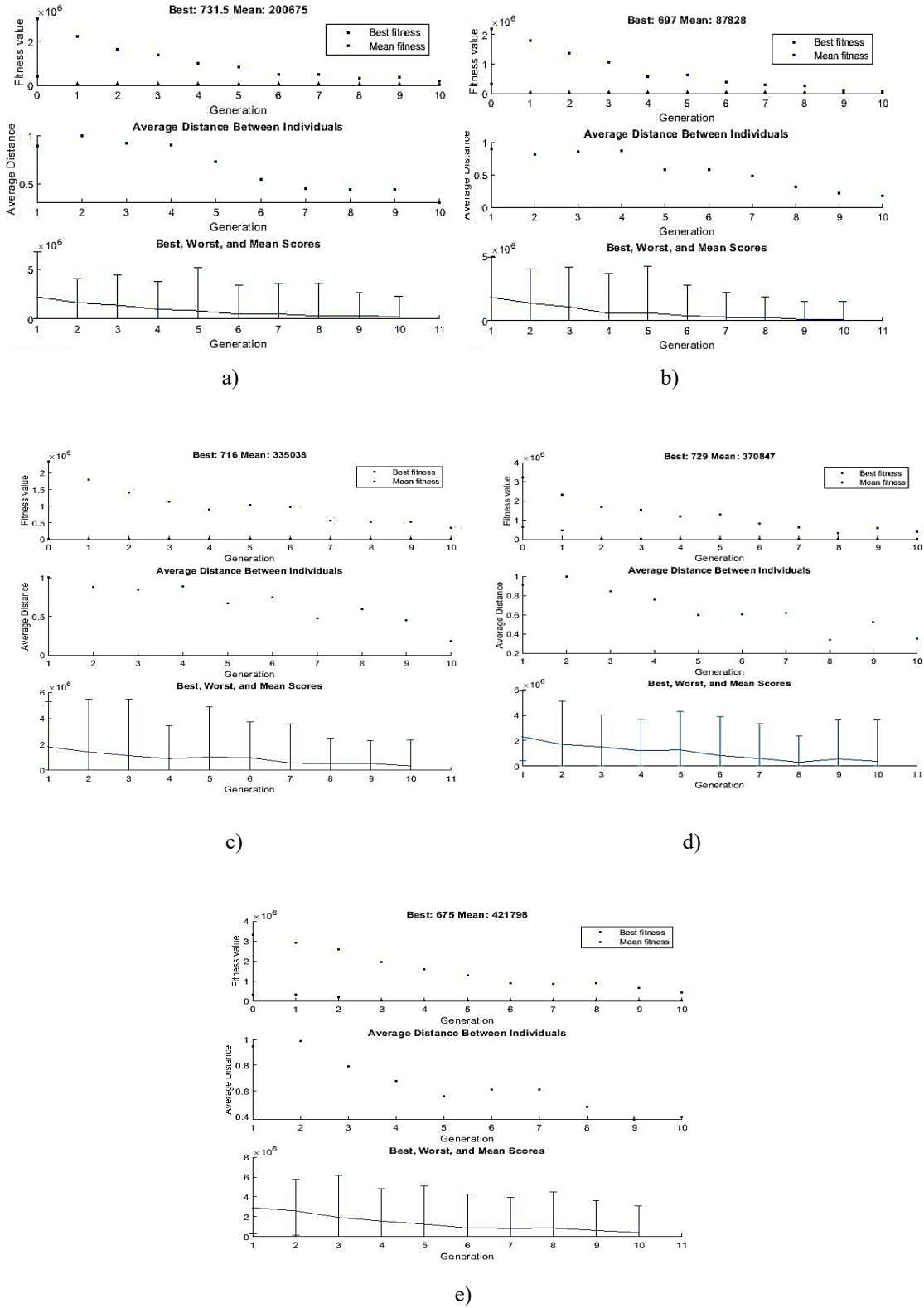


Figure 7. Optimization process in GA-based path planning: a) For Map 1, b) For Map 2, c) For Map 3, d) For Map 4, e) For Map 5

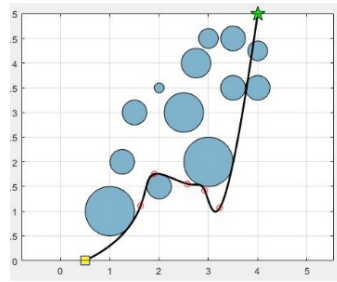


Figure 8. PSO algorithm's obstacle conflict

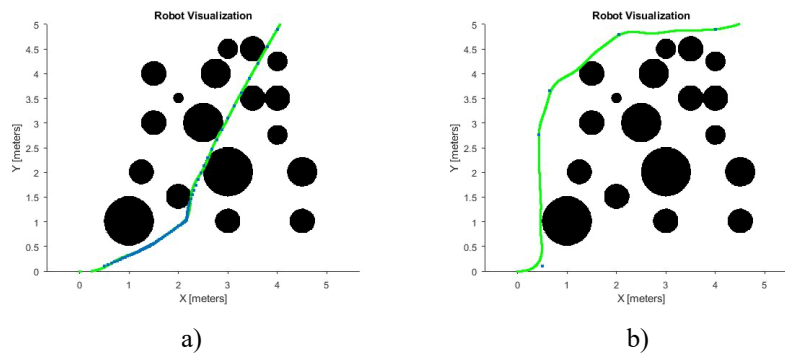


Figure 9. Real time simulation experiment. a) PSO b) GA

Table 1. Comparison of GA and PSO algorithms in object density

	PSO				GA			
	Distance	Time	Curvature	Processing Speed	Distance	Time	Curvature	Processing Speed
1. Case	6.3273	123.2	~3	50.7748	7.3150	144.8	2	34.6343
2. Case	6.0448	109.1	~1	57.3396	6.9700	132.1	3	25.7731
3. Case	7.2769	130.2	~2	58.4811	7.1600	139.3	3	27.6668
4. Case	6.8704	127.1	~3	67.9069	7.2900	140.1	2	27.2910
5. Case	6.2153	113.2	1	69.4000	6.7500	132.6	3	24.8320

Path plans were obtained from GA and PSO algorithms for the environment consisting of 5 different maps. PSO algorithm has found soft paths. GA found a faster solution compared to the PSO algorithm. However, as the environment got more complex, the search times of both algorithms increased. PSO struggled to produce solutions in complex environments. Even in a very complex environment, in cases where the number of iterations was not enough, it also produced solutions by ignoring the obstacles as in Figure 8. However, GA continued to seek conclusions at high transaction times. Although GA spent a lot of time in an environment considered to be unsolvable, it was able to offer limited solutions. The PSO algorithm generated different road routes each time. However, GA produced the same or very close paths for the same environment. It can be seen in Table 1 that GA searches for safer roads and causes longer distances. As seen in Figure 8, it was observed that in real-time applications, path smoothing algorithms are required for GA, curved paths increase deviations from the road and the distance increases even more due to oscillations. Since the processing times of the algorithms are very high, they cannot respond to instant changes in real-time applications. Therefore, they are generally used in offline static environments. In online road planning, they are used as a hybrid in optimization according to advanced road information.

4. Results

In this paper, the performance of meta-heuristic PSO and GA algorithms in object density in static environments was analysed. As a result of the analysis, they produced very successful results offline in static environments. Optimization successes revealed the prevalence of hybrid usage with other algorithms. Choosing the appropriate algorithm for the density of objects in the environment ensures more successful task and motion planning. With the selection of sensors suitable for the nature of the environment, less processing load, energy consumption and unnecessary movements are avoided. In the next study, it is aimed to measure the performance of GA and PSO algorithms in different object density in dynamic environments

References

- [1] Ma, J., Liu, Y., Zang, S., Wang, L. Robot path planning based on genetic algorithm fused with continuous bezier optimization. *Computational intelligence and neuroscience*, 2020.
- [2] Pellegrinelli, S., Borgia, S., Pedrocchi, N., Villagrossi, E., Bianchi, G., Tosatti, L. M. Minimization of the energy consumption in motion planning for single-robot tasks. *Procedia Cirp*, 2015; 29: 354-359.
- [3] Gul, F., Rahiman, W., Alhady, S. S. N. A comprehensive study for robot navigation techniques. *Cogent Engineering*, 2019; 6(1): 1632046.
- [4] Zakaria, M. A., Zamzuri, H., Mamat, R., Mazlan, S. A. A path tracking algorithm using future prediction control with spike detection for an autonomous vehicle robot. *International Journal of Advanced Robotic Systems*, 2013;10(8): 309.
- [5] Zhang, H. Y., Lin, W. M., Chen, A. X. Path planning for the mobile robot: A review. *Symmetry*, 2018; 10(10): 450.
- [6] Gürgöze, G., Türkoğlu, İ. Algorithms used in robot systems. *Turkish Journal of Nature and Science*, 2019; 8(1): 17-31.
- [7] Ibraheem, I. K., & Ajeil, F. H. Multi-objective path planning of an autonomous mobile robot in static and dynamic environments using a hybrid PSO-MFB optimisation algorithm. 2018; arXiv preprint arXiv:1805.00224.
- [8] Hassani, I., Maalej, I., Rekik, C. Robot path planning with avoiding obstacles in known environment using free segments and turning points algorithm. *Mathematical Problems in Engineering*, 2018; Article ID 2163278, DOI: <https://doi.org/10.1155/2018/2163278>.
- [9] Li, W., Wang, G. Y. (2010, October). Application of improved PSO in mobile robotic path planning. In 2010 International Conference on Intelligent Computing and Integrated Systems, 2010; pp. 45-48. IEEE.
- [10] Davoodi, M., Panahi, F., Mohades, A., Hashemi, S. N. Clear and smooth path planning. *Applied Soft Computing*, 2015; 32: 568-579.
- [11] Das, P. K., Behera, H. S., Panigrahi, B. K. A hybridization of an improved particle swarm optimization and gravitational search algorithm for multi-robot path planning. *Swarm and Evolutionary Computation*, 2016; 28: 14-28.
- [12] Purcaru, C., Precup, R. E., Iercan, D., Fedorovici, L. O., Petriu, E. M., Voisan, E. I. Multi-robot GSA-and PSO-based optimal path planning in static environments. In *9th International Workshop on Robot Motion and Control*, 2013; pp. 197-202. IEEE.
- [13] Roberge, V., Tarbouchi, M., Labonté, G. Comparison of parallel genetic algorithm and particle swarm optimization for real-time UAV path planning. *IEEE Transactions on industrial informatics*, 2012; 9(1): 132-141.
- [14] Shivgan, R., Dong, Z. Energy-Efficient Drone coverage path planning using Genetic Algorithm. In 2020 IEEE 21st International Conference on High Performance Switching and Routing (HPSR), 2020; pp.1-6. IEEE.
- [15] Tao, W., Yan, S., Pan, F., Li, G. AUV Path planning based on improved Genetic Algorithm. In 2020 5th International Conference on Automation, Control and Robotics Engineering (CACRE) 2020; pp. 195-199. IEEE.
- [16] Abhishek, B., Ranjit, S., Shankar, T., Eappen, G., Sivasankar, P., Rajesh, A. Hybrid PSO-HSA and PSO-GA algorithm for 3D path planning in autonomous UAVs. *SN Applied Sciences*, 2020; 2(11): 1-16.
- [17] Yan, Z., Li, J., Wu, Y., & Zhang, G. A real-time path planning algorithm for AUV in unknown underwater environment based on combining PSO and waypoint guidance. *Sensors*, 2019; 19(1): 20.
- [18] Shakiba, R., Najafipour, M., Salehi, M. E. An improved PSO-based path planning algorithm for humanoid soccer playing robots. In 2013 3rd Joint Conference of AI & Robotics and 5th RoboCup Iran Open International Symposium 2013; pp. 1-6. IEEE.
- [19] Zhang, H., Zhang, Y., Yang, T. A survey of energy-efficient motion planning for wheeled mobile robots. *Industrial Robot: the international journal of robotics research and application*, 2020.
- [20] Liu, F., He, H., Li, Z., Guan, Z. H., Wang, H. O. Improved potential field method path planning based on genetic algorithm. In 2020 39th Chinese Control Conference (CCC) 2020; pp. 3725-3729. IEEE.
- [21] Châari, I., Koubaa, A., Bennaceur, H., Trigui, S., Al-Shalfan, K. Smart PATH: A hybrid ACO-GA algorithm for robot path planning. In 2012 IEEE congress on evolutionary computation 2012; pp. 1-8. IEEE.
- [22] Masehian, E., Sedighzadeh, D. Multi-objective robot motion planning using a particle swarm optimization model. *Journal of Zhejiang University SCIENCE C*, 2010; 11(8): 607-619.
- [23] Hafez, A. T., & Kamel, M. A. Cooperative task assignment and trajectory planning of unmanned systems via HFLC and PSO. *Unmanned Systems*, 2019; 7(02): 65-81.
- [24] Olabode, A. O., Abdulkareem, B. Q., Ajao, T. A. Comparative analysis of some selected metaheuristic algorithms for solving intelligent path planning problem of mobile agents.

- [25] Gürgüze, G., Türkoğlu, İ. Position control of differential mobile robot with known dynamic model with Pure Pursuit Algorithm. International Congress on Human Computer Interaction, Optimization and Robotic Applications (HORA), 2019; 4(5): 199-202,
- [26] Hirpo, B. D., Zhongmin, W. Design and control for differential drive mobile robot. International Journal of Engineering Research & Technology (IJERT), 2017; 6(10):327-334.

Effect of Nitrogen Source on Growth and Protein and Lipid Amounts of a Freshwater Microalga *Scenedesmus acutus*

Ahmet ÇOBAN¹, Gökçe KENDİRLİOĞLU ŞİMŞEK², A. Kadri ÇETİN^{*3}

¹Ministry of Agriculture and Forestry, Fisheries Research Institute, Elazığ, Turkey

²Faculty of Science, Department of Biology, Firat University, Elazığ, Turkey

¹ahmetcoban729@gmail.com, ²gkendirlioglu58@gmail.com, ^{3*}kcetin@firat.edu.tr

(Geliş/Received: 26/02/2021;

Kabul/Accepted: 22/04/2021)

Abstract: *Scenedesmus acutus* (*S. acutus*) is a green freshwater microalga. This study investigated the impact of nitrogen sources on growth, protein and lipid amounts of *S. acutus*. The reaction of *S. acutus* to different N sources was tested in liquid nutrients by adding KNO₃, CaNO₃, NaNO₃, NH₄NO₃, and (NH₄)₂SO₄, instead of nitrogen sources, separately in a standard medium. KNO₃ and CaNO₃ resulted in the highest growth. The amount of protein was highest in KNO₃ and NH₄NO₃ cultures, while the amount of lipid was highest in KNO₃ and NaNO₃ cultures.

Key words: Nitrogen sources, *Scenedesmus acutus*.

Azot Kaynaklarının *Scenedesmus acutus*' un Gelişim, Protein ve Lipit Miktarına Etkisi

Öz: Bu çalışma, yeşil mikroalg *Scenedesmus acutus*' un gelişim, protein ve lipit miktarı üzerinde azot kaynağının etkilerini incelemeyi amaçlamıştır. Bu amaçla *Scenedesmus acutus*' un farklı azot kaynaklarına tepkileri standart besiyeri ortamındaki azot kaynakları yerine sadece KNO₃, CaNO₃, NaNO₃, NH₄NO₃ ve (NH₄)₂SO₄, ayrı ayrı ilave edilerek sıvı besi ortamlarında test edildi. Test edilen beş farklı azot kaynağı arasında KNO₃ ve CaNO₃ en yüksek gelişimi sağladı. Protein miktarı azot kaynağı olarak KNO₃ ve NH₄NO₃ kullanılan kültürlerde maksimum olurken lipit miktarı KNO₃ ve NaNO₃ kullanılan kültürlerde en yüksek miktarda tespit edildi.

Anahtar kelimeler: Azot kaynağı, *Scenedesmus acutus*.

1. Introduction

Microalgae have long been used for different purposes. However, natural, renewable, and eco-friendly products have become more prevalent in recent years. Microalgae are once again the center of attention because they are a source of valuable compounds [1-3]. When we think about overcoming protein deficit, the first source that comes to mind is algae. Microalgae have an important place in human and animal nutrition as they contain proteins, carbohydrates, amino acids, lipids, vitamins, and pigments [4-6]. Microalgal biomass cultivation is affected by physicochemical factors, such as nutrients, temperature, light source, pH, and salinity. However, production costs are the greatest problem in the cultivation of microalgae. Nutrients and light should be used efficiently in microalgae cultures to produce large quantities of low-cost biomass. Nitrogen, in particular, is a critical nutrient for growth. It is a macro element essential for the synthesis of nucleic acids, amino acids, proteins, and pigments, and thus, cellular growth. The cell growth rate and biochemical composition of microalgae depend on nitrogen concentration in a culture medium. Research shows that nitrogen starvation in a culture medium slows down the cell growth rate of microalgae and reduces protein synthesis by increasing lipid or carbohydrate content [7]. Many microalgae species use inorganic nitrogen sources (nitrate, nitrite, and ammonium) and synthesize cellular organic nitrogen compounds. Some microalgae (*Dunaliella tertiolecta* and *Botryococcus braunii*) prefer nitrate [8-9], while some *Chlorella* species prefer ammonium for growth [10-11]. Nitrogen source affects the biochemical content of microalgae. For example, *Dunaliella salina* has twice as much protein in nitrate media as in ammonium media [12], while *Chlorella sorokiniana* has twice as much lipid in ammonium media as in nitrate and urea media [13]. Different algae species need different nitrogen sources for growth. Not only growth but also biochemical content depend on the nitrogen source and amount. Therefore, we need to compare nitrogen sources and choose the best one for each type of microalgae. We need to identify suitable culture media to increase the efficiency of target products (lipid, protein, carbohydrate, etc.) and reduce culture costs.

*Corresponding author: kcetin@firat.edu.tr. ORCID number of authors: ¹0000-0001-1931-0469, ²0000-0001-8896-2893, ³0000-0002-8687-2912

This study investigated the impact of nitrogen sources on growth and protein and lipid amounts of *Scenedesmus acutus* (*S. acutus*).

2. Material and Method

2.1. Medium and Culture Condition

S. acutus was sampled from the *Keban* Dam Lake, Turkey, and isolated at the algal biotechnology laboratory of Firat University. The samples were cultured in a Jaworski's medium with 80 mg NaNO₃, 20 mg Ca(NO₃)₂·4H₂O, 36 mg Na₂HPO₄·12H₂O, 12.4 mg KH₂PO₄, 50 mg MgSO₄·7H₂O, 2.25 mg EDTAFeNa, 15.9 mg NaHCO₃, 2.25 mg EDTANA₂, 2480 µg H₃BO₃, 1390 µg MnCl₂·4H₂O, 1000 µg (NH₄)₆Mo₇·4H₂O, 40 µg biotin, 40 µg cyanocobalamin (B12), and 40 µg thiamin (B1). The culture medium was sterilized for 15 minutes at 121 °C and an atmospheric pressure of 1. The culture medium, called "standard medium," was used as control cultures. Liquid nutrient media with equal final concentrations were generated by adding only KNO₃, CaNO₃, NaNO₃, NH₄NO₃, or (NH₄)₂SO₄, instead of nitrogen sources, separately in the standard medium to determine the reaction of *S. acutus* to different N sources.

The samples were inoculated into 250-mL flasks with a 100-mL standard medium. The Erlenmeyer flasks were left to grow at a light intensity of 55 µmol photon m⁻²sec⁻¹ at 23±1 °C in a conditioning chamber. The cultures were sampled (10 mL) after they reached a certain density. The standard medium was used for control cultures. Modified media were used for experimental cultures. The modified media were media with CaNO₃, NaNO₃, NH₄NO₃, and (NH₄)₂SO₄ added into the standard medium with all nitrogen sources removed. The samples were inoculated into the modified media. The control and experimental cultures were allowed to grow for ten days in a climate cabinet at 23 ±1 °C under a 16h light/8h dark regime and 55 µmol photon m⁻²sec⁻¹ light intensity. The Erlenmeyer flasks were shaken three times a day.

2.2. Growth, Lipid and Protein Content

Growth was calculated at the optical density (OD) of 680 nm using a visible density spectrophotometer. Measurements were performed three times.

Lipid content was determined gravimetrically using a solution of chloroform and methanol mixture [14]. A mixture of 40 mL methanol and 80 mL chloroform was added onto a 0.2 g sample, and 20 mL of 0.4% CaCl₂ was added to the mixture, which was then filtered through filter paper and left in the dark overnight. The following day, a fraction of methanol and water was separated using a separatory funnel, and the chloroform was evaporated in a 60 °C water bath. The remaining part was kept in an oven at 90 °C for one hour to allow the chloroform to evaporate completely and then was weighed.

Total protein content was measured using the Lowry method [15]. 0.1-mL DOC solution was added in a 1-mL sample, which was then kept at room temperature for ten minutes. Afterward, 0.1-mL TCA was added onto the sample, which was then centrifuged at 7500 rpm for ten minutes. Following the removal of the supernatant, 1-mL Lowry solution was added to the precipitate, which was then kept at room temperature for 20 minutes. Later on, 1-mL folin reagent was added to the sample and kept for 30 minutes. Lastly, absorbance was plotted at 750 nm to generate a standard curve, which was used to evaluate the results.

3. Results and Discussion

Nitrogen is essential for synthesizing amino acids, proteins, nucleic acids, coenzymes, and chlorophylls, which are vital to all living things. Nitrogen deficiency significantly affects the growth of microalgae as well as all living things [6]. Nitrogen source is important for protein and lipid accumulation during microalgal growth. This study looked into the impact of different nitrogen sources on growth and protein and lipid amounts. Standard media were used as control cultures, and modified standard media were used as test cultures to determine which nitrogen source was effective in the growth of *S. acutus*. Figure 1 shows the trend of change in OD during cultivation. OD₆₈₀ was 0.040 in the standard and modified liquid cultures on the day of inoculation. From the first day after inoculation, the increase in cell density in both standard and modified cultures led to an increase in OD, which reached a maximum on day six. The control, KNO₃, NaNO₃, NH₄NO₃, (NH₄)₂SO₄, and CaNO₃ cultures had

an OD of 0.123, 0.358, 0.228, 0.315, 0.284, and 0.344, respectively. The optical density decreased after day six (Fig.1). Weak and short-term microalgal growth due to lack or insufficiency of nitrogen is observed in many algae [16]. Nitrate-N is a more common nitrogen source than ammonium nitrogen for microalgae [17]. However, some microalgae (e.g., *Isochrysis galbana*) can use ammonium-N as a nitrogen source and grow rapidly [18-19]. Some microalgae grow faster in ammonium media than in nitrate media. We found that the cells in all cultures continued to grow until day six but that the greatest growth took place in KNO_3 and CaNO_3 media, indicating that *S. acutus* prefers $\text{NO}_3\text{-N}$ for growth.

Proteins are large multi-atom organic molecules composed of carbon, hydrogen, oxygen, and nitrogen, as well as sulfur and phosphorus. Research shows that microalgal proteins are promising alternative sources of protein [4-5]. We collected samples from liquid media for ten days to determine the effect of nitrogen source on the protein amount of *S. acutus*. Figure 2 shows the changes in the protein amount of *S. acutus*. On the day of inoculation, all cultures had a protein content of 24.35 $\mu\text{g/ml}$, which increased until day six. The control, KNO_3 , NaNO_3 , NH_4NO_3 , $(\text{NH}_4)_2\text{SO}_4$, and CaNO_3 cultures had a protein content of 154.78, 275.65, 225.55, 260.40, 200.45, and 242.05 $\mu\text{g/ml}$, respectively, on day six, after which the protein content decreased.

We monitored the variation in the amount of lipid of *S. acutus* based on nitrogen sources for ten days. Figure 3 shows on the day of inoculation, all cultures had a lipid content of 9.20%, which increased until day six after inoculation. On day six, the control, KNO_3 , NaNO_3 , NH_4NO_3 , $(\text{NH}_4)_2\text{SO}_4$, and CaNO_3 cultures had protein contents of 58.35%, 78.64%, 68.15%, 45.65%, 40.35%, and 52.35% $\mu\text{g/ml}$, respectively.

Different strategies for improving microalgal growth and biochemical composition have become popular in recent years. Some of those strategies focus on increasing growth rates and protein, lipid, and pigment contents by altering environmental conditions [2, 20-25]. The primary objective of those strategies is to select the right nitrogen source and provide efficient and cost-effective microalgae cultivation for high-value products. Many microalgae can utilize different forms of nitrogen by following the pathways leading to the assimilation of nitrogen into amino acids [26]. For example, NH_4NO_3 cultures increase the growth rate and lipid content of *Scenedesmus abundans* and *Chlorella ellipsoidea* [27], while nitrate cultures are better for the growth of *Tetraselmis* cells, as they result in twice as much biomass as ammonium cultures [28].

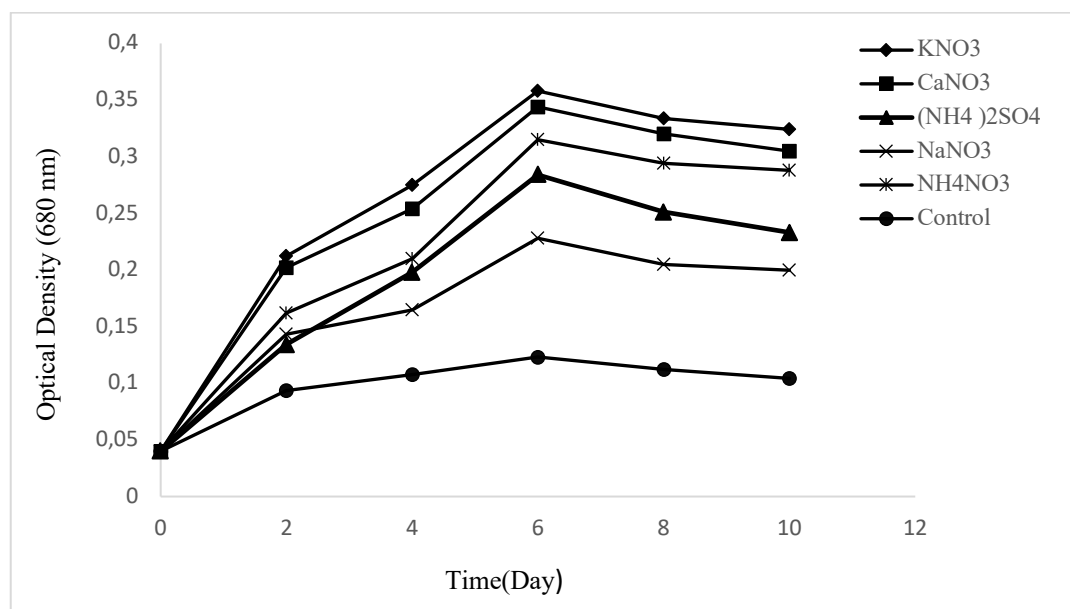


Figure 1. Effects of different nitrogen sources on growth of *Scenedesmus acutus*.

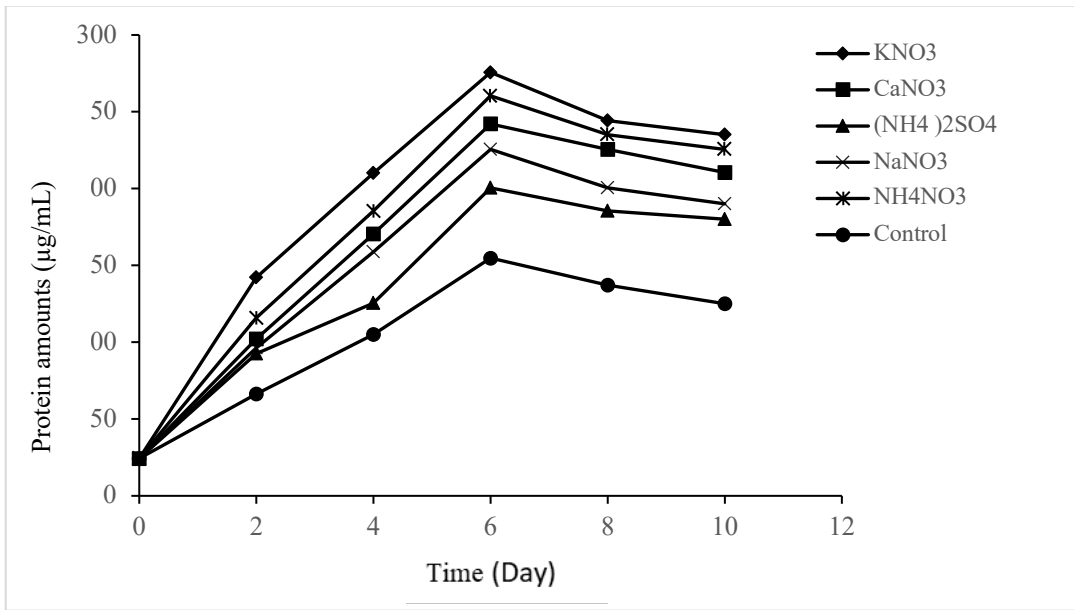


Figure 2. Effects of different nitrogen sources on protein amounts of *Scenedesmus acutus*.

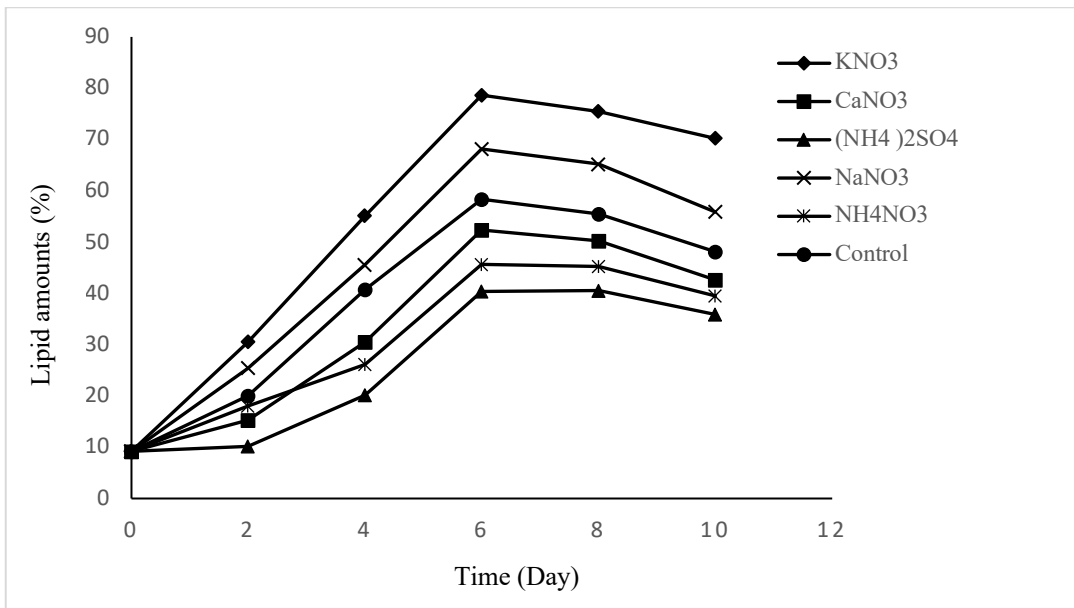


Figure 3. Effects of different nitrogen sources on lipid amounts of *Scenedesmus acutus*.

4. Conclusion

The results show that microalgae prefer different sources of nitrogen. The highest growth was observed in KNO₃ and CaNO₃ cultures. The protein content was highest in KNO₃ and NH₄NO₃ cultures, while the lipid content was the highest in KNO₃ and NaNO₃ cultures. If we are interested in increasing biomass in *S. acutus*, we should use KNO₃ or CaNO₃ cultures as nitrogen sources. We should use KNO₃ or NH₄NO₃ cultures to obtain high amounts of protein, and we should use KNO₃ or NaNO₃ cultures to obtain high amounts of lipid. However, more research is warranted to optimize the culture parameters necessary for high cultivation rates of *S. acutus*. We think that this study will pave the way for further research.

Acknowledgements

This research was funded by Firat University (Project No: FUBAB, FF.18.01). We would like to thank FUBAB for its financial support.

References

- [1] Singh R, Parihar P, Singh M, Bajguz A, Kumar J, Singh S, Singh VP, Prasad SM. Uncovering potential applications of cyanobacteria and algal metabolites in biology, agriculture and medicine: current status and future prospects. *Front Microbiol* 2017; 8:515.
- [2] Sharma J, Kumar SS, Sharma P, Gupta S, Malyan SK, Bishnoi NR. Effect of different nitrogen sources on growth of algal consortia. *Annals of Agri-Bio Research*. 2017; 22(2): 150-153.
- [3] Vasileva IA, Ivanova JG, Gigova LG. Selection of nitrogen source affect the growth and metabolic enzyme activities of *Chlorella vulgaris* (Beijerinck) strain R-06/2 (Chlorophyta). *Arch Biol Sci*. 2020; 72(2): 291-300.
- [4] Becker EW. Micro-algae as a source of protein. *Biotechnology Advances*. 2007; 25:207-210.
- [5] Barka A, Blecker C. Microalgae as a potential source of single-cell proteins. A review. *Biotechnol Agron Soc Environ*. 2016; 20(3): 427-436.
- [6] Vasileva I, Marinova G, Gigova L. Effect of nitrogen source on the growth and biochemical composition of a new Bulgarian isolate of *Scenedesmus* sp. *J BioSci. Biotechnol*, 2015; SE/ONLINE: 125-129.
- [7] Agirman N, Cetin AK. Effect of nitrogen limitation on growth, total lipid accumulation and protein amount in *Scenedesmus acutus* as biofuel reactor candidate. *Natural Science and Discovery*. 2017; 3(3): 33-38.
- [8] Chen M, Tang H, Ma H, Holland TC, Ng KYS, Salley SO. Effect of nutrients on growth and lipid accumulation in the green algae *Dunaliella tertiolecta*. *Bioresource Technology*, 2011; 102:1649-1655.
- [9] Ruangsomboon S. Effect of different media and nitrogen sources and levels on growth and lipid of green microalga *Botryococcus braunii* KMITL and its biodiesel properties based on fatty acid composition. *Bioresource Technology*. 2015; 191: 377-384.
- [10] Li T, Zheng Y, Yu L, Chen S. High productivity cultivation of a heat-resistant microalga *Chlorella sorokinina* for biofuel production. *Bioresource Technology*. 2013;13:60-67.
- [11] Muthuraj M, Kumar V, Palabhanvi B, Das D. Evaluation of indigenous microalgal isolate *Chlorella* sp. FC IITC as a cell factory for biodiesel production and scale up in outdoor conditions. *J. Ind. Microbiol. Biotechnol*. 2014; 41: 499-511.
- [12] Norici A, Dalsass A, Giordano M. Role of phosphoenolpyruvate carboxylase in anaplerosis in the green microalga *Dunaliella salina* cultured under different nitrogen regimes. *Physiol. Plant*. 2002;116: 186-191.
- [13] Wan MX, Wang RM, Xia JL, Rosenberg JN, Nie ZY, Kobayashi N, Oyler GA, Betenbaugh MJ. Physiological evaluation of a new *Chlorella sorokiniana* isolated for its biomass production and lipid accumulation in photoautotrophic and heterotrophic cultures. *Biotech. Bioeng*. 2012; 109:1958-1964.
- [14] Blight EG, Dyer WJ. A rapid method for total lipid extraction and purification. *Can J Biochem Physiol*. 1959;37:911-917.
- [15] Lowry OH, Rosebrough NJ, Farr AL, Randall RJ. Protein measurement with the folin phenol reagent. *The J Biol Chem*. 1951;193:265-275.
- [16] Gigova LG, Ivanova NJ. Microalgae respond differently to nitrogen availability during culturing. *J. Biosci*. 2015;40(2): 365-374.
- [17] Yongmanitchai W, Ward OP. Growth of and omega-3 fatty acid production by *Phaeodactylum tricoratum* under different culture conditions. *Appl Environ Microbiol*. 1991; 57(2): 419-425.
- [18] Hersh CM, Grumtain WG. Atrazine tolerance of algae isolated from two agricultural streams. *Environ Toxicol Chem*. 1989; 8: 327-332.
- [19] Molina GE, Sanchez PJA. EPA from *Isochrysis galbana*. Growth conditions and productivity. *Process Biochem*. 1992; 27: 299-305.
- [20] Harwati TU, Willke T, Vorlop KD. Characterization of the lipid accumulation in a tropical freshwater microalga *Chlorococcum* sp. *Bioresource Technology* 2012; 121, 54-60.
- [21] Xu N, Zhang X, Fan X, Han L, Zeng C. Effect of nitrogen source and concentration on growth rate and fatty acid composition of *Ellipsoidion* sp. (Eustigmatophyta). *Journal of Applied Phycology* 2001; 13: 463-469.
- [22] Sharma T, Gour RS, Kant A, Chauhan RS. Lipid content in *Scenedesmus* species correlates with multiple genes of fatty acid and triacylglycerol biosynthetic pathways. *Algal Research* 2015;12, 341-349.
- [23] Kendirlioglu G, Cetin AK. Effect of nitrogen sources on growth, protein, total lipid amount and pigment content in *Chlorella vulgaris*. *Fresenius Environmental Bulletin* 2017; 28, 4A:3065-3072.
- [24] Kendirlioglu Simsek G, Cetin AK. Effect of different wavelengths of light on growth, pigment content and protein amount of *Chlorella vulgaris*. *Fresenius Environmental Bulletin* 2019; 26, 12A:7974-7980.
- [25] Kumar DA, Gopal T, Harinath K, Sibi G. Responses in growth and lipid productivity of *Chlorella vulgaris* to different nitrogen sources. *SOJ Microbiol InfectDis*. 2017; 5(2): 1-6.
- [26] Podevin M, De Francisci D, Holdt SL, Angelidaki I. Effect of nitrogen source and acclimatization on specific growth rates of microalgae determined by a high-throughput in vivo microplate autofluorescence method. *J Appl Phycol* 2015;27: 1415-1423.

- [27] Gonzalez-Garcinuno A, Tabernero A, Sanchez-Alvarez JM, Martin del Valle. Effect of nitrogen source on growth and lipid accumulation in *Scenedesmus abundans* and *Chlorella ellipsoidea*. *Bioresource Technology* 2014;173: 334-341.
- [28] Kim G, Mujtaba G, Lee K. Effects of nitrogen sources on cell growth and biochemical composition of marine chlorophyte *Tetraselmis sp.* for lipid production. *Algae* 2016; 31(3): 257-266.

Special Curves According to Extended Darboux Frame Field in \mathbb{E}_1^4

Esra ERDEM^{1*}, Mihriban ALYAMAÇ KÜLAHÇI², Münevver YILDIRIM YILMAZ³

Department of Maths, Faculty of Science, Firat University, Elazığ, Turkey

¹ esra.6666.23@gmail.com, ² mihribankulahci@gmail.com, ³ myildirim@firat.edu.tr

(Geliş/Received: 23/04/2021;

Kabul/Accepted: 26/06/2021)

Abstract: In this study, the involute of a curve is investigated in Minkowski space-time by using extended Darboux frame field and curves of the AW (k) type are studied in Minkowski space-time.

Key words: Involute curve, Minkowski space-time, Extended Darboux frame field.

\mathbb{E}_1^4 de Genişletilmiş Darboux Çatı Alanına Göre Özel Eğriler

Öz: Bu çalışma da Genişletilmiş Darboux çatı alanı kullanılarak Minkowski uzayında bir eğrinin involütü ve AW(k) tipli eğriler incelenmiştir.

Anahtar kelimeler: İnvölüt eğri, Minkowski uzayı, Genişletilmiş Darboux çatı alanı.

1. Introduction

In differential geometry, there are many significant results and properties of curves. Scientists follow studies about the curves. In the light of existing studies authors introduce new works by using frame fields. The Darboux frame field is known as one of the frame field of the differential geometry. Many mathematicians have presented studies using the Darboux frame field. One of them is the study of Şahin and Dirişen. Şahin and Dirişen gave position vectors of curves with respect to Darboux frame in the Galilean space G^3 [1]. In [2], Altunkaya and Aksoyak's obtained curves of constant breadth according to Darboux frame. In [3], Dülül et al. introduced extended Darboux frame field.

Involutes of a curve is another attractive research subject among geometers. The idea of a string involute is due to C. Huygens (1658), who is also known for his work in optics. He discovered involutes trying to build a more accurate clock [4]. After, a characterization of space-like involute-evolute curve couple in Minkowski space-time were given in [5]. T. Soyfidan and M. A. Güngör studied a quaternionic curve Euclidean 4-space \mathbb{E}^4 and gave the quaternionic involute-evolute curves for quaternionic curve [6]. Another is As and Sarioğlugil study's. They obtained the Bishop curvatures of involute-evolute curve couple in \mathbb{E}^3 [7].

Many studies related to curves of AW(k)-type have been done by several authors and many interesting results on AW(k)-type curves have been obtained by many mathematicians (see [8-11]). In [12-13] the authors obtained some characterizations related to these curves in \mathbb{E}^m . Kılıç and Arslan considered curves and surfaces of AW(k)-type and they also gave related examples of curves and surfaces sufficient AW(k)-type conditions [14].

In this paper, involute curve is given in Minkowski space-time \mathbb{E}_1^4 by using extended Darboux frame field. In addition, considering extended Darboux frame field, AW(k)-type curves are studied in \mathbb{E}_1^4 .

2. Preliminaries

The Minkowski space-time \mathbb{E}_1^4 is a Euclidean space provided with the indefinite flat metric given by

$$g = -dx_1^2 + dx_2^2 + dx_3^2 + dx_4^2$$

where (x_1, x_2, x_3, x_4) is a rectangular coordinate system of \mathbb{E}_1^4 . Recall that an arbitrary vector $v \in \mathbb{E}_1^4 - \{0\}$ can be spacelike, timelike or null (lightlike vector), if holds $g\langle v, v \rangle > 0$, $g\langle v, v \rangle < 0$ or $g\langle v, v \rangle = 0$ respectively.

* Corresponding author: esra.6666.23@gmail.com. ORCID Number of authors: ¹ 0000-0001-8656-0196, ² 0000-0002-8621-5779, ³ 0000-0003-1278-3981

Especially, the vector $\nu = 0$ is spacelike. Besides an arbitrary curve $\alpha = \alpha(s)$ in \mathbb{E}_1^4 can locally be spacelike, timelike or null (lightlike) if all of its velocity vectors $\alpha'(s)$ are spacelike, timelike or null respectively. The norm of a vector ν is given by $\|\nu\| = \sqrt{|g\langle\nu,\nu\rangle|}$. Thus $\bar{\nu}$ is a unit vector if $g\langle\nu,\nu\rangle = \pm 1$. For an arbitrary curve $\alpha(s)$ in \mathbb{E}_1^4 the curve is named a spacelike, a timelike and a null (lightlike) curve, if all of its velocity vectors $\alpha'(s)$ are spacelike, timelike, and null (lightlike), respectively [15].

A hypersurface in the Minkowski space-time \mathbb{E}_1^4 is called a spacelike or a timelike hypersurface if the induced metric on the hypersurface is a positive definite Riemannian metric or a Lorentzian metric, respectively. The normal vector on the spacelike or the timelike hypersurface is, respectively, a timelike or a spacelike vector. Let M be an orientable non-null hypersurface

$$\alpha : I \subset \mathbb{R} \rightarrow M$$

be a unit speed non-null curve in \mathbb{E}_1^4 . Let's indicate by $\{t, n, b_1, b_2\}$ the acting Frenet frame along the curve $\alpha(s)$ in the space \mathbb{E}_1^4 . Then $\{t, n, b_1, b_2\}$ are, respectively, the unit tangent, the principal normal, the first binormal and the second binormal vector fields. If k_1, k_2, k_3 are named the curvature functions of the unit speed non-null curve α , then for the non-null frame vectors, we obtain Frenet equations as follows:

$$\begin{aligned} t' &= \varepsilon_n k_1 n \\ n' &= -\varepsilon_t k_1 t + \varepsilon_{b_1} k_2 b_1 \\ b_1' &= -\varepsilon_n k_2 n - \varepsilon_t \varepsilon_n \varepsilon_{b_1} k_3 b_2 \\ b_2' &= -\varepsilon_{b_1} k_3 b_1 \end{aligned}$$

where $\varepsilon_t = \langle t, t \rangle$, $\varepsilon_n = \langle n, n \rangle$, $\varepsilon_{b_1} = \langle b_1, b_1 \rangle$, $\varepsilon_{b_2} = \langle b_2, b_2 \rangle$ whereby $\varepsilon_t, \varepsilon_n, \varepsilon_{b_1}, \varepsilon_{b_2} \in \{-1, 1\}$, $1 \leq i \leq 4$ and $\varepsilon_t \varepsilon_n \varepsilon_{b_1} \varepsilon_{b_2} = -1$, [16].

3. Extended Darboux Frame Field in \mathbb{E}_1^4

Let M be an orientable non-null hypersurface, N be its non-null unit normal vector field in \mathbb{E}_1^4 and $x(s)$ be a non-null Frenet curve parametrized by arc-length parameter s lying on M . If the non-null unit tangent vector field of x is indicated by T , and the non-null unit normal vector field of M restricted to x is indicated by N , we attain

$$x'(s) = T(s) \tag{1}$$

and

$$N(x(s)) = N(s) \tag{2}$$

[17].

As in Euclidean 4- space \mathbb{E}^4 [3], the extended Darboux frame can be construct in two different cases in Minkowski space-time \mathbb{E}_1^4 with respect to whether the set $\{N, T, x''\}$ is linearly independent or linearly dependent.

Let us show the ED-frame field is first kind and the second kind if the set $\{N, T, x''\}$ is linearly independent and linearly dependent, respectively, [17].

Now, let us construct the ED-frame fields for the non-null Frenet curve α in \mathbb{E}_1^4 . As explained in [3], using the Gram-Schmidt orthonormalization method, we obtain

$$E = \frac{x''' - \langle x''', N \rangle N - \langle x''', T \rangle T}{\|x''' - \langle x''', N \rangle N - \langle x''', T \rangle T\|} \tag{3}$$

[17]. If we detect

$$-D = N \otimes T \otimes E \tag{4}$$

for both cases, we obtain the orthonormal frame field $\{T, E, D, N\}$ another from Frenet frame field $\{T, n, b_1, b_2\}$ along the curve x . According to the orthonormal frame $\{T, E, D, N\}$, the vector fields $\{T', E', D', N'\}$ have the following decompositions:

$$\begin{aligned} T' &= \varepsilon_1 \langle T', T \rangle T + \varepsilon_2 \langle T', E \rangle E + \varepsilon_3 \langle T', D \rangle D + \varepsilon_4 \langle T', N \rangle N \\ E' &= \varepsilon_1 \langle E', T \rangle T + \varepsilon_2 \langle E', E \rangle E + \varepsilon_3 \langle E', D \rangle D + \varepsilon_4 \langle E', N \rangle N \\ D' &= \varepsilon_1 \langle D', T \rangle T + \varepsilon_2 \langle D', E \rangle E + \varepsilon_3 \langle D', D \rangle D + \varepsilon_4 \langle D', N \rangle N \\ N' &= \varepsilon_1 \langle N', T \rangle T + \varepsilon_2 \langle N', E \rangle E + \varepsilon_3 \langle N', D \rangle D + \varepsilon_4 \langle N', N \rangle N \end{aligned}$$

where $\varepsilon_1 = \langle T, T \rangle, \varepsilon_2 = \langle E, E \rangle, \varepsilon_3 = \langle D, D \rangle, \varepsilon_4 = \langle N, N \rangle$ whereby $\varepsilon_1, \varepsilon_2, \varepsilon_3, \varepsilon_4 \in \{-1, 1\}$. Moreover, when $\varepsilon_i = -1$, then $\varepsilon_j = 1$ for all $j \neq i, 1 \leq i, j \leq 4$ and $\varepsilon_1 \varepsilon_2 \varepsilon_3 \varepsilon_4 = -1$, [17].

If

$$\langle D', N \rangle = \tau_g^2, \langle T', E \rangle = \kappa_g^1, \langle E', D \rangle = \kappa_g^2, \tag{5}$$

where κ_g^i and τ_g^i are the geodesic curvature and the geodesic torsion of order $i, (i = 1, 2)$ respectively, then the differential equations for ED-frame field is obtained, if

$$\begin{pmatrix} T' \\ E' \\ D' \\ N' \end{pmatrix} = \begin{pmatrix} 0 & 0 & 0 & \varepsilon_4 \kappa_n \\ 0 & 0 & \varepsilon_3 \kappa_g^2 & \varepsilon_4 \tau_g^1 \\ 0 & -\varepsilon_3 \kappa_g^2 & 0 & 0 \\ -\varepsilon_1 \kappa_n & -\varepsilon_2 \tau_g^1 & 0 & 0 \end{pmatrix} \tag{6}$$

[17].

Theorem 3.1: Let $x : I \rightarrow \mathbb{E}_1^4$ be a regular unit speed non-null Frenet curve and any real non-null Frenet curve $\bar{x} : I \rightarrow \mathbb{E}_1^4$ be the involute of x . The Serret-Frenet apparatus of non-null Frenet curve \bar{x} can be formed by apparatus of x .

Proof: Let $\alpha = \alpha(s)$ be a regular unit speed non-null Frenet curve. Without loss of generality, suppose that $\bar{\alpha} = \bar{\alpha}(s)$ is the involute of α . Therefore, we obtain

$$\bar{\alpha}(s) = \alpha(s) + \lambda_1(s)T_x(s) \tag{7}$$

By using Equation (6) and differentiating Equation (7) with respect to s , we get

$$\bar{\alpha}'(s) = [1 + \lambda_1'(s)]T_x(s) + \lambda_1(s)\varepsilon_4\kappa_n N_x(s).$$

Moreover, we have

$$\langle T_x'(s), T_x(s) \rangle = 0, \quad \langle T_x(s), N_x(s) \rangle = 0, \quad \langle T_x(s), T_x(s) \rangle = \varepsilon_1.$$

Thus, we get

$$\begin{aligned} (1 + \lambda_1'(s))\varepsilon_1 &= 0 \\ \lambda_1(s) &= c - s \end{aligned}$$

Hence, we attain

$$\bar{\alpha}'(s) = (c - s)\varepsilon_4\kappa_n N_x(s). \tag{8}$$

$$T_x'(s) = (c - s)\varepsilon_4\kappa_n N_x(s). \tag{9}$$

By using equation Equation (6) and differentiating Equation (8) twice with respect to s , we have

$$\begin{aligned} \bar{\alpha}''(s) &= -[(c - s)\varepsilon_1\varepsilon_4(\kappa_n)^2]T_x(s) - (c - s)\varepsilon_2\varepsilon_4\tau_g^1\kappa_n E_x(s) \\ &\quad + [(c - s)\kappa_n'\varepsilon_4 - \kappa_n\varepsilon_4]N_x(s), \end{aligned} \tag{10}$$

$$\begin{aligned} \bar{x}'''(s) = & \left[2\varepsilon_1\varepsilon_4(\kappa_n)^2 - 3(c-s)\varepsilon_1\varepsilon_4(\kappa_n)\kappa_n' \right] T_x(s) \\ & + \left[\begin{array}{l} 2\varepsilon_2\varepsilon_4\tau_g^1 - (c-s)\varepsilon_2\varepsilon_4(\tau_g^1)' \kappa_n \\ -2(c-s)\varepsilon_2\varepsilon_4\tau_g^1(\kappa_n)' \end{array} \right] E_x(s) \\ & - \left[(c-s)\varepsilon_2\varepsilon_3\varepsilon_4\tau_g^1\kappa_n(\kappa_n)' \right]^2 D_x(s) \\ & + \left[\begin{array}{l} -2\varepsilon_4\kappa_n' + (c-s)\kappa_n''\varepsilon_4 - (c-s)\varepsilon_1(\varepsilon_4)^2(\kappa_n)^3 \\ -(c-s)\varepsilon_2(\varepsilon_4)^2(\kappa_n)(\tau_g^1)^2 \end{array} \right] N_x(s). \end{aligned}$$

Consequently, substituting

$$\bar{x}'''(s) = AT_x(s) + BE_x(s) - CD_x(s) + FN_x(s). \tag{11}$$

then, by using the Equation (2), we obtain

$$\begin{aligned} N_x(s) = & \frac{\left[-(c-s)(\varepsilon_1)(\kappa_n)^2 \right] T_x(s) - \left[(c-s)(\varepsilon_2)(\tau_g^1)(\kappa_n) \right] E_x(s) \\ & + \left[(c-s)(\kappa_n') - (\kappa_n) \right] N_x(s)}{W = \left\| \bar{x}''(s) \right\|}. \end{aligned} \tag{12}$$

From the Equation (11) and Equation (12), we get

$$\begin{aligned} \langle \bar{x}'''(s), N_x(s) \rangle = & -A(c-s)(\varepsilon_1)^2(\kappa_n)^2 - B(c-s)(\varepsilon_2)^2(\tau_g^1)(\kappa_n) \\ & + F \left[(c-s)(\kappa_n') - (\kappa_n) \right] \varepsilon_4. \end{aligned}$$

Consequently, substituting

$$\begin{aligned} P = & -A(c-s)(\varepsilon_1)^2(\kappa_n)^2 - B(c-s)(\varepsilon_2)^2(\tau_g^1)(\kappa_n) \\ & + F \left[(c-s)(\kappa_n') - (\kappa_n) \right] \varepsilon_4. \end{aligned}$$

we obtain

$$\langle \bar{x}'''(s), N_x(s) \rangle N_x(s) = \frac{P}{W} \left[\begin{array}{l} \left[-(c-s)(\varepsilon_1)(\kappa_n)^2 \right] T_x(s) \\ - \left[\begin{array}{l} (c-s)(\varepsilon_2) \\ (\tau_g^1)(\kappa_n) \end{array} \right] E_x(s) \\ + \left[(c-s)(\kappa_n') - (\kappa_n) \right] N_x(s) \end{array} \right]. \tag{13}$$

By using Equation (9) and Equation (11), we have

$$\langle \bar{x}'''(s), T_x(s) \rangle T_x(s) = F(c-s)^2 (\varepsilon_4)^3 (\kappa_n)^2 N_x(s), \quad (14)$$

and if we write the Equations (11),(13) and Equation (14) into Equation (3), we get

$$E_x(s) = \frac{\begin{aligned} & \left[A + \frac{p}{w} \left[(c-s)(\varepsilon_1)(\kappa_n)^2 \right] \right] T_x(s) \\ & \left[B + \frac{p}{w} \left[(c-s)(\varepsilon_2)(\tau_g^1)(\kappa_n) \right] \right] E_x(s) - CD_x(s) \\ & \left[F - \frac{p}{w} \left[(c-s)(\kappa_n') - (\kappa_n) \right] - F(c-s)^2 (\varepsilon_4)^3 (\kappa_n)^2 \right] N_x(s) \end{aligned}}{L = \left\| \bar{x}''' - \langle \bar{x}''', N \rangle N - \langle \bar{x}''', T \rangle T \right\|}. \quad (15)$$

Then, we have

$$E_x'(s) = UT_x(s) + VE_x(s) + YD_x(s) + ZN_x(s). \quad (16)$$

Similarly, using the Equations (4), (9), (12), and Equation (15) and essential arrangements, $D_x(s)$ is obtained as follows that

$$D_x(s) = -\frac{1}{WL} \begin{bmatrix} \left[-(c-s)^2 \varepsilon_2 \varepsilon_4 C(\tau_g^1)(\kappa_n)^2 \right] T_x(s) \\ \left[(c-s)^2 \varepsilon_1 \varepsilon_4 C(\kappa_n)^3 \right] E_x(s) \\ \left[(c-s)^2 \varepsilon_4 (\kappa_n)^2 (\varepsilon_1 B - \varepsilon_2 (\tau_g^1) A) \right] D_x(s) \end{bmatrix}. \quad (17)$$

By using Equation (6) and differentiating Equation (17) with respect to s , we obtain

$$D_x'(s) = \left[-\frac{1}{WL} \right] \begin{bmatrix} \left[-(c-s)^2 \varepsilon_2 \varepsilon_4 C(\tau_g^1)(\kappa_n)^2 \right] T_x(s) \\ \left[+(c-s)^2 \varepsilon_1 \varepsilon_4 C(\kappa_n)^3 \right] E_x(s) \\ \left[+(c-s)^2 \varepsilon_4 (\kappa_n)^2 (\varepsilon_1 B - \varepsilon_2 (\tau_g^1) A) \right] D_x(s) \end{bmatrix} \\
 - \frac{1}{WL} \left[\begin{array}{l} \left[\begin{array}{l} 2(c-s) \varepsilon_2 \varepsilon_4 C(\tau_g^1)(\kappa_n)^2 \\ -(c-s)^2 \varepsilon_2 \varepsilon_4 C(\tau_g^1)(\kappa_n)^2 \\ -(c-s)^2 \varepsilon_2 \varepsilon_4 C(\tau_g^1)(\kappa_n)^2 \\ -2(c-s)^2 \varepsilon_2 \varepsilon_4 C(\tau_g^1)(\kappa_n)(\kappa_n) \end{array} \right] T_x(s) \\ \left[\begin{array}{l} -2(c-s) \varepsilon_1 \varepsilon_4 C(\kappa_n)^3 \\ +3(c-s)^2 \varepsilon_1 \varepsilon_4 C(\kappa_n)^2(\kappa_n) \\ -(c-s)^2 \varepsilon_2 \varepsilon_4 (\tau_g^1)(\kappa_n)^2 \\ \kappa_g^2 (\varepsilon_1 B - \varepsilon_2 (\tau_g^1) A) \\ (c-s)^2 \varepsilon_1 \varepsilon_4 C(\kappa_n)^3 \end{array} \right] E_x(s) \\ \left[\begin{array}{l} (c-s)^2 \varepsilon_1 \varepsilon_3 \varepsilon_4 C \kappa_g^2 (\kappa_n)^3 \\ -2(c-s) \varepsilon_4 (\kappa_n)^2 (\varepsilon_1 B - \varepsilon_2 (\tau_g^1) A) \\ +2(c-s)^2 (\varepsilon_4)(\kappa_n) \\ (\kappa_n) (\varepsilon_1 B - \varepsilon_2 (\tau_g^1) A) \\ (c-s)^2 \varepsilon_4 (\kappa_n)^2 \\ \left(\begin{array}{l} \varepsilon_1 B \\ -(\varepsilon_2 (\tau_g^1) A + \varepsilon_2 (\tau_g^1) A) \end{array} \right) \end{array} \right] D_x(s) \end{array} \right] \quad (18)$$

and if we write the Equation (18), we have

$$D_x'(s) = - \left[\left[\frac{1}{WL} \right] - \frac{1}{WL} \right] [MT_x(s) + NE_x(s) + RD_x(s)].$$

Finally, taking into consideration of the Equation (6) and making essential arrangement, we get

$$\tau_g^2 = - \left[\frac{1}{WL} \right] \frac{1}{W} \left[-M(c-s)(\varepsilon_1)^2 (\kappa_n)^2 - N(c-s)(\varepsilon_2)^2 (\tau_g^1)(\kappa_n) \right]$$

$$\kappa_g^1 = \frac{1}{L} \begin{bmatrix} -(c-s)(\varepsilon_1)^2 \varepsilon_4 (\kappa_n)^2 \left[A + \frac{p}{w} (c-s) \varepsilon_1 (\kappa_n)^2 \right] \\ -(c-s)(\varepsilon_2)^2 \varepsilon_4 (\tau_g^1) (\kappa_n) \left[B + \frac{p}{w} (c-s) \varepsilon_2 (\tau_g^1) (\kappa_n) \right] \\ \left(+ \varepsilon_4 \left((c-s) (\kappa_n)' - \varepsilon_4 \kappa_n \right) \right) \left[F - \frac{p}{w} \left((c-s) (\kappa_n)' - \kappa_n \right) \right] \\ - F (c-s)^2 (\varepsilon_4)^3 (\kappa_n)^2 \end{bmatrix}$$

$$\kappa_g^2 = -\frac{1}{WL} \begin{bmatrix} -U (c-s)^2 \varepsilon_2 \varepsilon_4 C (\tau_g^1) (\kappa_n)^2 \\ + V (c-s)^2 \varepsilon_1 \varepsilon_4 C (\kappa_n)^3 \\ + Z \left[(c-s)^2 \varepsilon_4 (\kappa_n)^2 (\varepsilon_1 B - \varepsilon_2 (\tau_g^1) A) \right] \end{bmatrix}$$

This completes the proof. (Remark 3.1 : $\langle E', D \rangle$ is left to reader.)

4. AW (k)-Type Curves

Let $x : I \rightarrow \mathbb{E}_1^4$ be a unit speed curve in \mathbb{E}_1^4 . The curve $x(s)$ is a Frenet curve of osculating order d when its higher order derivatives $x'(s), x''(s), \dots, x^{d+1}(s)$ are linearly independent, and $x'(s), x''(s), \dots, x^{d+1}(s)$ are no longer independent for all $s \in I$. Each frenet curve of osculating order d is associated with an orthonormal d -frame v_1, v_2, \dots, v_d along $x(s)$ (such that $x'(s) = T$) known as the Frenet frame as well as the functions $\kappa_1(s), \kappa_2(s), \dots, \kappa_{d-1}(s) : I \rightarrow \mathbb{R}$ known as Frenet curvatures [12].

In this section we consider AW (k)-type curves of order 3 in Minkowski space. Let $x : I \rightarrow \mathbb{E}_1^4$ be a curve with an extended Darboux frame $\{T(s), E(s), D(s), N(s)\}$, {as it is given in (6)}.

Proposition 4.1. Let $x : I \rightarrow \mathbb{E}_1^4$ be a unit speed curve, therefore, we have

$$\begin{aligned} x'(s) &= T(s) \\ x''(s) &= \varepsilon_4 (\kappa_n) N \\ x'''(s) &= -\varepsilon_1 \varepsilon_4 (\kappa_n)^2 T - \varepsilon_2 \varepsilon_4 \kappa_n \tau_g^1 E + \varepsilon_4 (\kappa_n)' \\ x''''(s) &= -3\varepsilon_1 \varepsilon_4 \kappa_n (\kappa_n)' T + \left[-2\varepsilon_2 \varepsilon_4 \tau_g^1 (\kappa_n)' - \varepsilon_2 \varepsilon_4 \kappa_n (\tau_g^1)' \right] E \\ &\quad - \varepsilon_2 \varepsilon_3 \varepsilon_4 \kappa_n \tau_g^1 \kappa_g^2 D + \left[-\varepsilon_1 (\varepsilon_4)^2 (\kappa_n)^3 - \varepsilon_2 (\varepsilon_4)^2 (\kappa_n)' \right. \\ &\quad \left. + (\varepsilon_4) (\kappa_n)'' \right] N \end{aligned}$$

Notation. Let us write

$$N_1(s) = \varepsilon_4(\kappa_n)N \tag{19}$$

$$N_2(s) = -\varepsilon_2\varepsilon_4\kappa_n\tau_g^1E + \varepsilon_4(\kappa_n)' \tag{20}$$

$$N_3(s) = -\varepsilon_2\varepsilon_3\varepsilon_4\kappa_n\tau_g^1\kappa_g^2D + \begin{bmatrix} -\varepsilon_1(\varepsilon_4)^2(\kappa_n)^3 - \varepsilon_2(\varepsilon_4)^2(\kappa_n) \\ +(\varepsilon_4)(\kappa_n)'' \end{bmatrix}N \tag{21}$$

Remark 4.1. $x'(s), x''(s), x'''(s)$ and $x''''(s)$ are linearly dependent if and only if $N_1(s), N_2(s)$ and $N_3(s)$ are linearly dependent.

Definition 4.1. Frenet curves are

(i) of type AW (1) if they satisfy

$$N_3(s) = 0,$$

(ii) of type AW (2) if they satisfy

$$\|N_2(s)\|^2 N_3(s) = \langle N_3(s), N_2(s) \rangle N_2(s). \tag{22}$$

(iii) of type AW (3) if they satisfy

$$\|N_1(s)\|^2 N_3(s) = \langle N_3(s), N_1(s) \rangle N_1(s). \tag{23}$$

Theorem 4.1. Let $x(s)$ be a Frenet curve of order 3 according to extended Darboux frame in \mathbb{E}_1^4 . Therefore, $x(s)$ is AW (1) -type curve if and only if

$$-\varepsilon_2\varepsilon_3\varepsilon_4\kappa_n\tau_g^1\kappa_g^2 = 0, \tag{24}$$

and

$$-\varepsilon_1(\varepsilon_4)^2(\kappa_n)^3 - \varepsilon_2(\varepsilon_4)^2(\kappa_n) + (\varepsilon_4)(\kappa_n)'' = 0. \tag{25}$$

Proof: Let $x(s)$ be a Frenet curve of type AW (1). From Definition (4.1.i), $N_3(s) = 0$. Then from Equation (21) equality, we get

$$-\varepsilon_2\varepsilon_3\varepsilon_4\kappa_n\tau_g^1\kappa_g^2D + \begin{bmatrix} -\varepsilon_1(\varepsilon_4)^2(\kappa_n)^3 - \varepsilon_2(\varepsilon_4)^2(\kappa_n) \\ +(\varepsilon_4)(\kappa_n)'' \end{bmatrix}N = 0.$$

Besides, since D and N are linearly independent, one can attain Equation (24) and Equation (25). This completes the proof of the theorem.

Theorem 4.2 Let $x(s)$ be a Frenet curve of order 3 according to extended Darboux frame in \mathbb{E}_1^4 . Therefore,

$x(s)$ is AW(2) -type curve if and only if

$$-\varepsilon_2 \varepsilon_3 (\varepsilon_4)^4 \kappa_n (\kappa_n')^2 \tau_g^1 \kappa_g^2 = 0. \quad (26)$$

Proof: Since $x(s)$ is type of AW (2) , Equation (22) holds on x . Substituting Equation (20) and Equation (21) into Equation (22) , one can attain Equation (26) . Thus, the proof of the theorem completes.

Theorem 4.3 Let $x(s)$ be a Frenet curve of order 3 according to extended Darboux frame in \mathbb{E}_1^4 . Therefore, $x(s)$ is AW (3) -type curve if and only if

$$-\varepsilon_2 \varepsilon_3 (\varepsilon_4)^4 (\kappa_n')^3 \tau_g^1 \kappa_g^2 = 0. \quad (27)$$

Proof: If $x(s)$ is type of AW (3), Equation (23) holds on x . So, substituting Equation (19) and Equation (21) into Equation (23), we get Equation (27) . This proves statement (iii) of the definition (4.1).

5. Conclusion

This study contains special curves according to extended Darboux frame field in \mathbb{E}_1^4 . That is, are investigated Serret-Frenet apparatus of involute of a curve and AW (k) Type curves using extended Darboux frame field in \mathbb{E}_1^4 . As a result of these, this study fills an important gap in literature and some findings in this work can be considered as an attractive by researchers, who are interested in special curve. Moreover, it can be a light for those who want to work in the future.

References

- [1] Dirişen BC, Şahin T. Position vectors of with respect to Darboux frame in the Galilean space . arXiv:1707. 03930v2.(2017).
- [2] Altunkaya B, Aksoyak FK. Curves of constant breadth according to Darboux frame, Commun. Fac. Sci. Univ. Ank. Series A1. (2017); 66(2):44-52.
- [3] Dldl M, Dldl B, Kuruođlu N, zdamar E. Extension of the Darboux frame into Euclidean 4-space and its invariants. Turkish Journal of Mathematics. (2017); 41: 1628-1639.
- [4] Boyer C. A history of mathematics New York: Wiley, (1968).
- [5] Turgut M, Yilmaz S. On the Frenet frame and a characterization of space-like involute-evolute curve couple in Minkowski space-time. Int. Math. Forum. (2008); 3(16): 793-801.
- [6] Soyfidan T, Gngr MA. On the quaternionic involute-evolute curves. arXiv: 1311.0621.[math. GT]. (2013).
- [7] As E, Sariođlugil A. On the Bishop curvatures of involute-evolute curve couple in \mathbb{E}^3 . International Journal of Physical Sciences.(2014); 9(7):140-145 .
- [8] Klahcı M, Bektaş M, Ergt M. Curves of AW (k) -type in 3-dimensional nul cone. Phys. Lett. A. (2007); 371:275-277.
- [9] Sun J, Pei D. Null Cartan Bertrand curves of AW (k) -type in Minkowski 4-space. School of Mathematics and Statistics. Northeast Normal University. Changchun, 130024, PR China. (2012).
- [10] Arslan K, elik Y, Deszcz R, zgr C. Submanifolds all of whose normal sections are W-curves. Far East J. Math. Sci. (1997); 5(4): 537-544.
- [11] Yoon D.W. General helices of AW(k) -type in the Lie group. J. Appl. Math, (2012).
- [12] Arslan K, zgr C. Curves and surfaces of AW (k) type. Geometry and Topology of Submanifolds IX. World Scientific. (1997). pp 21-26.
- [13] zgr C, Gezin F. On some curves of AW(k)-type. Differential Geometry-Dynamical Systems. (2005); 7:74-80.
- [14] Kılıç B, Arslan K. On curves and surfaces of AW(k)-type. BA Fen Bil. Enst. Dergisi. (2004); 6(1):52-61.
- [15] O'Neill B. Semi Riemannian geometry. Academic Press. New York-London.(1983).
- [16] İlarıslan K, Nesovic E. Spacelike and timelike normal curves in Minkowski space time. Publications de L'institut Mathematique, Nouvelle serie. (2009); 85:111-118.
- [17] Dldl B. Extended Darboux frame field in Minkowsk space-time \mathbb{E}_1^4 . Malaya Journal of Matematik. (2018); 6(3): 473-477.

Detection of Phishing Attacks on Websites with Lasso Regression, Minimum Redundancy Maximum Relevance Method, Machine Learning Methods, and Deep Learning Model

Mesut TOĞAÇAR^{1*}

¹ Department of Computer Technologies, Technical Sciences Vocational School, Fırat University, Elazığ, Turkey

*¹ mtogacar@firat.edu.tr

(Geliş/Received: 29/06/2021;

Kabul/Accepted: 04/07/2021)

Abstract: Phishing attacks are malicious software designed to steal personal or public. These types of attacks generally use e-mail addresses or aim to impersonate web-based pages to trap users. In such applications, they use textual or visual-based attractive content to lure users into their network. The internet environment is a large network platform with billions of users, and on this platform, users must be able to safely conduct their transactions without being harmed. To ensure the security of web pages simultaneously on a platform with billions of users, artificial intelligence-based software has been developed recently and this situation continues. In this study, analyzes were performed using two datasets. The two datasets consist of a total of 12454 website content. The first dataset consists of 11054 websites and the second dataset consists of 1400 websites. The datasets are divided into two classes, "phishing" and "legitimate". The contributions of machine learning methods, deep learning models, and feature selection methods in detecting phishing attacks were analyzed. The best accuracy success rate for the first dataset was 97.26%. The best accuracy success rate for the second dataset was 94.76%. As a result, it has been observed that feature selection methods contribute to the experimental analysis in general.

Keywords: Phishing attack, deep learning, machine learning, feature selection.

Kement Regresyon, Minimum Yedeklilik Maksimum Alaka Yöntemi, Makine Öğrenimi Yöntemleri ve Derin Öğrenme Modeli ile Web Sitelerine Yönelik Oltalama Saldırıların Tespiti

Öz: Kimlik avı saldırıları, kişisel veya genel olarak çalmak için tasarlanmış kötü amaçlı yazılımlardır. Bu tür saldırılar genellikle e-posta adreslerini kullanır veya kullanıcıları tuzağa düşürmek için web tabanlı sayfaları taklit etmeyi amaçlar. Bu tür uygulamalarda, kullanıcıları ağlarına çekmek için metin veya görsel tabanlı çekici içerikler tercih edilir. İnternet ortamı milyarlarca kullanıcısı olan büyük bir ağ platformudur ve bu platformda kullanıcıların işlemlerini güvenli bir şekilde zarar görmeden yapabilmeleri gerekmektedir. Milyarlarca kullanıcıya sahip bir platformda eş zamanlı olarak web sayfalarının güvenliğini sağlamak için son zamanlarda yapay zekâ tabanlı yazılımlar geliştirilmektedir. Bu çalışmada, iki veri seti kullanılarak analizler gerçekleştirilmiştir. İki veri seti toplam 12454 web sitesi içeriğinden oluşmaktadır. İlk veri seti 11054 web sitesinden ve ikinci veri seti 1400 web sitesinden oluşmaktadır. Veri kümeleri "oltalama" ve "legal" olmak üzere iki sınıfa ayrılır. Kimlik avı saldırılarını tespit etmede makine öğrenmesi yöntemleri, derin öğrenme modelleri ve özellik seçme yöntemlerinin katkıları analiz edildi. İlk veri seti için en iyi doğruluk başarı oranı %97.26'ydı. İkinci veri seti için en iyi doğruluk başarı oranı %94,76'ydı. Sonuç olarak, öznetelik seçme yöntemlerinin genel olarak deneysel analizlere katkı sağladığı gözlemlendi.

Anahtar kelimeler: Oltalama saldırısı, derin öğrenme, makine öğrenme, özellik seçimi.

1. Introduction

Phishing attacks are coded malicious software aimed at stealing users' personal information by using content that attracts users in the form of gifts, discounts, and awards through web applications or e-mails. Phishing attacks have an old history and are still used effectively by malicious people keeping up with technological developments [1,2]. Phishing attacks are an electronic fraud method that aims to drive users into their network by imitating corporate, commercial, or personal web addresses, e-mail addresses. The Internet is a large network used by billions of users around the world simultaneously. Thanks to this network, people have fast access to information, shopping, commerce, bill payment, etc. They can easily perform their operations. Security should be at the forefront as much as fast information exchange on the Internet. Precautionary internet protocols or security software have been developed. However, when technological developments are used by malicious people, this state of trust can be shaken [1,3]. Wandera stated in the Mobile Threat Landscape 2020 report that a new website is opened with phishing attacks every 20 seconds. In the same report, 87% of the attacks from mobile applications originate from messaging, social media, and game content web pages [4]. Anti-Phishing Working Group's 2020

* Corresponding author: mtogacar@firat.edu.tr. ORCID Number of author: ¹ 0000-0002-8264-3899

study stated that the rate of phishing attacks with SSL protection is 75% [5]. Recently, most phishing attacks are carried out using the keyword "Novel Coronavirus". Google company blocked more than 240 million spam messages labeled "Coronavirus" in a week [6]. According to the security report published by IBM for 2020, it was reported that the health sector was negatively affected by phishing attacks the most [7].

Internet users' card information, password information, personal or public information, etc. Developing software-based systems that can simultaneously protect their security has become an indispensable need and studies on this are still ongoing. Recently, Artificial Intelligence (AI) - based software has been developed that can provide information security on a platform with billions of users [8]. If some of these studies are examined; Ozgur Sahingoz et al [9]. detected phishing attacks with machine learning methods in their study. They used the Natural Language Processing (NLP) technique on their websites with the approach they suggested. Then, they achieved a 97.98% success rate with the Random Forest (RF) method. Erzhou Zhu et al. [10] classified phishing attacks using the Decision Tree (DT) method and the Artificial Neural Network (ANN) model together in their study. Using the Optimal feature selection (OFS) algorithm with the approach they proposed, they increased productivity. The success of classification they obtained with the feature selection method without improving the data was 95.76%. S. Sountharajan et al. [11] performed the classification process for phishing attacks of websites in their study. They used the Deep Boltzmann Machine (DBM) and the Stacked Auto-encoder (SAE) methods to select features in the dataset. Then, they trained the dataset with the deep learning model and their classification success was 94%. Ping Yi et al. [12] using Deep Faith Networks (DBNs), detected phishing attacks of websites on internet protocols (IP). They trained the features that websites use on IP data with the DBN model. They used Boltzmann machines for the classification method and achieved an 89.6% success rate. Mustafa Kaytan et al. [13] performed the classification process by using Extreme Learning Machines (ELM) to detect phishing attacks. They separated the dataset using the cross-validation method in the classification process and their classification accuracy success was 95.93%.

This paper, using the website data where phishing attacks occurred, as input, is to detect with machine learning methods and designed a deep learning model. It was also to observe whether feature selection methods contributed to the classification process. The summary of the other section of the study is as follows; information about the data set used in the experimental analysis is given in the second section. Information about machine learning methods, deep learning models, and feature selection methods used in the experimental analysis is given in the third section. Information about the experimental analysis and results are included in the fourth section. The last two sections consisted of Discussion and Conclusion, respectively.

2. Datasets

The experiment of this study consists of the analysis of two datasets. The first dataset consists of two files with extensions "txt" and "CSV", containing 11055 website content. Each website has parameters containing 30 features, and the label groups of these parameters consist of $\{-1, 1\}$ or $\{-1, 0, 1\}$ values. Information about the 30 features used as parameter values is given in Table 1. The data consists of websites that are designed for the binary classification model and where phishing attacks occur and are legitimate. This dataset is made available to the public [14].

Table 1. Website parameters and values in the first dataset.

Feature no	Website parameters	Label Values	Feature no	Website parameters	Label Values
1	UsingIP	$\{-1, 0, 1\}$	16	ServerFormHandler	$\{-1, 1\}$
2	LongURL	$\{-1, 0, 1\}$	17	InfoEmail	$\{-1, 1\}$
3	ShortURL	$\{-1, 1\}$	18	AbnormalURL	$\{-1, 1\}$
4	Symbol@	$\{-1, 1\}$	19	WebsiteForwarding	$\{-1, 0, 1\}$
5	Redirecting//	$\{-1, 1\}$	20	StatusBarCust	$\{-1, 1\}$
6	PrefixSuffix-	$\{-1, 1\}$	21	DisableRightClick	$\{-1, 1\}$
7	SubDomains	$\{-1, 0, 1\}$	22	UsingPopupWindow	$\{-1, 1\}$
8	HTTPS	$\{-1, 0, 1\}$	23	IframeRedirection	$\{-1, 1\}$
9	DomainRegLen	$\{-1, 1\}$	24	AgeofDomain	$\{-1, 1\}$
10	Favicon	$\{-1, 1\}$	25	DNSRecording	$\{-1, 0, 1\}$
11	NonStdPort	$\{-1, 1\}$	26	WebsiteTraffic	$\{-1, 1\}$
12	HTTPSDomainURL	$\{-1, 1\}$	27	PageRank	$\{-1, 1\}$
13	RequestURL	$\{-1, 1\}$	28	GoogleIndex	$\{-1, 0, 1\}$
14	AnchorURL	$\{-1, 0, 1\}$	29	LinksPointingToPage	$\{-1, 1\}$
15	LinksInScriptTags	$\{-1, 0, 1\}$	30	StatsReport	$\{-1, 1\}$

A second dataset was used to confirm the success of the proposed approach. This dataset is made available to the public. It has two classes: phishing and legitimate. The second dataset consists of a total of 1401 websites, 901 of which are phishing and 500 are legitimate. The dataset contains 10 features for each website [15]. These features are given in Table 2. The file format of the dataset is "xlsx". For this study, we converted the file format of the second dataset to the "CSV" file type.

Table 2. Website parameters and values in the second dataset.

Feature no	Website parameters	Label Values	Feature no	Website parameters	Label values
1	Having @ Symbol	{-1, 1 }	6	No.of Dots	{-1, 1 }
2	Presence of IP Address	{-1, 1 }	7	No. of Hyphen in Host Address	{-1, 1 }
3	Length of URL	{-1, 1 }	8	"Email" Keyword	{-1, 1 }
4	No. of Slashes	{-1, 1 }	9	URLs do not have "https"	{-1, 1 }
5	Special Character	{-1, 1 }	10	Age of URL	{-1, 1 }

In all of the experimental analyzes, 30% of the datasets were separated as test data, and 70% as training data. In addition, the cross-validation method ($k = 10$) was chosen and applied in the classification of datasets.

3. Models, Methods, and Proposed Approach

3.1. Nearest Neighbor Method (kNN)

The kNN method is a machine learning approach that is included in the supervised learning model and, can solve the classification problem of input data in the algorithm model. In the classification process, features that are similar to data features are labeled in the same class. While calculating this, sample data features are randomly selected and the distances of other data features are calculated according to sample data features. As a result, for each feature, the number of nearest neighbor features are looked at (as many as k). Here, the parameter k is usually chosen values such as $\{2,3,5,7, ..\}$. The disadvantage of the kNN method is that it needs a memory requirement to keep distance information for each feature data [16]. For distance measurements between features; one of the "Euclidean", "Manhattan", "Minkowski" methods is preferred. With the Euclidean formula, the distance (d) is calculated according to Eq. (1). Here, the variables p and q represent features [17].

$$d(p, q) = \sqrt{(p_1 - q_1)^2 + (p_2 - q_2)^2} \quad (1)$$

In this study, the kNN method supported by the Sklearn library was used. The Euclidean method was used for distance measurement and k value was selected as three.

3.2. Decision Tree Method

The Decision Tree (DT) method, consisting of root nodes and leaf nodes; is a machine learning approach preferred in classification processes. In the classification process, nodes are divided into sub-nodes using recursive methods, and this situation continues until it does not affect the classification process [18]. In the classification process, the "Entropy" method called information gain measurement is used to distinguish the data features. The uncertainties of the data are measured with the entropy method and the data features are classified with the obtained probability values. The formula used for measuring entropy (E) is given in Eq. (2). While N variable expresses the data number in Eq. (2). P is i . refers to the probability value of the data [19].

$$E = - \sum_{i=1}^N P_i \log_2 P_i \quad (2)$$

In this study, other important parameters were preferred for the DT method; criterion value Gini was selected, maximum depth value was selected 30. Other parameter values are the default values accepted in the Sklearn library [20].

3.3. Random Forest Method

Random Forest (RF) method is a machine learning approach used in regression and classification processes. The RF method creates multiple sets of decision trees and then combines these clusters to make the classification process more accurate. It aims to bring together as many different decision trees as possible, thus creating a low-correlation forest community. In the classification process, random nodes are selected and the best node is chosen among randomly selected variables. The Gini parameter is used to measure the homogeneity of classes. If the Gini measurement value of the lower node is lower than the Gini measurement value of the parent node, the branch with the nodes is considered successful. The Gini measurement is calculated according to Eq. (3). All data is represented by variable N and selected data is represented by n . Also, the variable p_i represents the square of the result consisting of the division of the number of elements smaller than the selected data and the number of elements larger than itself [21,22].

$$Gini(N) = 1 - \sum_{i=1}^n p_i^2 \quad (3)$$

In this study, other important parameters were preferred for the RF method; criterion value Gini was selected, maximum depth value was selected 30. Other parameter values are the default values accepted in the Sklearn library.

3.4. Feature Selection Methods

The minimum Redundancy Maximum Relevance (mRMR) algorithm is a filtering method that tries to select the most relevant features among the features it obtains from the data. It performs a ranking among the features it associates and tries to minimize the weakest associated features (redundancy features). In other words; treats each feature as a separate overlap variable and measures the level of similarity between the two features using mutual information between them [23]. Here, f_i is defined as the variable representing the features, and the ordering of the features vectorially is in the form of $f_i = [f_i^1, f_i^2, f_i^3, \dots, f_i^N]$. The $I(F_i, F_j)$ variable carries the mutual information values between the i and j features. The mRMR algorithm measures the similarity between two features and also measures the similarity between class tags for each feature. This situation is represented vectorially by the variable $h = [h^1, h^2, \dots, h^N]$ and the measurement value is represented by the variable $I(H, F_i)$. Here S represents the selected set of features and $|S|$ represents the number of selected features. The best properties are achieved by meeting two conditions (minimum redundancy and maximum relevance). For the minimum redundancy, the formula in Eq. (4) is used, and for the maximum relevance, the formula in Eq. (5) is used. Combined combination of two conditions is given in Eq. (6) and Eq. (7) [24,25].

$$\min W, W = \frac{1}{|S|^2} \sum_{F_i, F_j \in S} I(F_i, F_j) \quad (4)$$

$$\max V, V = \frac{1}{|S|} \sum_{F_i \in S} I(F_i, H) \quad (5)$$

$$\max (V - W) \quad (6)$$

$$\max (V/W) \quad (7)$$

The LASSO is preferred for the methods in which textual-based statistical calculations are performed and was created inspired by the linear regression method. This method minimizes the sum of square errors with an upper bound on the sum of the absolute feature values by processing the feature values obtained from the data. The formula used in the LASSO method is given in Eq. (8). The variable λ represents the amount of shrinkage. The variable t is inversely proportional to the variable λ , and as t becomes infinite, the problem becomes ordinary least squares. The variable β_j represents the coefficient and depends on the variable λ . In this case, features with a coefficient value equal to zero are extracted by the algorithm. The X and Y variables represent the features associated with the algorithm [26].

$$\min \left(\frac{\|Y - X\beta\|_2^2}{n} \right); \sum_{j=1}^k \|\beta_j\|_1 < t \quad (8)$$

In this study, the mRMR [25] and LASSO [27] feature selection algorithms were compiled in Python and used for two datasets. Among the 30 features in the first dataset, the feature with a low level of relation was extracted and classification was performed with 29 features. Among the 10 features in the second dataset, the feature with a low level of association was removed and classification was made with 9 features.

3.5. Deep Learning Model

In this study, the sequential model of the Keras library is used [28]. The designed model consists of Dense layers. Dense layers are regular layers and are called Dense because each neuron receives all the neurons from the previous layers as input [29]. For the first dataset, the number of input neurons of the experiment layer was 60 and the number of hidden neurons was chosen as 30. For the second dataset, the number of input neurons of the experiment layer was 30 and the number of hidden neurons was chosen as 10. The activation function was selected as ReLU. ReLU is a unit of functions that linearizes nonlinear input values [30]. The ReLU function takes $[0, +\infty]$ values and does not contain negative values. The Adam was chosen as the optimization method and the learning rate of this optimization method was selected 10^{-3} . The data showing the layer and parameter values of the designed model are given in Table 3. Also, the loss parameter of the designed model "mean_squared_error" was selected. After trying all the used parameters of this model, the ones showing the best success were preferred.

Table 3. Deep learning model layers were designed for this study.

Layer	Activation	Input Neuron	Hidden Neuron	Input Size
Dense	ReLU	Input dimensions	Input dimensions	Input dimensions
Dense	ReLU	Dataset #1: 60 Dataset #2: 30	Dataset #1: 30 Dataset #2: 10	-
Dense	ReLU	1	-	-
Output		ReLU		Two Classes

3.6. Proposed Approach

The proposed approach is aimed at successfully detecting phishing attacks on the website that have recently increased their effectiveness. Feature selection methods (mRMR, LASSO) were used to accomplish this. Among the parameter features of the websites, the most inefficient feature was removed and given as an input to the machine learning and deep model network. Thus, the detection of phishing attacks was achieved with a hybrid approach. The overall design of the proposed approach is shown in Fig. 1. The experimental analysis codes of this study were compiled in Python language [31].

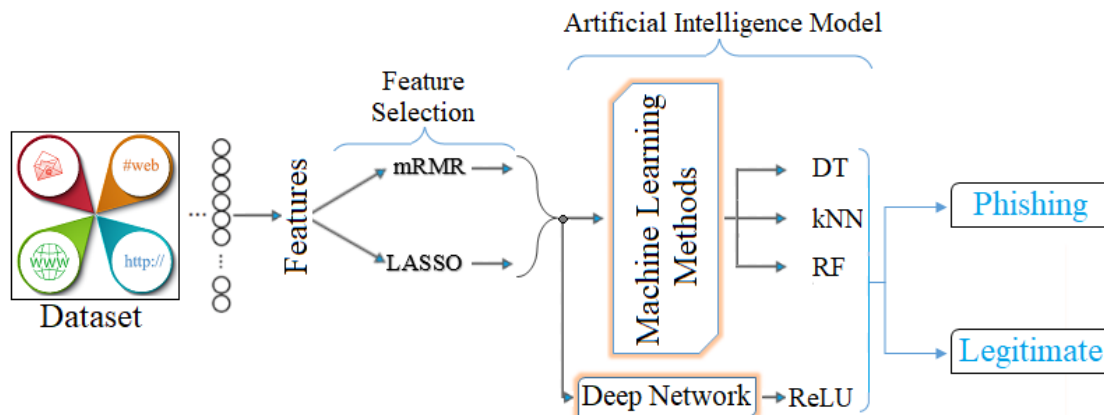


Figure 1. The general design of the proposed artificial intelligence supported approach.

4. Experimental Analysis and Results

Experimental analyzes were carried out using Python software codes. The Google Colab server was used for hardware requirements and for compiling the codes. Confusion matrix was used as a measurement in experimental analysis. The measurement metrics of the confusion matrix are; Specificity (Spe), Prediction (Pre), Recall, F-score (F-scr), and Accuracy (Acc). Metric results are calculated by equations between Eq. (9) and Eq. (13). Meanings of variables used in equations; True Positive (TP), True Negative (TN), False Positive (FP), False Negative (FN) [32,33].

$$\text{Spe} = \frac{\text{TN}}{\text{TN} + \text{FP}} \quad (9)$$

$$\text{Pre} = \frac{\text{TP}}{\text{TP} + \text{FP}} \quad (10)$$

$$\text{Recall} = \frac{\text{TP}}{\text{TP} + \text{FN}} \quad (11)$$

$$\text{F-scr} = \frac{2 \times (\text{Recall} \times \text{Pre})}{\text{Recall} + \text{Pre}} \quad (12)$$

$$\text{Acc} = \frac{\text{TP} + \text{TN}}{\text{TP} + \text{TN} + \text{FP} + \text{FN}} \quad (13)$$

The experimental analysis consisted of two steps for each dataset. In the first step, the success of machine learning methods and designed deep network model is analyzed. In the second step, it was analyzed whether feature selection methods (Lasso and mRMR) contributed to the success achieved. In all steps of the experiment, the data sets were separated as 30% test data and analyzes were carried out. In addition, the validity of the analyzes was checked using the cross-validation method (choosing $k = 10$).

The first analysis was performed using 30% test data of the first dataset. Accuracy achievements were analyzed using machine learning methods (DT, kNN, RF) and deep network model. An accuracy success of 96.26% was achieved with the DT method; an accuracy success of 93.46% was achieved with the kNN method; an accuracy success of 96.83% was achieved with the RF method, and an accuracy of 95.57% was achieved with the deep network model. The confusion matrices of the first analysis are shown in Fig. 2. The second analysis was performed by separating the data with the cross-validation method of the first dataset. Accuracy achievements were analyzed using machine learning methods (DT, kNN, RF) and deep network model. An accuracy success of 95.90% was achieved with the DT method; an accuracy of 93.37% was achieved with the kNN method; an accuracy of 97.03% was achieved with the RF method and an accuracy of 95.50% with the deep network model. The accuracy graphs of the second analysis are shown in Fig. 4. The accuracy results of the second analysis and first analysis approximately corresponded to each other. In both analyzes, it was observed that the RF method was more successful. The third analysis was performed using 30% test data of the second dataset. Accuracy achievements were analyzed using machine learning methods (DT, kNN, RF) and deep network model. An accuracy success of 94.05% was achieved with the DT method; an accuracy success of 92.62% was achieved with the kNN method; an accuracy success of 94.05% was achieved with the RF method, and an accuracy of 93.81% was achieved with the deep network model. The confusion matrices of the third analysis are shown in Fig. 3. The fourth analysis was performed by separating the data with the cross-validation method of the second dataset. Accuracy achievements were analyzed using machine learning methods (DT, kNN, RF) and deep network model. An accuracy success of 94.18% was achieved with the DT method; an accuracy of 93.98% was achieved with the kNN method; an accuracy of 94.18% was achieved with the RF method and an accuracy of 94.18% with the deep network model. The accuracy graphs of the fourth analysis are shown in Fig. 5. The accuracy results of the third analysis and fourth analysis approximately corresponded to each other. In both analyzes, it was observed that the DT, RF, Deep Network methods were more successful. Detailed analysis results of the confusion matrices obtained from the first step of the experiment are given in Table 4.

In the second step of the experiment, the feature selection methods (Lasso, mRMR) made a classification by determining the most inefficient feature among the features obtained from datasets. Thus, 30 features in the first dataset were reduced to 29 features, and 10 features in the second dataset were reduced to 9 features. Then, the analyzes performed in the first step of the experiment were re-performed. The Lasso feature selection method was used for the fifth, sixth, seventh, eighth analyzes. In the ninth, tenth, eleventh, twelfth analyzes, the mRMR feature selection method was used. The fifth analysis was performed using 30% test data of the first dataset (29 featured). Accuracy achievements were analyzed using machine learning methods (DT, kNN, RF) and deep network model.

An accuracy success of 96.50% was achieved with the DT method; an accuracy success of 93.76% was achieved with the kNN method; an accuracy success of 96.83% was achieved with the RF method, and an accuracy of 95.75% was achieved with the deep network model. The confusion matrices of the fifth analysis are shown in Fig. 6. The sixth analysis was performed by separating the data with the cross-validation method of the first dataset. Accuracy achievements were analyzed using machine learning methods (DT, kNN, RF) and deep network model. An accuracy success of 96.04% was achieved with the DT method; an accuracy of 93.29% was achieved with the kNN method; an accuracy of 97.05% was achieved with the RF method and an accuracy of 95.98% with the deep network model. The accuracy graphs of the sixth analysis are shown in Fig. 7. As a result of the fifth and sixth analyzes, it was observed that the Lasso method contributed to the classification success. Other than the kNN method, the success of other analysis results has increased. The seventh analysis was performed using 30% test data of the second dataset (9 featured). Accuracy achievements were analyzed using machine learning methods (DT, kNN, RF) and deep network model. An accuracy success of 94.05% was achieved with the DT method; an accuracy success of 92.86% was achieved with the kNN method; an accuracy success of 94.29% was achieved with the RF method, and an accuracy of 93.81% was achieved with the deep network model. The confusion matrices of the seventh analysis are shown in Fig. 8. The eighth analysis was performed by separating the data with the cross-validation method of the second dataset. Accuracy achievements were analyzed using machine learning methods (DT, kNN, RF) and deep network model. An accuracy success of 94.18% was achieved with the DT method; an accuracy of 92.84% was achieved with the kNN method; an accuracy of 94.29% was achieved with the RF method and an accuracy of 94.18% with the deep network model. The accuracy graphs of the eighth analysis are shown in Fig. 9. As a result of the seventh and eighth analyzes, it was observed that the Lasso method contributed to the classification success. The reduction of the number of features with the Lasso method was equivalent to the results obtained in previous analyzes or increased.

Table 4. Analysis results of datasets obtained by machine learning methods and deep network model (%).

Dataset	Test Rate	Feature	Model, Method	Spe	Pre	Recall	F-scr	Acc
Dataset #1	30%	30	DT	95.06	96.08	97.23	96.65	96.26
			kNN	92.29	93.83	94.40	94.11	93.46
			RF	95.67	96.56	97.77	97.16	96.83
			Deep Network	96.35	97.0	94.94	95.96	95.57
Dataset #2	30%	10	DT	99.30	98.26	83.09	90.04	94.05
			kNN	97.18	93.39	83.09	87.94	92.62
			RF	99.30	98.26	83.09	90.04	94.05
			Deep Network	99.30	98.25	82.35	89.60	93.81

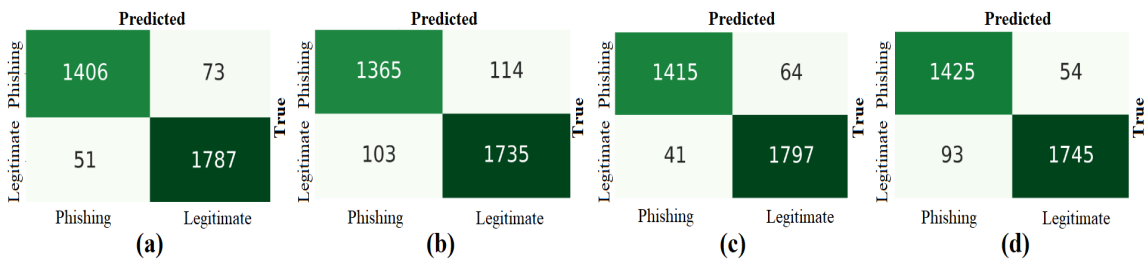


Figure 2. Confusion matrices were obtained from 30% test data of the first dataset.

Detection of Phishing Attacks on Websites with Lasso Regression, Minimum Redundancy Maximum Relevance Method, Machine Learning Methods, and Deep Learning Model

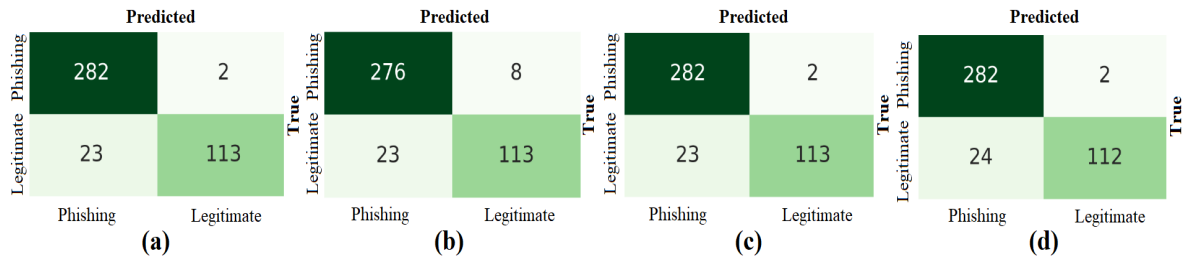


Figure 3. Confusion matrices were obtained from 30% test data of the second dataset.

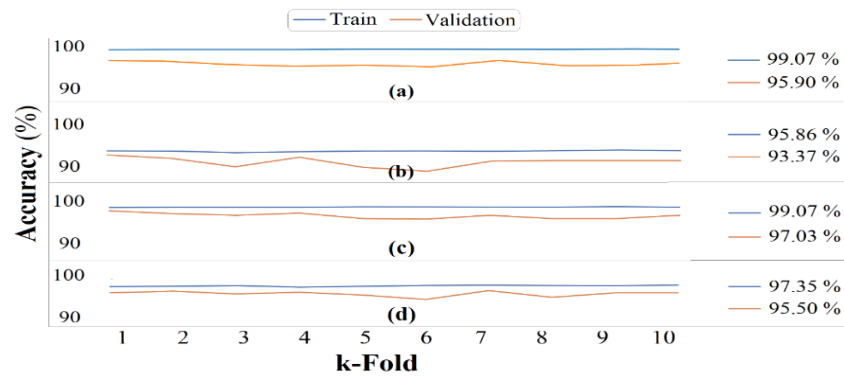


Figure 4. Success graphs and accuracy results were obtained from data separated by the cross-validation method of the first dataset.

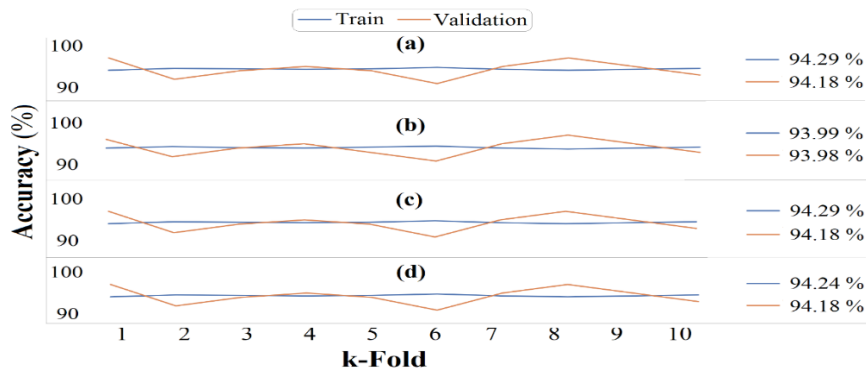


Figure 5. Success graphs and accuracy results were obtained from data separated by the cross-validation method of the second dataset.

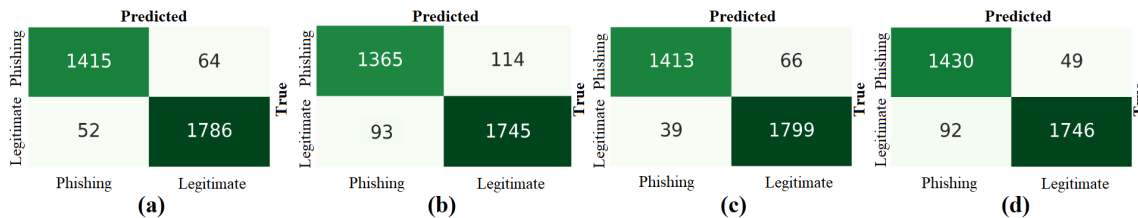


Figure 6. Confusion matrices were obtained after applying the Lasso feature selection method to 30% test data of the first dataset.

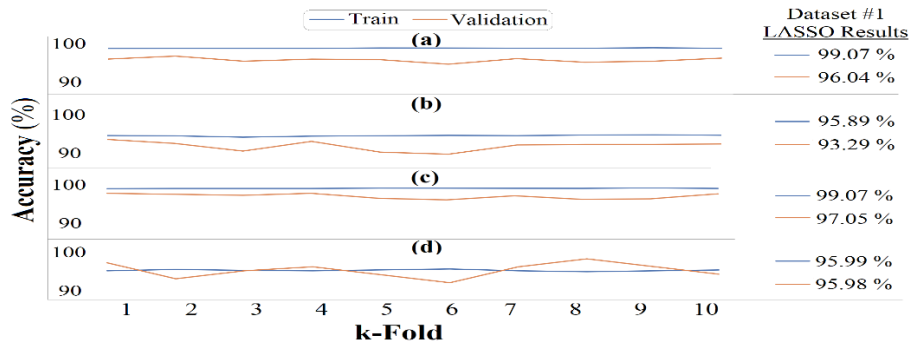


Figure 7. Success graphs and accuracy results were obtained from data separated by the cross-validation method after the Lasso feature selection method of the first dataset.

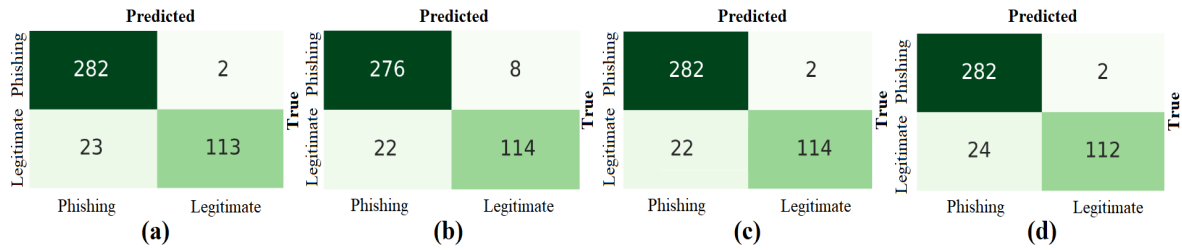


Figure 8. Confusion matrices were obtained after applying the Lasso feature selection method to 30% test data of the second dataset.

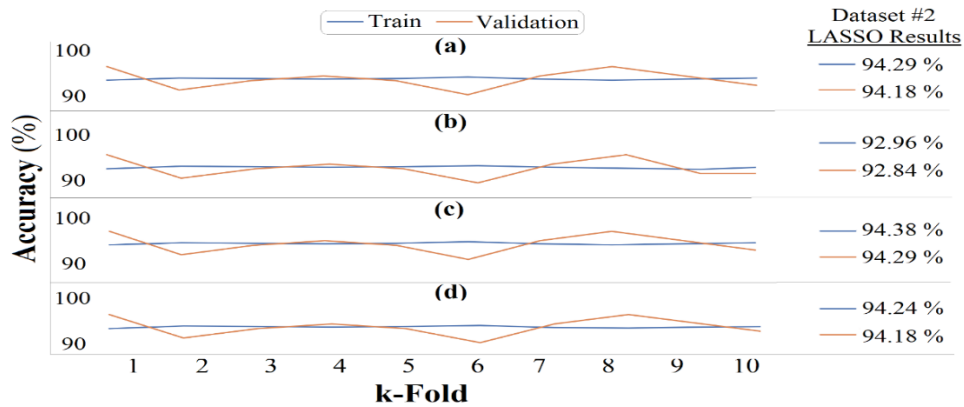


Figure 9. Success graphs and accuracy results were obtained from data separated by the cross-validation method after the Lasso feature selection method of the second dataset.

The ninth analysis was performed using 30% test data of the first dataset (29 featured). Accuracy achievements were analyzed using machine learning methods (DT, kNN, RF) and deep network model. An accuracy success of 96.59% was achieved with the DT method; an accuracy success of 93.76% was achieved with the kNN method; an accuracy success of 97.26% was achieved with the RF method, and an accuracy of 96.14% was achieved with the deep network model. The confusion matrices of the ninth analysis are shown in Fig. 10. The tenth analysis was performed by separating the data with the cross-validation method of the first dataset. Accuracy achievements were analyzed using machine learning methods (DT, kNN, RF) and deep network model. An accuracy success of 96.54% was achieved with the DT method; an accuracy of 93.41% was achieved with the kNN method; an accuracy of 96.96% was achieved with the RF method and an accuracy of 95.78% with the deep network model. The accuracy graphs of the ninth analysis are shown in Fig. 11. The validity of the accuracy results obtained from the ninth analysis was confirmed by the tenth analysis. The eleventh analysis was performed using

30% test data of the second dataset (9 featured). Accuracy achievements were analyzed using machine learning methods (DT, kNN, RF) and deep network model. An accuracy success of 94.29% was achieved with the DT method; an accuracy success of 92.62% was achieved with the kNN method; an accuracy success of 94.76% was achieved with the RF method, and an accuracy of 93.81% was achieved with the deep network model. The confusion matrices of the eleventh analysis are shown in Fig. 12. The twelfth analysis was performed by separating the data with the cross-validation method of the second dataset. Accuracy achievements were analyzed using machine learning methods (DT, kNN, RF) and deep network model. An accuracy success of 94.18% was achieved with the DT method; an accuracy of 93.98% was achieved with the kNN method; an accuracy of 94.18% was achieved with the RF method and an accuracy of 93.69% with the deep network model. The accuracy graphs of the twelfth analysis are shown in Fig. 13. As a result of the eleventh and twelfth analyzes, it was observed that the mRMR method contributed to the classification success.

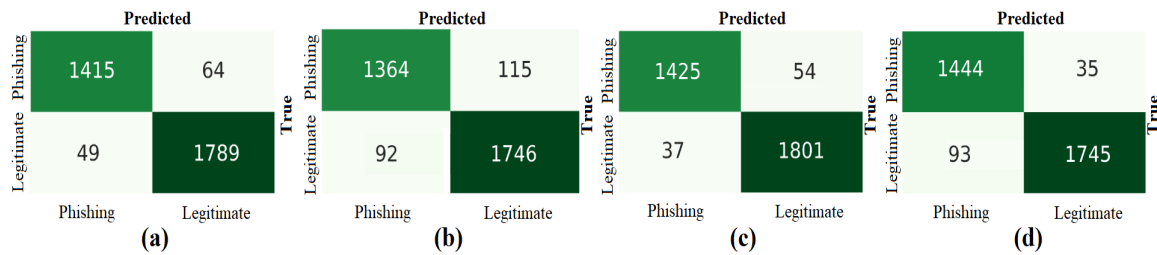


Figure 10. Confusion matrices were obtained after applying the mRMR feature selection method to 30% test data of the first dataset.

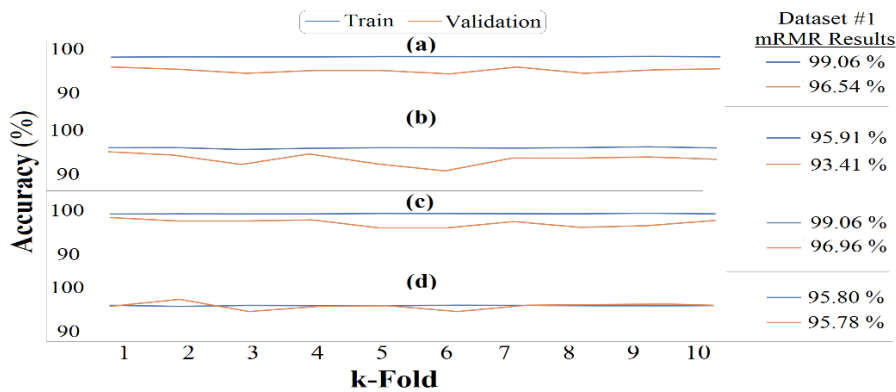


Figure 11. Success graphs and accuracy results were obtained from data separated by the cross-validation method after the mRMR feature selection method of the first dataset.

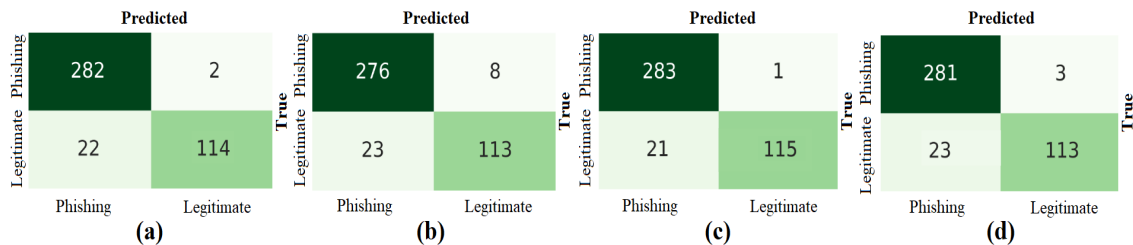


Figure 12. Confusion matrices were obtained after applying the mRMR feature selection method to 30% test data of the second dataset.

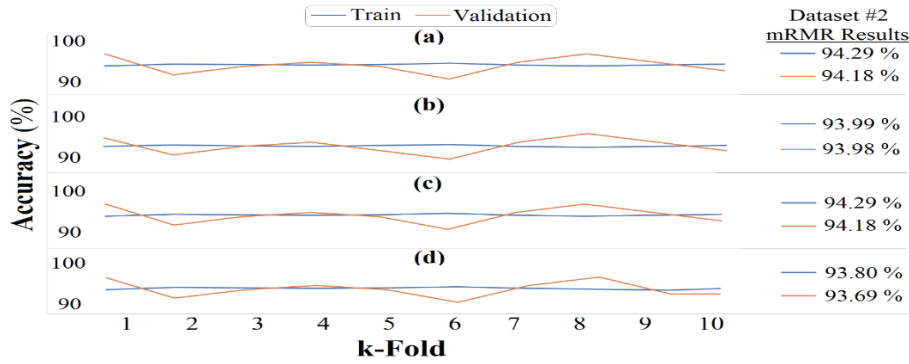


Figure 13. Success graphs and accuracy results were obtained from data separated by the cross-validation method after the mRMR feature selection method of the second dataset.

Detailed results of the analyzes performed in the second step of the experiment are given in Table 5. These results showed us the efficiency of feature selection methods in two datasets. It was also observed that the mRMR method was more effective than the Lasso method.

Table 5. Analysis results were obtained from 30% of test data after the feature selection methods are applied to datasets (%).

Dataset	Test Rate	Method, Total Feature	Model, Method	Spe	Pre	Recall	F-scr	Acc
Dataset #1	30%	LASSO / 29	DT	95.67	96.54	97.17	96.85	96.50
			kNN	93.87	93.62	93.74	92.95	93.76
			RF	95.54	96.46	97.88	97.16	96.83
			Deep Network	96.69	97.27	94.99	96.12	95.75
Dataset #2	30%	LASSO / 9	DT	99.30	98.26	83.09	90.04	94.05
			kNN	97.18	93.44	93.03	94.85	92.86
			RF	98.28	99.30	95.52	95.92	94.29
			Deep Network	99.30	98.25	82.35	89.60	93.81
Dataset #1	30%	mRMR / 29	DT	96.55	95.67	96.60	96.16	96.59
			kNN	93.82	92.22	93.70	92.95	93.76
			RF	97.09	96.35	97.28	96.91	97.26
			Deep Network	98.03	97.63	95.99	95.76	96.14
Dataset #2	30%	mRMR / 9	DT	98.28	99.30	95.52	95.92	94.29
			kNN	97.18	93.39	83.09	87.94	92.62
			RF	99.14	99.65	96.11	96.26	94.76
			Deep Network	97.41	98.94	94.92	95.58	93.81

5. Discussion

In this paper, phishing attacks against websites that threaten information security were detected. The approach suggested in my study has been successful in detecting e-fraud. Among the limited aspects of my proposed approach; it can be shown that the number of features of the dataset is not too much. This situation limited the success of the classification process. But, perhaps a combination of natural language processing methods for features in datasets would increase success. Because the datasets had information such as the domain names of the websites. I did not use this information in the suggested approach. In the proposed approach, feature selection methods affected the results positively. The success graph showing this performance situation is shown in Fig. 14. It was observed in Fig. 14 that the Lasso and mRMR method effectively increase the success. In addition, we used

the dataset training-test and cross-validation methods to reliable the proposed approach. As a result, I have seen through experimental analysis that our approach applies to the detection of phishing attacks.

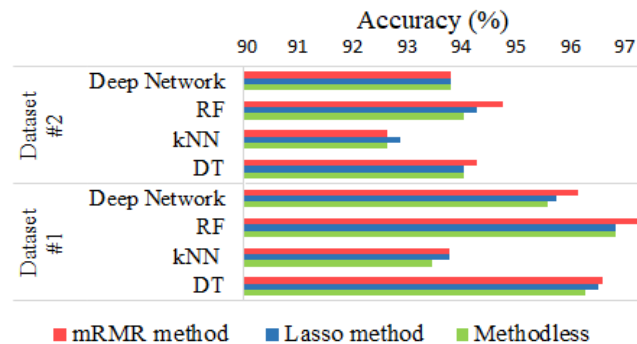


Figure 14. Bar graph showing the performance of the proposed approach on datasets.

6. Conclusion

This paper analyzed the AI-assisted detection of phishing attacks on websites. In the internet environment with billions of users, such attacks are frequently seen and the AI-based approaches are needed to minimize these attacks [34]. The experimental analysis of this study shows that the AI-based approaches are successful in the detection of phishing attacks. In the analysis of this study, the AI-based machine learning methods (DA, kNN, RF) were used to perform the classification process. In addition, the designed deep network model has also been used in the training and classification process of datasets. Feature selection methods (Lasso, mRMR) made the most important contribution to the proposed approach. The best performance results in both datasets were achieved with RF - mRMR methods. Analysis results of the first dataset with RF-mRMR methods; specificity success was 97.09%, prediction success was 96.35%, recall success was 97.28%, f-score success was 96.91% and Accuracy success was 97.26%. Likewise, analysis results of the second dataset with RF-mRMR methods; specificity success was 99.14%, prediction success 99.65%, recall success 96.11%, f-score success 96.26% and accuracy success 94.76%.

In the next study, the proposed approach for phishing attacks in web applications is planned to be used together with meta-heuristic optimization methods.

Funding

There is no funding source for this article.

Ethical approval

This article does not contain any data, or other information from studies or experimentation, with the involvement of human or animal subjects.

Conflicts of interest

The author declares that there is no conflict of interest related to this paper.

References

- [1] S.S.M. Motiur Rahman, T. Islam, M.I. Jabiullah, PhishStack: Evaluation of Stacked Generalization in Phishing URLs Detection, *Procedia Comput. Sci.* 167 (2020) 2410–2418. doi:<https://doi.org/10.1016/j.procs.2020.03.294>.
- [2] H. Önal, Phishing (Oltalama) Saldırısı Nedir? | BGA Security, BGA Secur. (2021). <https://www.bgasecurity.com/2019/09/phishing-oltalama-saldirisi-nedir/> (accessed June 10, 2021).
- [3] D. Goel, A.K. Jain, Mobile phishing attacks and defence mechanisms: State of art and open research challenges, *Comput. Secur.* 73 (2018) 519–544. doi:<https://doi.org/10.1016/j.cose.2017.12.006>.

- [4] WANDERA, Mobile Threat Landscape Report 2020 | Wandera, 2020. <https://www.wandera.com/mobile-threat-landscape/> (accessed August 18, 2020).
- [5] APWG, Phishing Activity Trends Report Q1 2020, 2020. www.apwg.org.
- [6] Phishing Statistics: The 29 Latest Phishing Stats to Know in 2020 - Hashed Out by The SSL Store™, Hashedout. (2021). <https://www.thesslstore.com/blog/phishing-statistics-latest-phishing-stats-to-know/> (accessed June 10, 2021).
- [7] M. Abdelhamid, The Role of Health Concerns in Phishing Susceptibility: Survey Design Study, *J Med Internet Res.* 22 (2020) e18394. doi:10.2196/18394.
- [8] J. Chen, C. Su, Z. Yan, AI-Driven Cyber Security Analytics and Privacy Protection, *Secur. Commun. Networks.* 2019 (2019) 1859143. doi:10.1155/2019/1859143.
- [9] O.K. Sahingoz, E. Buber, O. Demir, B. Diri, Machine learning based phishing detection from URLs, *Expert Syst. Appl.* 117 (2019) 345–357. doi:<https://doi.org/10.1016/j.eswa.2018.09.029>.
- [10] E. Zhu, Y. Ju, Z. Chen, F. Liu, X. Fang, DTOF-ANN: An Artificial Neural Network phishing detection model based on Decision Tree and Optimal Features, *Appl. Soft Comput.* 95 (2020) 106505. doi:<https://doi.org/10.1016/j.asoc.2020.106505>.
- [11] S. Sountharajan, M. Nivashini, S.K. Shandilya, E. Suganya, A.B. Banu, M. Karthiga, *Advances in Cyber Security Analytics and Decision Systems*, 2020. doi:10.1007/978-3-030-19353-9.
- [12] P. Yi, Y. Guan, F. Zou, Y. Yao, W. Wang, T. Zhu, Web Phishing Detection Using a Deep Learning Framework, *Wirel. Commun. Mob. Comput.* 2018 (2018) 4678746. doi:10.1155/2018/4678746.
- [13] M. Kaytan, D. Hanbay, Effective Classification of Phishing Web Pages Based on New Rules by Using Extreme Learning Machines, *Anatol. J. Comput. Sci.* 2 (2017) 15–36. <https://dergipark.org.tr/download/article-file/333655>.
- [14] E. Chand, Phishing website Detector, Kaggle. (2021). <https://www.kaggle.com/eswarchandt/phishing-website-detector> (accessed June 7, 2021).
- [15] A. J., Phishing Websites Detection, Kaggle. (2020). <https://www.kaggle.com/akshaya1508/phishing-websites-detection?> (accessed August 19, 2020).
- [16] C. Sitawarin, D. Wagner, On the Robustness of Deep K-Nearest Neighbors, in: *2019 IEEE Secur. Priv. Work.*, 2019: pp. 1–7. doi:10.1109/spw.2019.00014.
- [17] A. Niwatkar, Y.K. Kanse, Feature Extraction using Wavelet Transform and Euclidean Distance for speaker recognition system, in: *2020 Int. Conf. Ind. 4.0 Technol.*, 2020: pp. 145–147. doi:10.1109/I4Tech48345.2020.9102683.
- [18] S. Zhang, Z. Shi, G. Wang, R. Yan, Z. Zhang, Groundwater radon precursor anomalies identification by decision tree method, *Appl. Geochemistry.* 121 (2020) 104696. doi:<https://doi.org/10.1016/j.apgeochem.2020.104696>.
- [19] Y. Wang, S.-T. Xia, J. Wu, A less-greedy two-term Tsallis Entropy Information Metric approach for decision tree classification, *Knowledge-Based Syst.* 120 (2017) 34–42. doi:<https://doi.org/10.1016/j.knosys.2016.12.021>.
- [20] Scikit-learn kütüphanesi, Scikit Learn. (2021). https://scikit-learn.org/stable/supervised_learning.html#supervised-learning (accessed August 20, 2020).
- [21] C. Aldrich, Process variable importance analysis by use of random forests in a shapley regression framework, *Minerals.* 10 (2020) 1–17. doi:10.3390/min10050420.
- [22] H. Han, X. Guo, H. Yu, Variable selection using Mean Decrease Accuracy and Mean Decrease Gini based on Random Forest, in: *2016 7th IEEE Int. Conf. Softw. Eng. Serv. Sci.*, 2016: pp. 219–224. doi:10.1109/ICSESS.2016.7883053.
- [23] M. Toğaçar, B. Ergen, Z. Cömert, Detection of lung cancer on chest CT images using minimum redundancy maximum relevance feature selection method with convolutional neural networks, *Biocybern. Biomed. Eng.* (2019). doi:<https://doi.org/10.1016/j.bbe.2019.11.004>.
- [24] M. Cıbuk, U. Budak, Y. Guo, M.C. Ince, A. Sengur, Efficient deep features selections and classification for flower species recognition, *Measurement.* 137 (2019) 7–13. doi:<https://doi.org/10.1016/j.measurement.2019.01.041>.
- [25] Hanchuan Peng, Python binding to mRMR Feature Selection algorithm, (n.d.). <https://github.com/fbrundu/pymrmmr>.
- [26] V. Fonti, Feature Selection using LASSO, VU Amsterdam. (2017) 1–26. doi:10.1109/access.2017.2696365.
- [27] Feature selection - LASSO, Scikit-Learn. (2020). https://scikit-learn.org/stable/modules/feature_selection.html (accessed August 21, 2020).
- [28] The Sequential model, Keras. (2020). <https://keras.io/api/models/sequential/> (accessed August 21, 2020).
- [29] Y. Yang, S. Liu, Non-porous thin dense layer coating: Key to achieving ultrahigh peak capacities using narrow open tubular columns, *Talanta Open.* 1 (2020) 100003. doi:<https://doi.org/10.1016/j.talo.2020.100003>.
- [30] D. Zou, Y. Cao, D. Zhou, Q. Gu, Gradient descent optimizes over-parameterized deep ReLU networks, *Mach. Learn.* 109 (2020) 467–492. doi:10.1007/s10994-019-05839-6.
- [31] S.A. Khan, Phishing Websites Classification using Deep Learning, GitHub. (2020). <https://github.com/sohailahmedkhan173/Phishing-Websites-Classification-using-Deep-Learning> (accessed August 9, 2020).
- [32] D. Chicco, G. Jurman, The advantages of the Matthews correlation coefficient (MCC) over F1 score and accuracy in binary classification evaluation, *BMC Genomics.* 21 (2020) 6. doi:10.1186/s12864-019-6413-7.
- [33] M. Toğaçar, B. Ergen, Deep Learning Approach for Classification of Breast Cancer, in: *2018 Int. Conf. Artif. Intell. Data Process.*, 2018: pp. 1–5. doi:10.1109/idap.2018.8620802.
- [34] T. Lin, D.E. Capecci, D.M. Ellis, H.A. Rocha, S. Dommaraju, D.S. Oliveira, N.C. Ebner, Susceptibility to Spear-Phishing Emails: Effects of Internet User Demographics and Email Content, *ACM Trans. Comput. Hum. Interact.* 26 (2019) 32. doi:10.1145/3336141.

Against Digital Extinction: Cyber Peace

Muharrem Tuncay GENÇOĞLU*

* Technical sciences Vocational School, Fırat University, Elazığ, Turkey

* mt.gencoglu@firat.edu.tr

(Geliş/Received: 12/07/2021;

Kabul/Accepted: 10/08/2021)

Abstract:At a time when cyberattacks are becoming a part of our daily lives and small-scale attacks are becoming commonplace, it is obvious that digital infrastructures are widely and intensely used in our lives and that they can be used for hostile, non-peaceful purposes. This situation has become very serious especially for Turkey, due to the complex attacks taking place around the World.

The issue of cybersecurity around the world is not limited to certain cyberattacks but also brings the threat of these attacks turning into comprehensive cyber warfare. Therefore, the more important the security of the geographical borders, the more important the security of electronic systems and the data stored there. Since the most important component of security is peace, it is worth examining as a very important concept in Cyber Peace in response to the negative perceptions of cyberwar, cyber terrorism and cybercrime. This study, it is aimed to create a conceptual basis of cyber peace and contribute to this field to create a defense mechanism based on peaceful behaviors in cyberspace. For this purpose, the definition of cyber peace has been made, and it has been focused on establishing and protecting cyber peace. It was emphasized that cyber peace can be sustainable not through disarmament, but by reducing the risk through modernization of attack and defense capacities.

In this study, which we do not have much work on cyber peace and we can accept it as the first step in filling this gap; It was concluded that private and voluntary organizations must take a more active role in protecting cyber peace.

Key words: Peace, Cyber Peace, Cyber Peace Protection, Cyber.

Dijital Yokoluşa Karşı: Siber Barış

Öz: Siber saldırıların günlük hayatımızın bir parçası haline geldiği ve küçük çaplı saldırıların sıradanlaştığı bir dönemde, dijital altyapıların hayatımızda yaygın ve yoğun bir şekilde kullanıldığı ve düşmanca, barışçıl olmayan amaçlar için kullanılabilmesi aşırıdır. Bu durum, dünya genelinde yaşanan karmaşık saldırılar nedeniyle özellikle Türkiye için çok ciddi bir hal almıştır. Dünya genelinde siber güvenlik konusu belirli siber saldırılarla sınırlı kalmayıp, bu saldırıların kapsamlı bir siber savaşa dönüşme tehdidini de beraberinde getiriyor. Dolayısıyla coğrafi sınırların güvenliği ne kadar önemliyse, elektronik sistemlerin ve orada depolanan verilerin güvenliği de o kadar önemlidir. Güvenliğin en önemli bileşeni barış olduğu için siber savaş, siber terörizm ve siber suçlara ilişkin olumsuz algılara karşılık Siber Barışta çok önemli bir kavram olarak incelenmeye değerdir. Bu çalışma ile siber barışın kavramsal bir temelini oluşturulması ve bu alana siber uzayda barışçıl davranışlara dayalı bir savunma mekanizması oluşturulmasına katkı sağlanması amaçlanmaktadır. Bu amaçla siber barışın tanımı yapılmış ve siber barışın kurulması ve korunması üzerinde durulmuştur. Siber barışın silahsızlanma yoluyla değil, saldırı ve savunma kapasitelerinin modernizasyonu ile risklerin azaltılması yoluyla sürdürülebilir olabileceği vurgulanmıştır. Siber barış konusunda çok fazla çalışmamızın olmadığı ve bu boşluğu doldurmanın ilk adımı olarak kabul edebileceğimiz bu çalışmada; Siber barışın korunmasında özel ve gönüllü kuruluşların daha aktif rol alması gerektiği sonucuna varılmıştır.

Anahtar kelimeler: Barış, Siber Barış, Siber Barışı Koruma, Siber

1. Introduction

We are in a period where cyber attacks are becoming a part of our daily lives and small-scale attacks are becoming commonplace. It is obvious that digital infrastructures entered our lives extensively and intensely during this period and it is inevitable that they will be used for hostile and non-peaceful purposes. We have witnessed quite complex attacks around the world. The issue of cybersecurity around the world is not limited to certain cyberattacks but also brings the threat of these attacks to turn into comprehensive cyber warfare. Therefore, the more important the security of the geographical borders, the more important the security of electronic systems and the data stored there. Since the most important component of security is peace, it has taken its place in the literature as a very important concept in Cyber Peace in response to the negative perceptions of cyberwar, cyber terrorism and cybercrimes. For this reason, it is important to create a conceptual

* Corresponding author: mt.gencoglu@firat.edu.tr. ORCID: 0000-0000-0002-8784-9634

basis of cyber peace and contribute to this field to create a defense mechanism based on peaceful behavior in cyberspace.

The World Federation of Scientists has placed the concept of Cyber Peace at the center of its studies for the last few years, and the International Telecommunication Union (ITU) has been striving to make the concept more concrete with its recent and supported studies. One of the steps taken to ensure cybersecurity in the international arena is the "Paris Call for Trust and Security in Cyberspace" signed in November 2019. Among the supporters of the agreement, the majority of which are private sector organizations, are 67 states as well as 139 international institutions and non-governmental organizations. Although it is a comprehensive and positive step in the field of cybersecurity, the fact that countries with strong cybersecurity infrastructure such as the United States, Russia, Britain and Israel have not signed the agreement, the agreement has the nature of a declaration and the lack of sanction power raises questions about its effectiveness, but civil society is involved in the issue. It is of vital importance for the future of the subject.

The most striking developments in the field of cyber peace are; There are foundations and organizations established to ensure security in the cyber world. One of the last examples of initiatives developed against cyberattack threats is the Cyber Peace Institute, which was established in Geneva in September 2019. Established under the leadership of technology giants such as Microsoft, Hewlett Foundation and MasterCard, the main purpose of the institute is to make the internet a more stable and secure space. Although it was founded by the aforementioned technology giants, the institute is completely independent and set out with the slogan "Towards a safer online world for all", the institute's main strategies include helping civilian victims of cyber attacks, investigating and analyzing cyberattacks In addition to ensuring the establishment of international laws and norms in the field of cybersecurity. Declaring that it will support civilians who are in the most vulnerable position against cyber attacks, the institute will fill this serious gap in the field.

One of the few organizations working on cybersecurity is the Cyber Peace Foundation of India. I guess it would not be wrong to say that the foundation is the most active non-governmental organization in the field. The Foundation is a very successful example of a social enterprise model in the field of cybersecurity, with its work in different fields. Founded in 2013 under the leadership of a young entrepreneur, Vineet Kumar, the foundation conducts international studies in addition to India and also produces its policies based on the Sustainable Development goals of the United Nations. Kumar defines the foundation's main founding purpose as "to create a civil society movement against the proliferation of state-sponsored cyber attacks and cyber weapons"[4]. Cyber Peace Alliance and Cyber Peace Corps are two of the foundation's most important initiatives. The alliance, established in partnership with the Indiana University Ostrom Workshop, the Cyber Security and Internet Governance Program, and the Cyber Peace Foundation, was established to look at the concepts of cyber peace and cybersecurity from an interdisciplinary perspective and to conduct various researches. The Cyber Peace Union is a network of volunteers of the foundation and is called the "Volunteers Battalion" by Kumar. These volunteers work to help people of all ages who need cybersecurity in different areas[4].

In addition to these initiatives; Two initiatives such as the Cyber Security Technology Agreement (Cyber Security Tech Accord), signed under the leadership of Microsoft, and the Charter of Trust, which was initiated under the leadership of Siemens and signed during the 2018 Munich Security Conference, can be mentioned as important developments in this field.

Nations should try to reduce the emerging cyber arms race by establishing a foundation of trust. The international community has taken useful steps in this direction, for example, with the European Convention on Cybercrime, the UN report on cybersecurity that requires a series of actions to make information infrastructures more secure.

1.2. Literature Review

When the subject is scrutinized academically, there are quite a few valuable studies;

In Bloom and Saveg's studies; They emphasized that focusing on reducing national and international risk while discovering all cyber capabilities would be the best deterrent method against cyber conflict[5]. As Akatyev; emphasized the need for cyber peacekeeping and defined cyber peacekeeping goals[6]. Lynn emphasized the complexity and rapidly changing environment of cyberspace, highlighting the importance of coordinated and rapid response to threats for cyber peace [7]. Cahill, et al. Analyzed some principles, possible applications and technologies of cyber peacekeeping [9]. Kleffner and Dinnis examined the international legal aspects of cyber activity in cyber peacekeeping operations[10]. Şahin examined cyber peace as an alternative concept in the light of liberalism and realism[11].

2. Peace

Peace is not an unattainable goal; rather, it is a negotiation between the rights, lives, well-being and safety of each individual concerning others. This is not a hard-won war either, for then it would be the imposition of someone else's will on another, and that would be victory, not peace.

Generally, the concept of peace is interpreted both positively and negatively. On the positive side; It means good governance, regular resolution of conflict, harmony, gentleness and love. On the negative side; the absence of anything means the absence of chaos, tension, conflict and war [2]. By achieving positive cyber peace and eliminating structural forms of cyber violence, many of the challenges today can be addressed.

In the creation of a culture of peace and peace, not only the use of force and non-violence but also a common set of values, behavior patterns, laws, positive-dynamic-participatory processes should be established in the international arena. It is also vital to promote freedom, justice, democracy, tolerance, solidarity, cooperation, pluralism, cultural diversity, dialogue, understanding and conflict resolution. It is particularly important to create a cyber context in which the preconditions for peace, such as respect for everyone's right to freedom of expression, opinion and information, are particularly important, as well as the much-emphasized moral aspects of peace.

When viewed from this angle; Instead of finding another analogy of "what cyberspace looks like" or discussing how much individuals or firms can "back down", it would be better to start by examining the structure of cyberspace, and the types of violence that can occur in and through cyberspace. Only in this way is it possible to solve problems at their source. With the concept of Cyber Peace, the establishment of the universal order of cyberspace is aimed at as the basic principle. However, a basic definition still needs to be made.

In August 2019, the World Federation of Scientists, based on the Erice declaration, which determines certain actions and obligations to ensure peace and stability in the cyber field, determined the basic operational elements of cyber peace as follows;

1. The free circulation of information and ideas guaranteed by international law to individuals also applies to cyberspace. Restrictions should be within the legal process and to the extent necessary.

2. All countries should work together to develop a common code of cyber conduct and a harmonized global legal framework, including provisions on judicial investigation cooperation that respects confidentiality and human rights.

3. All users, service providers, and governments should work to prevent the use of cyberspace, especially young and vulnerable users, in a way that could lead to violence or exploitation.

4. The private sector, including governments, organizations, and individuals, should implement and maintain comprehensive security programs that leverage privacy and security technologies based on internationally accepted best practices and standards.

5. Software and hardware developers should strive to improve resilience and develop secure technologies that are resistant to vulnerabilities.

6. Governments should actively participate in the efforts of the United Nations to support global cybersecurity and cyber peace, as well as prevent the use of cyberspace for conflict.

If the concept of cyber peace is taken seriously, first of all, a legal framework should be determined to define what violates peace. They must undertake that they will not launch the first cyberattack and will not go unpunished by the cyber terrorists and attackers in their country. In addition, these commitments can include non-attack on critical national infrastructures, particularly those that serve basic humanitarian needs, and the inviolability of cross-border data networks. However, to be realistic; Such strategies and principles designed to promote cyber peace are likely to be sabotaged by countries with cyberwar potential. It will create distrust for other countries. At this point, when the current reports such as the systematic armament of cyberspace and the development of cyber-attack strategies are examined, the trust environment is problematic. Therefore, decisive enforcement action is needed to contribute to cyber peace, cyber stability and fundamental rights.

Cyber peace; aggression, counterattack, and retaliation should not be completely indispensable but should include feasible scenarios. The keyword here should be a restriction. A rigorous, ongoing threat and risk analysis should be carried out to prevent uncontrollable consequences, including the careful protection of humanitarian and socially indispensable critical infrastructures.

It is necessary to define cyber peace from both aspects of peace. Because we cannot define it simply by the absence of conflict and war; The reason is that these elements are not seen in the digital space. Therefore, in cyber peace, it is necessary to define the stable peace zone first. The region where peace is maintained based on mutual and consensus is called a stable peace zone. Sustainable, safe and flexible systems should be established to ensure peace in this region.

For the time being, a peaceful situation in cyberspace does not seem possible. However, if cooperation and trust between actors can be increased, a positive atmosphere can be created towards a stable peace environment. Action should be taken to stabilize cyberspace and reduce the potential effects of hostile actions.

Cyber peace can be achieved. Since human beings have created technology, human beings can find technological solutions to certain problems themselves. Man can find humane solutions to his problems. Cybersecurity and cyber peace are two sides of the same coin and should therefore be handled together.

2.1. Cyber Peace

It is a universal cyberspace order built on a healthy state of peace, disorder or discomfort and the absence of violence [1].

The International Telecommunications Union (ITU) has accelerated the work by pioneering some of the first studies in this field by defining cyber peace as a "universal cyberspace" system built on a "healthy state" in part. Based on these studies, we can define cyber peace as follows;

It is a regime that respects human rights, spreads internet access with best practices, promotes multi-stakeholder cooperation and prepares the ground for reducing the risk of cyberwar with a new cybersecurity approach that strengthens governance mechanisms.

Based on this definition; By helping to reduce the threats of cyber conflict, crime and espionage to comparable levels, by making clear the rules for companies and governments, it is possible to say that a multilevel network of regimes that promotes global, fair and sustainable security can only be built with cyber peace.

2.1.1. Ways to Achieve Cyber Peace

Although it seems unlikely that cyber warfare and conflicts can be prevented completely soon, it may be possible to reduce the likelihood and impact of conflicts and to move from a negative peace state to a stable state of peace. Namely;

- This Will lead to some degree of restriction on the attack as all stakeholders are interconnected
- Internet protocols are in place and will contribute to peace as they are widely accepted.
- The presence of defense organizations trying to increase Internet security and stability will contribute to the formation of a peaceful environment as it will provide an advantage in forming supranational groups.

Their offensive capabilities are also a deterrent in maintaining a stable peace. Because the attacker is afraid of retaliation, defensive measures reduce the likelihood of a successful attack. The two most important components of a stable cyber peace are flexible security and trust.

Technically flexible security is the most important factor that helps reduce the likelihood and impact of digital attacks. The higher the impact of this factor, the more reliable the infrastructure will be. Trust is an important component of collaboration for actors in the digital space. Based on security and trust, it is possible to exclude the risk of attack against government primary attacks. Because there are protocols, processes and agreements that create stable peace [2].

It is time to make critical decisions to change the world's cyber defense approach and provide viable solutions to the challenges it faces in cyberspace. For this reason, raising awareness of all individuals in the field of cyber peace requires the efforts of all sectors. On the other hand, there is a need for international and binding legal regulations that will prevent cyber attacks from being instrumentalized by states. Civil society has to undertake important tasks to create the necessary pressure tools for this to happen.

Establishing and maintaining cyber peace can be as challenging as starting a cyberwar. Because defining and promoting cyber peace is not as easy as it seems. However, all stakeholders should engage in a constructive dialogue, harmonizing different approaches to governance and ensuring a collaborative environment that is critical to achieving a point between internet sovereignty and freedom that both respects human rights and guarantees vital systems. However, by preparing the ground for cyber peace with these initiatives, cyberwar can be stopped before it starts [3].

3. Cyber Peace Protection

Cyber Peace Preservation is essential to protect an increasing number of people in cyberspace, establish inter-state arbitration to help prevent the escalation of cyber conflicts, and help build and maintain trust and openness.

Cyber Peace Protection is defined as rehabilitation that focuses on civil security by preventing, mitigating, later limiting and mitigating cyber conflict [6].

Cyber Peacekeeping works to promote online safety and security following international laws and treaties, whose main purpose is to protect civilians. A framework should be put forward to maintain permanent conditions of peace in cyber and physical areas affected by potential threats in cyberspace. Certain roles should be defined at different stages of peace conditions.

Each role of Cyber Peacekeeping can contribute to the safety and security of cyberspace at three different stages of a conflict, the absence of conflict, during and after conflict. Namely; monitoring potential threats when there is no conflict. It can be explained as stopping the spread of cyberattacks during conflict and as a last measure the creation of cyberweapons that respond with counter-attacks [8]. The relationships between roles, goals, and functions are shown below (Fig. 1).

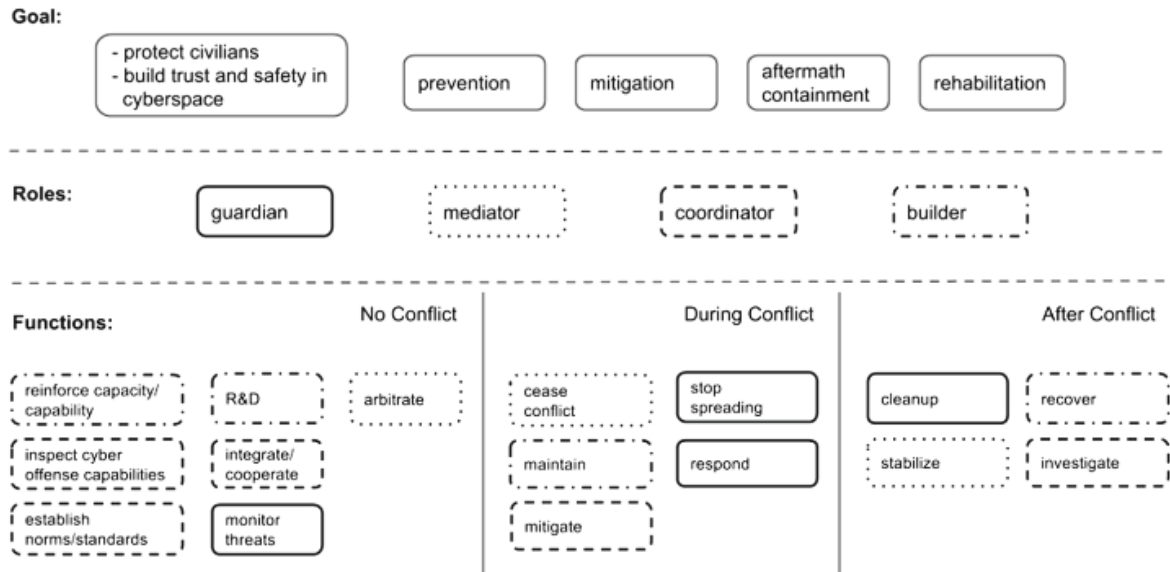


Fig. 1. Different stages of the conflict in cyber peacekeeping and the relationships between them [6]

We can say that there are generally eleven different activities carried out in the UN peacekeeping operation [12]. These activities are shown in the figure below (Fig. 2). Peacekeeping operations are the practical measure by which the UN fulfills this task and is the rationale for establishing peacekeeping operations [8]. If cyberwar threatens international peace and security, the UN should act on peacekeeping duty.

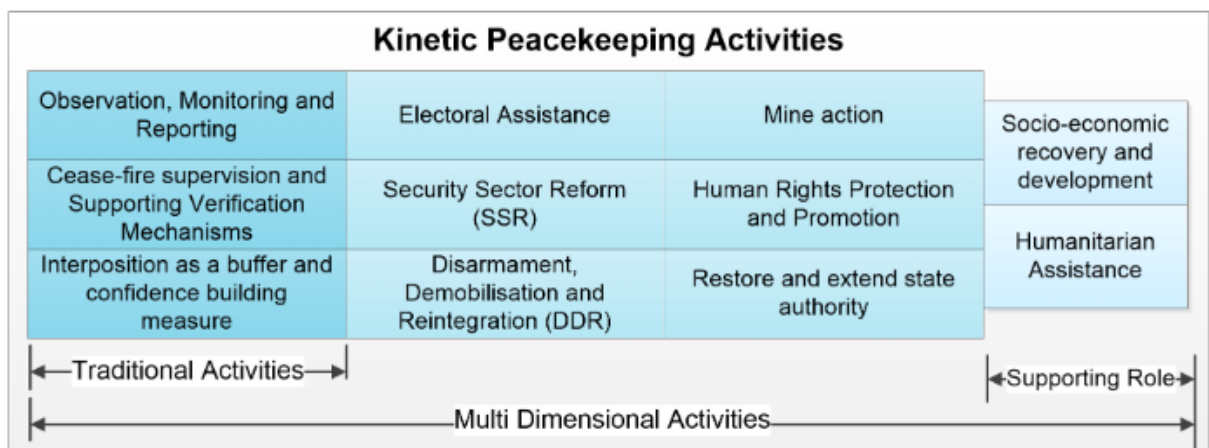


Fig. 2. Peacekeeping activities [13]

Cyber peacekeeping will be necessary for the future, and it is now important to define what cyber peacekeeping means. This is not simple, as to how to define peacekeeping is a constant source of debate [8]. To simplify the work, we can take the definition of the UN made; "The action taken in places where the conflict is

stopped to preserve the peace, even though it is fragile, and to help implement the agreements reached by the peacekeepers"[14].

3.1. The Challenges of Keeping Cyber Peace

Several challenges will be faced in maintaining cyber peace. However, it is necessary to consider both technical and political difficulties. It would be worth further researching the potential for resistance and how to overcome it.

Providing the required number of peacekeepers is a challenge in itself. Today's UN operations are carried out with the contribution of full-time UN staff and soldiers and experts from UN member states. However, it is also necessary to evaluate resources such as cybersecurity experts from the private sector and voluntary organizations.

There are probably many more obstacles. Each activity concluded to be necessary and feasible requires further investigation to discover where the additional barriers are and how to resolve them.

4. Conclusion and Recommendations

As a first step in reducing the risk of conflict, each country should make an internal assessment of their exposure to attack. First, critical infrastructure areas need to be studied thoroughly and clearly. Second, steps must be taken to improve the security of hardware and software. Third, it is necessary to work with other countries to share knowledge and establish norms of behavior, especially in times of crisis.

Cyber peace can be sustained not through disarmament, but risk reduction combined with the modernization of each rival country's attack and defense capacity. Organizations and individuals who believe that maintaining the status quo is in their interest will pose significant obstacles to reducing cyber risk. Innovative mechanisms will be required to overcome this organizational and individual resistance. Organizing these mechanisms around principles of behavior such as amnesty, community, internal transparency, competition, globalization, enforcement and international norms would be a good model for the change required to secure cyberspace. As this model requires extensive cooperation, states should be held directly responsible.

Cyber peacekeeping is a very difficult issue, but the fact that cyberspace hosts activities such as terrorism, espionage and war reveal the need for a practical solution. Cyber Peacekeeping is still a new and untested idea. Future work should be shaped by feedback from potential stakeholders.

While there is no need to maintain cyber peacekeeping today, it is clear that it will be needed shortly as cyber warfare becomes more common. Since operating in cyberspace will be an increasing necessity to keep the peace, official, private and voluntary organizations should take a more active role.

For Cyber Peace, you need to be ready for Cyber War!

References

- [1] Hamadoun, I. T. The Quest For Cyber Confidence, 77, 2011.
- [2] Inversini, R. Cyber Peace: And How It Can Be Achieved, The Ethics of Cybersecurity, Christen, M., Gordijn, B. ve Loi, M. (Ed.), 259-276, 2020.
- [3] Shackelford, S. J. Managing Cyber Attacks in International Law, Business, and Relations: In Search of Cyber Peace. Cambridge University Press, 2014.
- [4] Çakır, M. N. Siber Güvenlik İnisiyatifleri ve Sivil Toplum, 2019. <https://www.sivilsayfalar.org/tag/siber-baris-enstitusu/>
- [5] Bloom, L. Savag, J. E. On Cyber Peace. Atlantic Council, 2011.
- [6] Akatyev, N. Cyber Peacekeeping, Digital Forensics and Cyber Crime, 126-139, 2015.
- [7] Lynn III, W. J. Defending a new domain: the pentagon's cyber strategy. External Affairs, 89, 97–108, 2010.
- [8] Bellamy, A. and Williams, P. Understanding Peacekeeping. Polity, 2010.
- [9] Cahill, TP, Rozinov, K., Katir, C. : Cyber Warfare Peacekeeping, s. 100. In: Proceedings of the 2003 IEEE Workshop on Information Assurance, 2003.
- [10] Kleffner, JK, Dinnis, H.H. A. Cyber peacekeeping: international legal aspects of cyber activity in peacekeeping operations. International Law Studies. 89, 1, 2013.
- [11] Keskin, Ş. Realizm Ve Liberalizm Işığında Siber Savaş Ve Alternatif Bir Kavram Olarak Siber Barış'ın Değerlendirilmesi, TURAN-SAM Uluslararası bilimsel dergisi, 9(35), 287-297, 2017.
- [12] United Nations, United Nations Peacekeeping Operations: Capstone Doctrine. January 2008.
- [13] Robinson, M. Jones, K. Janicke, H and Maglaras, L. An Introduction to Cyber Peacekeeping, Senior Member, IEEE, 2017.
- [14] Mays, T. Historical Dictionary of Multinational Peacekeeping. Scarecrow Press, 2010.

Analysis of Mutated RNA-Type Breast Cancer Data with Machine Learning Methods

Rumeysa Hanife KARS^{1*}

¹ Biomedical Engineering, School of Engineering and Natural Sciences, Istanbul Medipol University, Istanbul, Turkey
*rhkars@st.medipol.edu.tr

(Geliş/Received: 13/07/2021;

Kabul/Accepted: 23/08/2021)

Abstract: According to the data for the year 2020, the three most common types of cancer in women are; breast, lung, and colorectal. These types of cancer make up 50% of other types of cancer seen in women. In addition, only breast cancer accounts for 30% of cancer types in women. Early diagnosis and treatment processes of breast cancer patients are important and the correct application of this process increases the survival rate of the patients. Artificial intelligence can contribute to the observational performance of radiologists in breast cancer screening. On the other hand, artificial intelligence-based approaches can also be used to increase the accuracy of digital mammography. The dataset used in this study consists of mutated RNA-type breast cancer data. The dataset includes the clinical and genetic characteristics of the patients. In the approach of the study, it is suggested to use various machine learning methods together. Support Vector Machines method has been decided the best performance with 97.55% in the analyzes performed. It has been observed that the recommended approach in the diagnosis of breast cancer gave successful results.

Key words: Artificial intelligence, Breast cancer, Machine learning, Mutation RNA

Mutasyona Uğramış RNA tipli Göğüs Kanseri Verilerinin Makine Öğrenme Yöntemleri ile Analizi

Öz: Kadınlarda görülen en yaygın üç kanser türü 2020 yılı verilerine göre; göğüs, akciğer ve kolorektaldır. Bu kanser türleri kadınlarda görülen diğer kanser türleri arasında %50'sini oluşturmaktadır. Ayrıca, kadınlarda görülen kanser türleri arasında yalnızca göğüs kanseri %30'unu oluşturmaktadır. Göğüs kanseri hastalarının, erken tanı ve tedavi süreçleri önemlidir ve bu sürecin doğru uygulanması hastaların hayatta kalma oranlarını artırır. Yapay zekâ, radyologların göğüs kanseri taramasındaki gözlemlene performanslarına katkı sağlayabilir. Öte yandan yapay zekâ tabanlı yaklaşımlar, dijital mamografinin doğruluğunu artırmak için de kullanılabilir. Bu çalışmada kullanılan veri kümesi mutasyona uğramış RNA tipi göğüs kanseri verilerinden oluşur. Veri kümesinde hastaların klinik özellikleri ile genetik özellikleri yer alır. Çalışmanın yaklaşımında çeşitli makine öğrenimi yöntemlerinin bir arada kullanılması önerildi. Gerçekleştirilen analizlerde en iyi performansı %97,55 oranında Destek Vektör Makineleri yöntemi verdi. Göğüs kanseri tanısında önerilen yaklaşımın başarılı sonuçlar verdiği gözlemlendi.

Anahtar kelimeler: Göğüs kanseri, Makine öğrenme, Mutasyon RNA, Yapay zekâ

1. Introduction

It is estimated that approximately 1.9 million people will have cancer in 2021 and it is predicted that approximately 608 thousand people will die from cancer patients. Today, breast cancer is the most common type of cancer detected in women, and it is the first cause of death due to cancer in such women. In addition, women living in the USA have an average of 13% risk of developing breast cancer [1]. Once breast cancer is detected early, the chances of survival will be very high. Specialists use certain tests to understand or cure breast cancer. Tests are used to find out if the cancer has spread to a body. Radiologists, on the other hand, are more active in mammography. Conditions such as these tests and treatment can take a lot of time and increase the workload of the doctor and radiologist. [2].

The use of Machine Learning (ML) and Deep Learning (DL) as tools in medical diagnosis has become a very useful application in breast cancer diagnosis [2]. ML methods can be used as an aid to radiologists struggling to improve cell detection performance in a cancer. Several new methods, including ML and DL, have been developed and applied to digital mammography. Preliminary research has shown that the aid of artificial intelligence systems to predict mammograms can increase the productivity of the radiologist in terms of time, specificity, and precision. These developed algorithms and tools have made the work of radiologists and doctors easier and reduced their workload [2].

Many studies have been carried out in the literature using the ML and DL approaches. In one study, they observed that the appropriate use of an AI tool increases the diagnostic efficiency of radiologists [3]. In another

* Corresponding author: rhkars@st.medipol.edu.tr. ORCID Number of authors: ¹ 0000-0002-2865-0414

study, they developed an artificial intelligence system that outperformed radiologists in the clinical processes of breast cancer detection [4]. They observed that the AI system produced more accurate and earlier results against scanning protocols. In another study, they observed a significant difference between the analyzes of radiologists and the analysis of the data obtained by the artificial intelligence-based system they developed. With their proposed approach, they reduced the heavy workload of radiologists and achieved successful results in the detection of cancer [5]. Dembrower et al. performed breast cancer classification on their mammograms with a cancer detector using artificial intelligence. They used machine learning methods in their study. Their proposed approach is able to interpret without radiologist evaluation [6]. The aim of this study is to obtain statistical results by analyzing features containing mutated RNA type breast cancer data and to achieve general success with artificial intelligence-based machine learning methods using this dataset.

2. Materials and Machine Learning Methods

2.1. Dataset

The dataset includes targeted sequencing data of 1,980 primary breast cancer samples. In addition, clinical features, m-RNA levels, z-score and gene mutations were examined for 1904 patients. The dataset contains 693 trait parameters for each patient, and their label groups have one of the values {text}, {number}, {positive, negative}, {0,1}, {0,1,2,3,4}. In addition, the “Status” parameter of breast cancer was used in the experimental analyses. There are two label values in the status parameter; “positive” and “negative”. If the patient’s status parameter is “positive”, the patient is breast cancer, otherwise the patient is not breast cancer [7].

Table 1. Parameters and label value of the patients that make up the dataset

The number of the feature	Original parameters available in the dataset	Label Value Type
1	Patient id	{numerical}
2	Age at diagnosis	{numerical}
3	Type of breast surgery	{text}
4	Cancer type	{text}
5	Cancer type detailed	{text}
6	Cellularity	{text}
7	Chemotherapy	{0,1}
8	Pam50 + claudin-low subtype	{text}
9	Cohort	{numerical}
10	Er status measured by ihc	{positive, negative}
11	Er status	{ positive, negative }
12	Neoplasm histologic grade	{numerical}
13	Her2 status measured by snp6	{text}
16	Hormone therapy	{0,1}
24	Mutation count	{numerical}
25	Overall survival months	{numerical}
30	Tumor size	{numerical}
31	Tumor stage	{0,1,2,3,4}
32	Death from cancer	{0,1}
33-693	Genetic features	{numerical, text}

The breast cancer status and count information used in the experimental analyzes are shown in Figure 1. Breast cancer status of 1459 patients is labeled as “positive” and status information of 445 patients is labeled as

“negative”. In addition, in all experimental analyzes of the dataset, 70% is reserved as training data and 30% is reserved as test data.

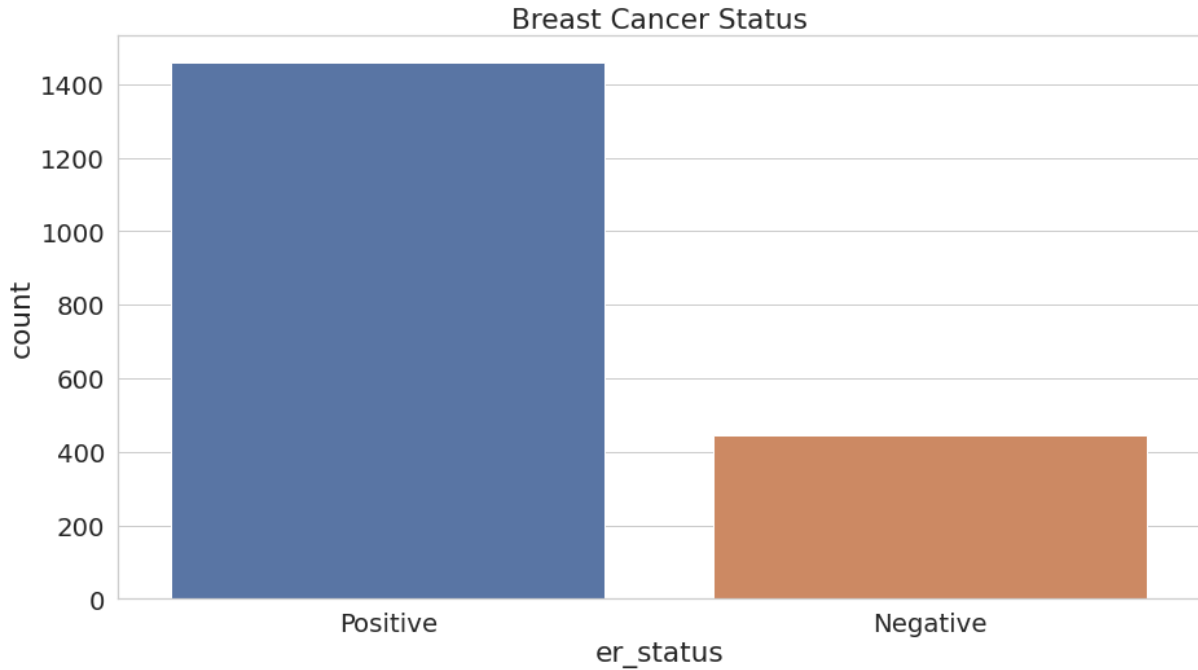


Figure 1. Breast cancer and census statistical information in the dataset.

2.2 Support Vector Machines Method

The Support Vector Machine (SVM) performs classification by finding the hyperplane that maximizes the margin between the two classes. The states that define the hyperplane are support vectors. The main purpose of SVM is to find the optimal hyperplane that linearly separates the data points in the two components by maximizing the margin [8]. It is still effective when the number of dimensions is greater than the number of samples. Another advantage of SVM is that there is a unique global minimum value if the data can be linearly separable. An ideal SVM analysis should produce a hyperplane that completely separates the vectors into two non-overlapping classes. However, perfect separation may not be possible or may result in a model in so many cases that the model cannot be correctly classified. In this case, the SVM finds the hyperplane that maximizes the margin and minimizes misclassifications. Hyper plane is calculated according to Eq. (1) and distance measurement between plane vectors is calculated according to Eq. (2) [9]. When the equations are examined; w is the vector in the hyperplane, b is the preset variable, x is the input vector, and T is the threshold value. The general design showing the operation of two-class data with the SVM method is shown in Figure 2.

$$H: wT(x) + b = 0 \quad (1)$$

$$\forall w \quad \forall^2 = \sqrt{w_1^2 + w_2^2 + w_3^2 + \dots w_n^2} \quad (2)$$

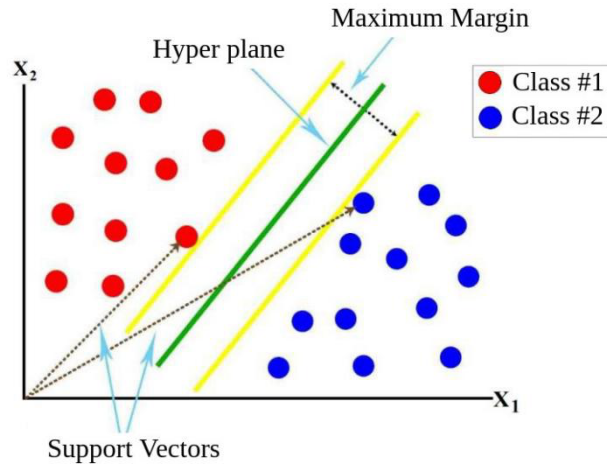


Figure 2. Classification process with SVM method [10].

2.3. Extreme Gradient Boosting Method

Extreme Gradient Boosting (EGB) is an open source approach that enables efficient and effective implementation of gradient boosting algorithm. This approach has led the applied machine learning community to move towards gradient boosting more generally. The EGB method is among the methods used to win solutions for classification and regression problems in machine learning competitions. In the AGA method, the gain parameter is used and it contributes to the transaction performance with this parameter. Gain parameter is calculated according to Eq. (3) and provides convenience in the partitioning process with an approach similar to the tree-root relationship in the classification process. The AGA method scales beyond billions of instances using far fewer resources than existing systems. The process of estimating the output value of the tree structure created in this method is calculated according to Eq. (4) [10].

$$Gain = Gain\ left + Gain\ right - root\ similarity \tag{3}$$

$$New\ prediction = First\ predicted\ value + Learning\ rate \times output\ value \tag{4}$$

2.4. Gradient Boosting Method

Gradient Boosting (GB) can produce a prediction model, typically in the form of a collection of weak prediction models such as decision trees; preferred machine learning method for solving classification and regression problems. This method is based on performing the processing steps by combining the best possible model approach with the previous model approaches, thus minimizing the overall estimation error. The outcome for each sample input in the dataset depends on how much the change in the prediction affects the overall prediction error. The steps to be applied in my classification process in the GB method are as follows;

- Placing a simple linear regression or decision tree on the data,
- Calculating error residuals according to Eq. (5),
- Placing a new model on the error residues as the target variable with the same input variables,
- Adding predicted residuals to previous forecasts,
- Placing another model on the remaining residues [11].

$$Error = True\ target\ value - predicted\ target\ value \tag{5}$$

2.5. Decision Tree Method

Decision tree (DT) is the popular machine learning method of choice for solving classification and prediction problems. DT is a flowchart-like tree structure where each internal node represents a test on an attribute, each branch represents a result of the test, and each leaf node holds a class label. The overall design of the KA is shown in Figure 3. Decision trees can handle both continuous and categorical variables. This method provides a clear indication of which areas are most important for forecasting or classification. As with all analytical methods, the decision tree method has limitations that users should be aware of. Its main disadvantage is that it may not work well, especially when using a small dataset. This problem may limit the generalizability and robustness of the emerging models [13].

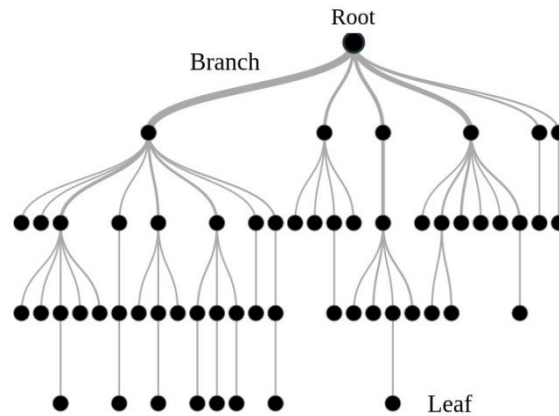


Figure 3. The general view of DT method [14].

2.6. Random Forest Method

Random Forest (RF) is a machine learning method that contains more than one decision tree in its algorithm structure. The overall design of the RF method is shown in Figure 4. To classify a new object from an input vector, insert the input vector into each of the trees in the forest. Each tree in the RF approach performs a classification and the result is calculated by performing voting. In the RF method, each input data chooses the classification with the most votes. This method generally works more efficiently on large datasets. The margin of error is important in calculating the efficiency, and in the RF method, the mean square error (MSE) formula given in Eq. (6) is used. In this equation; ,the variable N represents the number of data points, the variable f_i represents the value returned by the method. The actual value for each i in the data point is represented by the variable y_i . It also makes predictions about which variables are important in the classification, and the forests created are recorded for use in other data entries [15].

$$MSE = \frac{1}{N} \sum_{i=1}^N (f_i - y_i)^2 \quad (6)$$

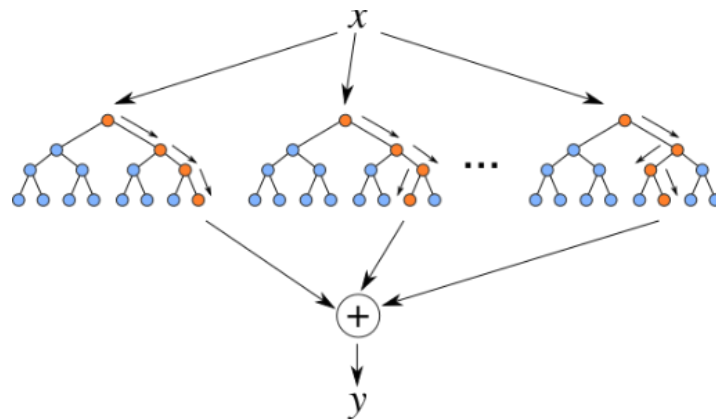


Figure 4. General representation of RT method [16].

3. Proposed Approach

The proposed method was used to determine the characteristics such as cancer status, age determination, cancer stage of breast cancer patients. The dataset contains mutated RNA type breast cancer data. To conclude the correlation between the proposed approach and the features in the mutated dataset with graphical analyzes and using machine learning methods, it is determined whether the patient has cancer or not. The overall design of the proposed approach is shown in Figure 5. Performance comparisons are made using SVM, EGB, GB, DT and RF methods, and the most appropriate method is determined to determine the patient's cancer status (Positive: Cancer-containing, Negative: Cancer-free).

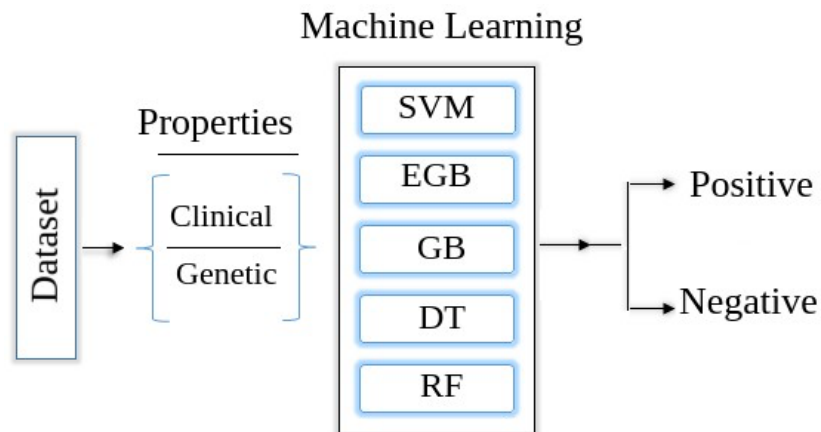


Figure 5. Design of the proposed approach.

4. Results

The analyzes of this study were carried out using the Google Colaboratory server installed on the Ubuntu-Linux operating system [17,18]. Python software language libraries (Sklearn, Numpy, Pandas) [19] were used for statistical analysis and Jupyter Notebook interface was used for compiling the codes. The confusion matrix was preferred as a criterion in the evaluation of breast cancer. The metric parameters of the confusion matrix are; accuracy, specificity, sensitivity and f-score. The formulas between Eq. (7) and Eq. (10) are used to calculate these metric parameters. For the validity and reliability of the analyzes, it is necessary to look at the True(T) and False(F) of positive (P), negative (N) decisions. The equations given below perform these operations [18,20].

$$\text{Sensitivity} = \frac{TP}{TP+FN} \tag{7}$$

$$\text{Specificity} = \frac{TN}{TN+FP} \tag{8}$$

$$\text{f score} = \frac{2 \times TP}{2 \times TP + FN + FP} \tag{9}$$

$$\text{Accuracy} = \frac{TP+TN}{TP+FP+TN+FN} \tag{10}$$

Experimental analyzes were carried out in two parts. In the first analysis, the statistical information of the dataset was extracted and some clinical-genetic features were used for this. The open source codes were compiled using the "seaborn" library and the results obtained in the first analysis are shown in Figure 6. Figure 6 shows the four trait parameters and their correlation with patient conditions. The incidence of breast cancer increases with age. Mutation amounts were observed to be more effective in patients with positive cancer status. Tumor size was not observed to be affected by positive and negative cases. Finally, tumor stages have been observed to be effective in positive cases.

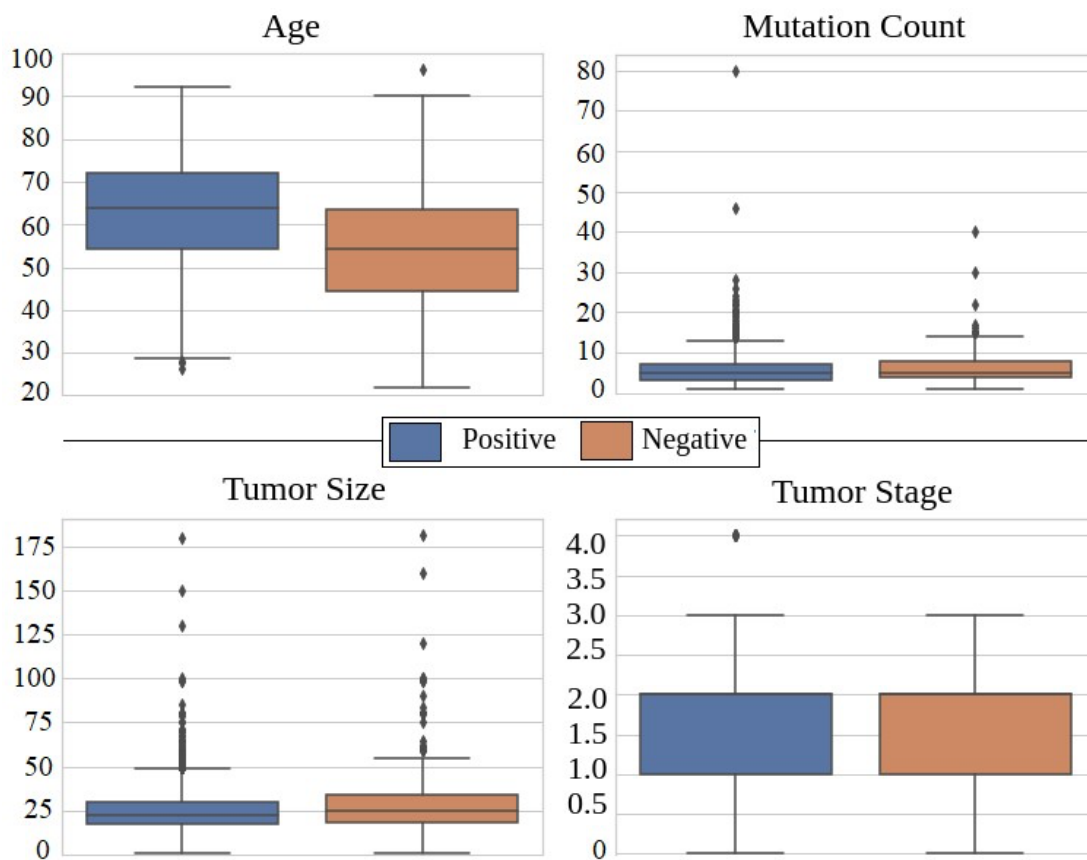


Figure 6. Statistical results of the dataset using some clinical-genetic features.

In the second analysis of the experiment, machine learning methods (SVM, EGB, GB, DT and RF) were used to determine whether the patients had breast cancer or not. The open source codes of the “Sklearn” library were used in machine learning methods and the preferred parameters in this study are the default values. The confusion matrix graphs obtained as a result of the second analysis are shown in Figure 7. Accordingly, 97.55% with the SVM method; 96.32% with EGB and GB methods; An accuracy rate of 92.65% was obtained with the DT method and 94.75% with the RF method. The SVM method provided the best performance in the recommended approach. With the SVM method, the sensitivity of the data with negative disease status was 93.83%; specificity success was 98.82% and f-score success was 95.13%. With the SVM method, the sensitivity of the data with positive disease status was 98.82%; specificity success of 93.83%; f-score success was 98.36%. The success information of the metric parameters obtained from the confusion matrices are given in Table 2.

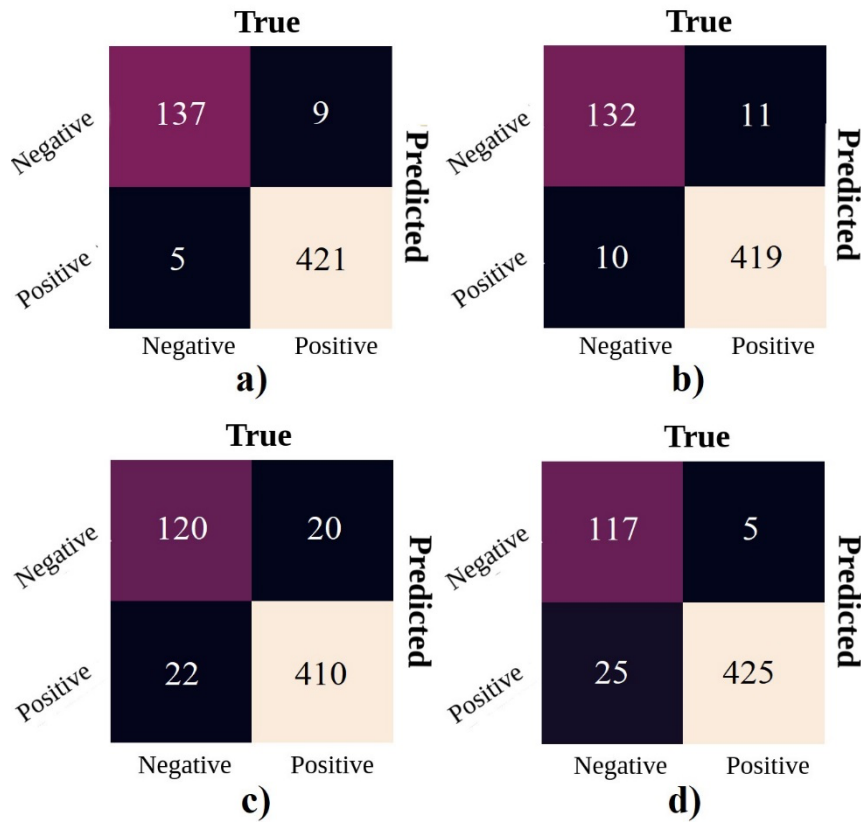


Figure 7. In the proposed approach, confusion matrices obtained by machine learning methods; a) SVM, b) EGB and GB, c) DT, d) RF.

Table 2. Analysis from confusion matrices of breast cancer (%).

Method	Class	Sensitivity	Specificity	f-score	Accuracy
SVM	Negative	93,83	98,82	95,13	97,55
	Positive	98,82	93,83	98,36	
EGB	Negative	92,30	97,66	92,63	96,32
	Positive	97,66	92,30	97,55	
GB	Negative	92,30	97,66	92,63	96,32
	Positive	97,66	92,30	97,55	
DT	Negative	85,71	94,90	85,10	92,65
	Positive	94,90	85,71	95,12	
RF	Negative	95,90	94,44	88,63	94,75
	Positive	94,44	95,90	96,59	

5. Discussion

Breast cancer is a disease that is frequently seen among women and causes an increase in the number of cases worldwide every year. To benefit from technological stakeholders in the diagnosis of this disease; It is important to increase the rate of accurate and fast decision making in early diagnosis processes. In this study, analyzes were performed using mutated breast cancer data. The use of various machine learning methods in the proposed

approach has given us an advantage over the analysis of datasets with different characteristics. Thus, analyzes were carried out without relying on a single machine learning method. I achieved the best performance with the SVM method in mutated breast cancer data. The disadvantage of the proposed approach is that it does not have an end-to-end algorithm. The analyzes of different studies that performed analyzes using the dataset are given in Table 3.

Table 3. Results of studies using the same dataset.

Study	Year	Method	Accuracy (%)
Felonneau et al. [21]	2018	Radial Basis Function (RBF)	66,20
Proposed Method	2021	SVM	97,55

In one study, they performed analyzes using two methods. These methods are; It was RBF and SVM. They also used different datasets in their study and presented a pipeline tool for easier analyzes across diseases on other datasets [21]. The analysis results were more productive than the work of Felonneau et al. In order for them to increase their classification success, they should have used various machine learning methods in experimental analysis. In addition, it cannot be said that the parameter values and optimization methods they use affect the classification results positively. The SVM method used in our study provided convenience for data that are not regularly distributed and whose distribution is unknown. As a result of this situation, an accuracy rate of 97.55% was achieved.

In this article, higher rate of accuracy has been achieved when it is compared to the work of Felonneau et al. bu utilizing SVM method. Machine learning methods have contributed to this kind of success. Importantly, SVM method gave the highest rate of success after investigating the dataset.

6. Conclusion

According to studies, the most common type of cancer in women is breast cancer. Thousands of women die every year because of this situation. In order to prevent this situation and to facilitate the work of doctors and radiologists, various artificial intelligence applications are being developed. Recently, interest in the classification of cancer datasets with deep learning methods has increased. In this study, mutated RNA type breast cancer data were examined. For this purpose, five different machine learning models were used to evaluate whether the patient had breast cancer, and criteria such as age, number of mutations, and tumor stage were examined. According to the results obtained, the SVM machine learning method came to the fore by showing the highest performance. Using this method, a success rate of 97.55% is achieved. In this study, the availability of statistical results by data analysis and the general success of general success with artificial intelligence-based machine learning methods were investigated using this dataset.

References

- [1] R.L. Siegel, K.D. Miller, H.E. Fuchs, A. Jemal, *Cancer Statistics, 2021*, CA: A Cancer Journal for Clinicians. 71 (2021) 7–33. <https://doi.org/10.3322/caac.21654>.
- [2] A. Aloraini, *Different Machine Learning Algorithms for Breast Cancer Diagnosis*, International Journal of Artificial Intelligence & Applications. 3 (2012) 21–30. <https://doi.org/10.5121/ijaia.2012.3603>.
- [3] S. Pacilè, J. Lopez, P. Chone, T. Bertinotti, J.M. Grouin, P. Fillard, *Improving Breast Cancer Detection Accuracy of Mammography with the Concurrent Use of an Artificial Intelligence Tool*, Radiology: Artificial Intelligence. 2 (2020) e190208. <https://doi.org/10.1148/ryai.2020190208>.
- [4] S.M. McKinney, M. Sieniek, V. Godbole, J. Godwin, N. Antropova, H. Ashrafian, and et al. *International evaluation of an AI system for breast cancer screening*, Nature. 577 (2020) 89–94. <https://doi.org/10.1038/s41586-019-1799-6>.

- [5] I. Sechopoulos, J. Teuwen, R. Mann, Artificial intelligence for breast cancer detection in mammography and digital breast tomosynthesis: State of the art, *Seminars in Cancer Biology*. (2020). <https://doi.org/10.1016/j.semcancer.2020.06.002>.
- [6] K. Dembrower, E. Wåhlin, Y. Liu, M. Salim, K. Smith, P. Lindholm, M. Eklund, F. Strand, Effect of artificial intelligence-based triaging of breast cancer screening mammograms on cancer detection and radiologist workload: a retrospective simulation study, *The Lancet Digital Health*. 2 (2020) e468–e474. [https://doi.org/10.1016/S2589-7500\(20\)30185-0](https://doi.org/10.1016/S2589-7500(20)30185-0).
- [7] B. Pereira, S.F. Chin, O.M. Rueda, H.K.M. Vollan, and et al., The somatic mutation profiles of 2,433 breast cancers refines their genomic and transcriptomic landscapes, *Nature Communications*. 7 (2016) 1–16. <https://doi.org/10.1038/ncomms11479>.
- [8] M. Marjanović, M. Kovačević, B. Bajat, V. Voženilek, Landslide susceptibility assessment using SVM machine learning algorithm, *Engineering Geology*. 123 (2011) 225–234. <https://doi.org/10.1016/j.enggeo.2011.09.006>.
- [9] T. Shon, Y. Kim, C. Lee, J. Moon, A machine learning framework for network anomaly detection using SVM and GA, in: *Proceedings from the 6th Annual IEEE System, Man and Cybernetics Information Assurance Workshop, SMC 2005*, 2005: pp. 176–183. <https://doi.org/10.1109/IAW.2005.1495950>.
- [10] Support Vector Machine Machine learning algorithm with example and code - Codershood, (n.d.). <https://www.codershood.info/2019/01/10/support-vector-machine-machine-learning-algorithm-with-example-and-code/> (accessed February 17, 2021).
- [11] A. Ibrahim Ahmed Osman, A. Najah Ahmed, M.F. Chow, Y. Feng Huang, A. El-Shafie, Extreme gradient boosting (Xgboost) model to predict the groundwater levels in Selangor Malaysia, *Ain Shams Engineering Journal*. (2021). <https://doi.org/10.1016/j.asej.2020.11.011>.
- [12] A. Natekin, A. Knoll, Gradient boosting machines, a tutorial, *Frontiers in Neurorobotics*. 7 (2013). <https://doi.org/10.3389/fnbot.2013.00021>.
- [13] Y.Y. Song, Y. Lu, Decision tree methods: applications for classification and prediction, *Shanghai Archives of Psychiatry*. 27 (2015) 130–135. <https://doi.org/10.11919/j.issn.1002-0829.215044>.
- [14] An Introduction to Machine Learning, (n.d.). <https://bioinformatics-training.github.io/intro-machine-learning-2017/decision-trees.html> (accessed February 18, 2021).
- [15] K. Fawagreh, M.M. Gaber, E. Elyan, Random forests: from early developments to recent advancements, *Systems Science & Control Engineering*. 2 (2014) 602–609. <https://doi.org/10.1080/21642583.2014.956265>.
- [16] Random Forest Regression. Random Forest Regression is a... | by Chaya Bakshi | Level Up Coding, (n.d.). <https://levelup.gitconnected.com/random-forest-regression-209c0f354c84> (accessed February 18, 2021).
- [17] T. Carneiro, R.V.M. da Nobrega, T. Nepomuceno, G. bin Bian, V.H.C. de Albuquerque, P.P.R. Filho, Performance Analysis of Google Colaboratory as a Tool for Accelerating Deep Learning Applications, *IEEE Access*. 6 (2018) 61677–61685. <https://doi.org/10.1109/ACCESS.2018.2874767>.
- [18] S. Walker, W. Khan, K. Katic, W. Maassen, W. Zeiler, Accuracy of different machine learning algorithms and added-value of predicting aggregated-level energy performance of commercial buildings, *Energy and Buildings*. 209 (2020) 109705. <https://doi.org/10.1016/j.enbuild.2019.109705>.
- [19] GitHub - scikit-learn-contrib/sklearn-pandas: Pandas integration with sklearn, (n.d.). <https://github.com/scikit-learn-contrib/sklearn-pandas> (accessed February 21, 2021).
- [20] D. Chicco, G. Jurman, The advantages of the Matthews correlation coefficient (MCC) over F1 score and accuracy in binary classification evaluation, *BMC Genomics*. 21 (2020) 1–13. <https://doi.org/10.1186/s12864-019-6413-7>.
- [21] G. Dubourg-Felonneau, T. Cannings, F. Cotter, H. Thompson, N. Patel, J.W. Cassidy, H.W. Clifford, A Framework for Implementing Machine Learning on Omics Data, *ArXiv*. (2018) 1–5.

The Characterizations Of Null Quaternionic Curves In Minkowski 3-Space

Şeyda ÖZEL^{1*}, Mihriban ALYAMAÇ KÜLAHÇI², Mehmet BEKTAŞ³

^{1,2,3} Mathematics, Faculty of Science Firat Universty, Elazığ, Turkey

*¹ s_demir2323@outlook.com, ² mihribankulahci@gmail.com, ³ mbektaş@firat.edu.tr

(Geliş/Received: 16/03/2021;

Kabul/Accepted: 23/08/2021)

Abstract: In this study, we investigate some characterizations of null quaternionic curves in the Minkowski 3-Space. Also, we research the characterizations of Null quaternion curves in Minkowski 3-Space.

Key words: Null Quaternionic curves, Serret-Frenet formula, Helices, Slant Helices.

Minkowski 3-Uzayda Null Kuaterniyonik Eğrilerin Karakterizasyonları

Öz: Bu çalışmada, Minkowski 3-uzayda null kuaterniyonik eğrilerin bazı karakterizasyonları incelendi. Ayrıca, Minkowski 3-uzayda null kuaterniyonik eğrilerin karakterizasyonları çalışıldı.

Anahtar Kelimeler: Null Kuaterniyonik Eğriler, Serret-Frenet Formülleri, Helis, Slant Helis

1. Introduction

The curve theory has been one of the most tried topics owing to existing a lot of implementation fields from geometry to the different twigs of science. Most mathematicians study the private curves like Bertrand and Mannheim curves. Lately, they have defined a new special curve named Smarandache curve in Minkowski 3-space time by Turgut and Yılmaz [1].

Quaternions were first defined by Irish Mathematician William Rowan Hamilton in 1843. Hamilton said that his adaptation was a generalization in which the real (scalar) axes were unaltered but completed by adding the vector in 1843. The Serret-Frenet formulas of the Null Quaternionic curves by Çöken and Tuna were defined for the Semi-Euclidean spaces, in 2015 [2-3]. The quaternionic curves in \mathbb{E}^3 and \mathbb{E}^4 were described by Baharathi and Nagaraj and they also carried out studies on differential geometry of space curves and with the help of their studies on quaternions, they introduced Frenet frames and formulae [4]. There are some curves which are particular in differential geometry. Having a crucial role, these curves satisfy some connections between their curvatures and torsions. Described by characteristic that tangent of curve makes a constant angle with a stable straight line called the axis of the general helix. Moreover, lately slant helix have been identify as a special curve [5]. Some characterizations of slant helices in Euclidean 3-space were analyzed by Kula and et al. [6].

In this study the characterizations of null quaternionic curves in Minkowski 3-space were analyzed. Also the characterizations of a null quaternionic curve to be helix, slant helix were given.

2. Preliminaries

In this part, we impart fundamental notions connected to the semi-real quaternions [2]. A series of semi-real quaternion is representable by

$$Q = \{q \mid q = ae_1 + be_2 + ce_3 + d; a, b, c, d \in \mathbb{R}\},$$

where

$$e_1, e_2, e_3 \in \mathbb{E}_1^3, h(e_i, e_i) = \varepsilon(e_i), 1 \leq i \leq 3$$

and

$$e_i \times e_i = -\varepsilon(e_i), \\ e_i \times e_j = \varepsilon(e_i)\varepsilon(e_j)e_k \in \mathbb{E}_1^3.$$

The cross product of semi-real quaternions for vectors p and q are described by

* Corresponding author: s_demir2323@outlook.com ORCID Number of authors: ¹ 0000-0002-1519-2418, ² 0000-0002-8621-5779, ³ 0000-0002-5797-4944

$$p \times q = S_p S_q + S_p V_q + S_q V_p + h(V_p, V_q) + V_p \wedge V_q.$$

In this place, we used scalar and vector products defined in \mathbb{E}_1^3 . To a semi real quaternion $q = ae_1 + be_2 + ce_3 + d$, conjugate αq of q and scalar product h_1 are denoted as $\alpha q = -ae_1 - be_2 - ce_3 + d$ and

$$h(p, q) = \frac{1}{2} [\varepsilon(p)\varepsilon(\alpha q)(p \times \alpha q) + \varepsilon(q)\varepsilon(\alpha p)(q \times \alpha p)]$$

respectively.

\mathbb{E}_1^3 is described as the space of null spatial quaternions $\{\gamma \in Q_{\mathbb{E}_1^3} \mid \gamma + \alpha\gamma = 0\}$ in an obvious manner,

$$\gamma(s) = \sum_{i=1}^3 \gamma_i(s) \vec{e}_i, \quad 1 \leq i \leq 3.$$

Let $\{l, n, u\}$ be the frenet trihedron for the differentiable null spatial quaternionic curve in \mathbb{E}_1^3 , we took the e_2 as time-like vector. After that, Frenet formulae is

$$\begin{bmatrix} l' \\ n' \\ u' \end{bmatrix} = \begin{bmatrix} 0 & 0 & k \\ 0 & 0 & \tau \\ -\tau & -k & 0 \end{bmatrix} \begin{bmatrix} l \\ n \\ u \end{bmatrix},$$

where k and τ are first and second curvatures of null spatial quaternionic curve, respectively. Furthermore, $h(l, l) = h(n, n) = h(l, u) = h(n, u) = 0$, $h(l, n) = h(u, u) = 1$, n, l are null vectors; u is a space-like vector. In this place, the quaternion product is dedicated as

$$\begin{aligned} l \times n &= -1 - u, & n \times l &= -1 + u, & n \times u &= -n, & u \times n &= n \\ u \times l &= -l, & l \times u &= l, & u \times u &= -1, & l \times l &= n \times n = 0. \end{aligned}$$

3. Characterizations Of Null Quaternionic Curves In Minkowski 3-Space

In this part, we first examined some characterizations of null quaternionic curves in Minkowski 3-Space.

Definition 3.1.

The curve formed by making a fixed angle in a fixed direction is called a helix. If ratio $\frac{k_1}{k_2}$ is constant, it means that the curves are helix [7].

Theorem 3.2.

Let's take an α null quaternionic curve in \mathbb{E}_1^3 , at the time α is a common helix only if $\frac{k_1}{k_2}$ is fixed.

Proof. When α is treated as a common helix, the slope axis of the curve α is denoted as $sp\{A\}$. Note this

$$\langle l, A \rangle = \text{cons.}$$

If we differentiate both sides of the equality above, by then we have

$$\langle l', A \rangle = 0.$$

By using equations $l' = k \cdot u$ and $A = \cos \theta \cdot n + \sin \theta \cdot u$,

$$\begin{aligned} \langle k.u, A \rangle &= 0 \\ k \langle u, A \rangle &= 0, k \neq 0 \\ \langle u, A \rangle &= 0. \end{aligned}$$

If we differentiate both sides of the equality above;

$$\langle u', A \rangle + \langle u, A' \rangle = 0$$

Since derivative of the constant is zero, then;

$$\begin{aligned} \langle u', A \rangle &= 0 \\ \langle -\tau l - kn, \cos \theta n + \sin \theta u \rangle &= 0 \\ \langle -\tau l, \cos \theta n \rangle + \langle -\tau l, \sin \theta u \rangle + \langle -kn, \cos \theta n \rangle + \langle -kn, \sin \theta u \rangle &= 0 \\ -\tau \cos \theta \langle l, n \rangle - \tau \sin \theta \langle l, u \rangle - k \cos \theta \langle n, n \rangle - k \sin \theta \langle n, u \rangle &= 0. \end{aligned}$$

Here, since

$$\langle l, n \rangle = \langle l, u \rangle = \langle n, u \rangle = 0 \text{ and } \langle n, n \rangle = 1,$$

the following expression is obtained;

$$\begin{aligned} -k \cos \theta &= 0 \\ k \cos \theta &= 0 \end{aligned}$$

the result is as follow:

- Case i)** $k = 0 \Rightarrow \cos \theta \neq 0$
Case ii) $k \neq 0 \Rightarrow \cos \theta = 0.$

Definition 3.3.

A unit speed curve α is dubbed a slant helix if the function $\langle n(s), U \rangle$ is constant, for a non-zero fixed vector field $U \in \mathbb{E}_1^3$. It is difficult to describe the aspect between the two vectors (apart for that both vectors are of time-like) unlike in the \mathbb{E}^3 spaced, it is an important point. To this case, we can not comment on the slope between the usual vector field $n(s)$ and U [7].

Theorem 3.3.

Let α be a null quaternionic curve in \mathbb{E}_1^3 , in that case α is slant helix only if $\frac{k}{\tau}$ is fixed.

Proof. Let α be a slant helix in \mathbb{E}_1^3 , $\langle n(s), U \rangle$ is fixed. According to description we have, α is a slant helix. So

$$\langle n(s), U \rangle = \text{cons.}$$

If we differentiate the equations both sides, then we have

$$\langle n'(s), U \rangle + \langle n(s), U' \rangle = 0.$$

Since the derivative of the constant is zero, then

$$\langle n'(s), U \rangle = 0.$$

By using equations $n' = \tau u$, the following expression is obtained;

$$\begin{aligned} \langle \tau u, U \rangle &= 0 \\ \tau \langle u, U \rangle &= 0, \tau \neq 0 \\ \langle u, U \rangle &= 0. \end{aligned}$$

Here, if we differentiate the equations both sides, by then we have

$$\langle u', U \rangle + \langle u, U' \rangle = 0.$$

Since derivative of the constant is zero, then;

$$\langle u', U \rangle = 0.$$

By using equations $u' = -\tau l - kn$ and $U = \cos \theta n + \sin \theta u$

$$\begin{aligned} &\langle -\tau l - kn, \cos \theta n + \sin \theta u \rangle = 0 \\ \langle -\tau l, \cos \theta n \rangle + \langle -\tau l, \sin \theta u \rangle + \langle -kn, \cos \theta n \rangle + \langle -kn, \sin \theta u \rangle &= 0 \\ -\tau \cos \theta \langle l, n \rangle - \tau \sin \theta \langle l, u \rangle - k \cos \theta \langle n, n \rangle - k \sin \theta \langle n, u \rangle &= 0. \end{aligned}$$

Here, since $\langle l, n \rangle = \langle l, u \rangle = \langle n, u \rangle = 0$ and $\langle n, n \rangle = 1$, the following expression is obtained;

$$\begin{aligned} -k \cos \theta &= 0 \\ k \cos \theta &= 0. \end{aligned}$$

Case i) $k = 0 \Rightarrow \cos \theta \neq 0$ or

Case ii) $k \neq 0 \Rightarrow \cos \theta = 0$.

Theorem 3.4.

Let α be a null quaternionic curve in \mathbb{E}_1^3 , α is a slant helix only if

$$\det(u', u'', u''') = (-\tau'' + 2k\tau^2) \cdot (2k^2\tau + (-k)'') \cdot (-3\tau'k - 2k'\tau + (-k)''\tau).$$

Proof. Suppose that $\frac{k}{\tau}$ be constant. From $u' = -\tau l - kn$, we have

$$\begin{aligned} u' &= -\tau l - kn \\ u'' &= (-\tau)'l + (-\tau).l' + (-k)'n + (-k).n'. \end{aligned}$$

Here, if

$$l' = k.u, n' = \tau u \quad \text{and } u' = -\tau l - kn \text{ equals are used}$$

$$u'' = (-\tau)'l + (-\tau)ku + (-k)'n - k\tau u$$

$$u'' = -\tau'l - 2k\tau u + (-k)'n$$

$$\begin{aligned} u''' &= (-\tau)'l + (-\tau)l' - 2[(k\tau)'u + (k\tau)u'] + (-k)''n + (-k)'n' \\ &= (-\tau)'l + (-\tau)'ku - 2[k'\tau u + k\tau'u + k\tau(-\tau l - kn)] + (-k)''n + (-k)'(\tau u) \\ &= (-\tau)''l + (-\tau)'ku - 2k'\tau u - 2k\tau'u + 2k\tau^2 l + 2k^2\tau n + (-k)''n + (-k)''\tau u \\ &= (-\tau'' + 2k\tau^2)l + (2k^2\tau + (-k)'')n + ((-\tau)'k - 2k'\tau - 2k\tau' + (-k)''\tau)u \\ &= (-\tau'' + 2k\tau^2)l + (2k^2\tau + (-k)'')n + (-3\tau'k - 2k'\tau + (-k)''\tau)u. \end{aligned}$$

Thus, the following equation is obtained

$$\begin{aligned} \det(u', u'', u''') &= \begin{vmatrix} -\tau'' + 2k\tau^2 & 0 & 0 \\ 0 & 2k^2\tau + (-k)'' & 0 \\ 0 & 0 & -3\tau'k - 2k'\tau + (-k)''\tau \end{vmatrix} \\ &= (-\tau'' + 2k\tau^2)(2k^2\tau + (-k)'')(-3\tau'k - 2k'\tau + (-k)''\tau). \end{aligned}$$

Theorem 3.5.

Let γ be a null quaternionic curve in \mathbb{E}_1^3 , γ is cylindrical helix $\Leftrightarrow \frac{k}{\tau}$ is constant.

Proof. Let γ be a null quaternionic curve in \mathbb{E}_1^3 , $\frac{\tau}{k} = c$ constant and

$$\alpha = \frac{c}{\sqrt{1+c^2}}l + \frac{1}{\sqrt{1+c^2}}u.$$

$$\alpha' = \frac{c}{\sqrt{1+c^2}}l' + \frac{1}{\sqrt{1+c^2}}u'$$

Here if $l' = k.u$ and $u' = -\tau l - kn$ equals are used, we get

$$\alpha' = \frac{c}{\sqrt{1+c^2}}ku + \frac{1}{\sqrt{1+c^2}}(-\tau l - kn).$$

Here, since $\theta \in (0, \pi)$, $\cot \theta = c$

$$\frac{1}{\sin^2 \theta} = \frac{\sin^2 \theta + \cos^2 \theta}{\sin^2 \theta} = \frac{\sin^2 \theta}{\cos^2 \theta} + \frac{\cos^2 \theta}{\sin^2 \theta} = 1 + \cot^2 \theta = 1 + c^2.$$

Also

$$\frac{1}{\sin^2 \theta} = 1 + c^2$$

$$\sin^2 \theta = \frac{1}{1+c^2}$$

and

$$\begin{aligned} \cos \theta &= \sin \theta \cot \theta \\ &= \frac{1}{\sqrt{1+c^2}} \cdot c \\ \cos \theta &= \frac{c}{\sqrt{1+c^2}}. \end{aligned}$$

Thus,

$$\begin{aligned} \sin \theta &= \frac{1}{\sqrt{1+c^2}} \\ \cos \theta &= \frac{c}{\sqrt{1+c^2}} \\ \langle l, \alpha \rangle &= \langle l, \frac{c}{\sqrt{1+c^2}}l + \frac{1}{\sqrt{1+c^2}}n \rangle \\ &= \langle l, l \rangle \frac{c}{\sqrt{1+c^2}} + \langle l, n \rangle \frac{1}{\sqrt{1+c^2}} \\ \langle l, \alpha \rangle &= \frac{c}{\sqrt{1+c^2}} = \cos \theta, \end{aligned}$$

where θ is the constant bevel between the vectors $l(t)$ and the vector α .

Let α be a constant unit vector and $\theta \in (0, \pi)$, $\langle l, \alpha \rangle = \cos \theta$, then we can write α vector as follows:

$$\alpha = \langle l, \alpha \rangle l + \langle n, \alpha \rangle n + \langle u, \alpha \rangle u.$$

Since

$$\begin{aligned} k. \langle n, \alpha \rangle &= \langle kn, \alpha \rangle = \langle l', \alpha \rangle = 0 \text{ and } k \neq 0 \\ \langle n, \alpha \rangle &= 0. \end{aligned}$$

Also

$$\alpha = \frac{c}{\sqrt{1+c^2}}l + \frac{1}{\sqrt{1+c^2}}u$$

$$\langle \alpha, u \rangle = \frac{c}{\sqrt{1+c^2}} \langle l, u \rangle + \frac{1}{\sqrt{1+c^2}} \langle u, u \rangle.$$

Here, since $\langle l, n \rangle = \langle l, u \rangle = \langle n, u \rangle = 0$ and $\langle n, n \rangle = 1$, the following expression is obtained

$$\begin{aligned} \langle \alpha, u \rangle &= \frac{1}{\sqrt{1+c^2}} = \sin \theta \\ \langle \alpha, u \rangle &= \sin \theta, \end{aligned}$$

and

$$\alpha = \cos \theta . l + \langle \alpha, u \rangle u.$$

Since α is constant unit vector,

$$\begin{aligned} \|\alpha\| &= \sqrt{\left(\frac{c}{\sqrt{1+c^2}}\right)^2 + \left(\frac{1}{\sqrt{1+c^2}}\right)^2} \\ &= \sqrt{\frac{c^2}{1+c^2} + \frac{1}{1+c^2}} \\ &= \sqrt{\frac{c^2+1}{1+c^2}} = 1 \end{aligned}$$

$$\|\alpha\|^2 = 1 = \cos^2 \theta + \sin^2 \theta.$$

Also, because $\langle \alpha, u \rangle = \sin \theta \Rightarrow \langle \alpha, u \rangle^2 = \sin^2 \theta$ and α is constant unit vector,

$$\begin{aligned} \langle u, \alpha \rangle &= \pm \sin \theta \\ \alpha &= \cos \theta . l \pm \sin \theta . u = 0 \\ \alpha' &= \cos \theta . l' \pm \sin \theta . u' = 0. \end{aligned}$$

Here, $l' = k . u$ and $u' = -\tau l - kn$ equals are used

$$\alpha' = \cos \theta . ku \pm \sin \theta . (-\tau l - kn).$$

Also

$$\begin{aligned} \langle \alpha', l \rangle &= \cos \theta . k \langle u, l \rangle + \sin \theta . (-\tau) \langle l, l \rangle + \sin \theta . (-k) \langle n, l \rangle = 0 \\ \langle \alpha', n \rangle &= \cos \theta . k \langle u, n \rangle + \sin \theta . (-\tau) \langle l, n \rangle + \sin \theta . (-k) \langle n, n \rangle = 0 \\ \langle \alpha', u \rangle &= \cos \theta . k \langle u, u \rangle + \sin \theta . (-\tau) \langle l, u \rangle + \sin \theta . (-k) \langle n, u \rangle = 0. \end{aligned}$$

Here, since $\langle l, n \rangle = \langle l, u \rangle = \langle n, u \rangle = 0$ and $\langle l, l \rangle = \langle n, n \rangle = \langle u, u \rangle = 1$, the following expression is obtained

$$\begin{aligned} \sin \theta . (-\tau) + \sin \theta . (-k) + \cos \theta . k &= 0 \\ \cos \theta . k &= \sin \theta . \tau + \sin \theta . k \\ \cos \theta . k &= \sin \theta . (\tau + k) \\ \frac{\cos \theta}{\sin \theta} &= \frac{(\tau+k)}{k} \\ \cot \theta &= \frac{\tau}{k} + 1 \\ \frac{\tau}{k} &= \cot \theta - 1 \end{aligned}$$

References

- [1] Turgut M, Yılmaz S. Smarandache Curves in Minkowski Space-Time. *Int. J. Math Comb.* 2008; Vol.3: 51-55.
- [2] Tuna Aksoy A, Çöken A.C. Null Quaternionic Curves in Semi-Euclidean 3-Space of Index ν , *Acta Physica Polonica A.* 2015; 2(128): 286-289.
- [3] Tuna Aksoy A, Çöken, A.C. Serret-Frenet Formulae for Null Quaternionic Curves in Semi Euclidean 4-Space \mathbb{R}_1^4 . *Acta Physica Polonica A.* 2015; 2(128): 293-296.
- [4] Baharathi K, Nagaraj M. Quaternion valued function of a real variable Serret-Frenet formulae. *Indian J. Pure Appl. Math.* 1987; 18(6): 507-511.
- [5] Izumiya S, Takeuchi N. New special curves and developable surfaces. *Turk. J. Math.* 2004; 28(2): 153-164.
- [6] Kula L, Ekmekçi N, Yaylı Y, İlarıslan K. Characterizations of Slant Helices in Euclidean 3-space. *Turkish Journal of Mathematics* 2010; 34(2): 261-274.
- [7] Ahmad T, Ali and Rafael Lopez. Slant Helices in Minkowski Space \mathbb{E}_1^3 . *J. Korean Math. Soc.* 2011; 48(1): 159-167.

Investigation of Electrophoretic Mobility of Various Nanofibers in Ethanol or Water

Sercan DEDE¹, Filiz LOKUMCU ALTAY^{2*}

¹ Department of Food Engineering, Faculty of Agricultural, Mustafa Kemal University, Hatay, 31000, Turkey

² Department of Food Engineering, Faculty of Chemical and Metallurgical, Istanbul Technical University, Istanbul, 34469, Turkey

¹ sdede@mku.edu.tr, ^{2*} lokumcu@itu.edu.tr

(Geliş/Received: 11/03/2020;

Kabul/Accepted: 26/04/2021)

Abstract: In this study, the electrophoretic mobility of nanofibers in ethanol or in water was calculated by using both equations from zeta potential values and related to their measured diffusion coefficients. Results showed that all samples in ethanol had positive zeta potential values, whereas all samples in water, except sample 3 containing gelatin, had negative zeta potential values. The samples with PVA or PVA-alginate had the most stable suspensions in water compared to other samples, regarding zeta potential values. The electrophoretic mobilities calculated by using the Smoluchowski and Henry equations of samples showed similar charge characteristics as zeta potential values. Gelatin might have charged by applied voltage during the electrospinning process. When results were related to the diffusion coefficient values, it was observed that the higher electrophoretic mobility and zeta potential values resulted in lower diffusibility. Moreover, adding limonene to the structure decreased the electrophoretic mobility and zeta potential values, and increased the diffusion coefficient. The adding different polymers revealed that molecular structure and charging behavior of the polymers are some of the most important factors on the electrophoretic mobility and zeta potential of nanofibers.

Key words: Electrophoretic mobility, Zeta potential, Smoluchowski equation, Henry Equation, Electrospun nanofibers, Electrospinning.

Çeşitli Nanoliflerin Etanol veya Sudaki Elektroforetik Hareketliliğinin İncelenmesi

Öz: Bu çalışmada, etanolde veya suda bulunan nanoliflerin elektroforetik hareketliliği hem zeta potansiyel değerlerinden hem de ölçülen difüzyon katsayısı değerlerinden hesaplanmıştır. Etanoldeki bütün örneklerin zeta potansiyel değerleri pozitif bulunurken 3 numaralı örnek hariç sudaki bütün nanoliflerin zeta potansiyelleri negatiftir. Zeta potansiyel değerleri göz önüne alındığında suda bulunan PVA'lı veya PVA-aljinatlı nanolifler diğer örneklere göre daha stabil olarak değerlendirilmiştir. Smoluchowski ve Henry denklemleri hesaplanan elektroforetik hareketlilikler zeta potansiyel değerleri yle benzer yük karakteristikleri göstermiştir. Jelatin elektroçirme sırasında uygulanan voltaj nedeniyle yüklenmiş olabilir. Elde edilen sonuçlar difüzyon katsayısı değerleriyle ilişkilendirildiğinde, yüksek elektroforetik hareketliliğe ve zeta potansiyel değerlerine sahip örneklerin difüzlenebilirliklerinin düşük olduğu belirlenmiştir. Buna ilave olarak nanolif yapısına limonen eklenmesinin elektroforetik hareketliliği ve zeta potansiyelini azalttığı, difüzyon katsayısını ise arttırdığı görülmüştür. Değişik polimerlerin ilavesiyle nanoliflerin elektroforetik hareketliliğine ve zeta potansiyeline etki eden en önemli faktörler polimerlerin moleküler yapısı ve yüklenme davranışdır.

Anahtar kelimeler: Elektroforetik hareketlilik, Zeta potansiyeli, Smoluchowski denklemi, Henry denklemi, Elektroçirilmiş nanolifler, Elektroçirme

1. Introduction

Nanofibers electrospun from biomaterials has become important in many fields [1] such as filtration [2], smart packaging [3], scaffolds in tissue engineering [4], drug delivery [5], enzyme immobilization, biosensors, energy generation, functional textile products, affinity membrane and cosmetics [6-8].

The transport property of nanofibers and the quality of products with nanofibers are related to their dispersion and aggregation tendencies [9-10]. These properties depend on the surface charging characteristics [1; 11-14].

Monaghan & White [15] investigated the effect of proteins on electrophoretic mobility and sedimentation velocity of red cells. They reported that mobility of red cells was unchanged or only slightly decreased when bulk viscosity was increased by added protein is interpreted as indicating that the red cell surfaces are hydrated [15]. Then, electrophoretic mobility could have decreased due to red cells somehow absorbed water molecules (or hydrated) under some circumstances (in this case, added proteins).

The dispersion and aggregation of colloidal particles are based on the interaction energy between particles. This interaction energy represented by Derjaguin, Landau, Verwey and Overbeek (DLVO) theory is charging behavior and attractive van der Waals energy influence the sum of repulsive electrostatic interactions. However, electrospun nanofibers seem not to be agree with the DLVO theory [1; 16].

* Corresponding author: lokumcu@itu.edu.tr. ORCID Number of authors: ² 0000-0002-5484-866X

The Smoluchowski equation can be applied for large particles compared with the thickness of electric double layer [1]. It appears that the Smoluchowski equation is mostly used for the calculation of zeta potential [13; 17-19]. On the other hand, the Smoluchowski equation can be inaccurate even for large spherical particles at low salt concentration due to the relaxation of the electric double layer [20-21]. Furthermore, Sato et al. [1] indicated that it is doubtful to apply the Smoluchowski neglects the effect of relaxation underestimating the zeta potential, therefore it is not valid for calculating the interaction energy and the capture efficiency. However, they used the equation for calculation electrophoretic mobilities of cellulose nanofibers in their study.

Electrophoretic mobility can also be expressed in terms of zeta potential [22]. The measured electrophoretic mobility (ue) is calculated from zeta potential (ζ) through Henry's equation which needs a constant called as the Henry function ($F(\kappa a)$) [19; 23]. This equation only applies for isolated particles of zeta potential less than around 25 mV and if $F(\kappa a)=1.5$; it is known as the Smoluchowski equation that applies where κa is large ($F(\kappa a)=$ around 100) and the double layer is thinner than the particle radius [1; 24-25]. Delgado et al. [23] revealed that according to Henry's, the electrophoretic mobility is lower than that calculated from Smoluchowski equation and the theory fails for low-to-moderate zeta potentials due to neglecting concentration polarization which decreases the mobility for sufficiently high zeta potential values [23].

In this paper, the electrophoretic mobility of nanofiber encapsulation systems in ethanol or in water were calculated by using the Smoluchowski equation and Henry's equation. Then the results were related to the measured diffusion coefficients.

2. Materials and Methods

2.1. Materials

(+/-)-Limonene used in the study was purchased from Alfa Aesar Co. (Germany) and ethanol used in the study was purchased from Sigma-Aldrich Co. (Germany). Type B gelatin powder from bovine skin, PVA, Na-alginate E-401, lactalbumin and acetic acid used in the study were purchased from Sigma (Germany), ZAG (Turkey), Sigma (Germany), FMC-Biopolymer (US), Sigma (Germany) and Merck (US), respectively.

2.2. Methods

2.2.1. Electrospinning

The preparation of the feed solutions and electrospinning process were given by Dede and Altay [26]. The uniaxial electrospinning was performed by using an electrospinning equipment (Inovenso NE100, Turkey) at room temperature. The applied voltage, the feed rate and the distance to the collector plate were 25 kV, 0.5 ml/h and 10 cm, respectively. The diffusion coefficient measurements and morphological characterization of the samples were reported in Dede and Altay [26].

2.2.2. Dynamic light scattering measurements

The zeta potential measurements of dispersions containing electrospun nanofiber samples were carried out using a dynamic light scattering instrument (Malvern Zetasizer Nano ZS, Worcestershire, UK) at 25 °C in triplicate. Ethanol or distilled water were used as dispersants and nanofibers were dispersed at 0.1% (w/v) [27].

2.2.3. Electrophoretic mobility calculations

Electrophoretic mobilities were calculated from the zeta potential by using the Smoluchowski equation [1; 22]:

$$ue = \frac{\epsilon_r \epsilon_0 \zeta}{\eta} \quad (1)$$

where ue is the electrophoretic mobility ($m^2/V.s$), ζ is the zeta potential (mV), η is the viscosity of the solution [1] or solvent [22], ϵ_r is the dielectric constant of the medium (for ethanol 24.3 and for water 80), ϵ_0 is the permittivity of vacuum, (for ethanol 2.2×10^{-12} C/V.m and for water 8.85×10^{-12} C/V.m) [1; 22]. We used η is

the viscosity of the solvent (for ethanol $1,074 \times 10^{-3}$ Pa.s and for water $8,94 \times 10^{-4}$ Pa.s) [22; 28]. The measured electrophoretic mobility (u_e) was calculated from zeta potential (ζ) through Henry's equation:

$$u_e = \frac{2\varepsilon\zeta F(\kappa a)}{3\eta} \quad (2)$$

where ε is the dielectric constant of the dispersant, $F(\kappa a)$ is the Henry function and η is the viscosity [19; 23]. We acknowledged all assumptions made by Sato et al. [1] for nanofiber morphology and surface charge characteristics.

2.2.4. Statistical analysis

Excel 2016 (Microsoft, WA, USA) was employed for statistical analysis. The results of zeta potential, were evaluated by the two-way ANOVA ($\alpha=0.05$). Significant differences among samples were determined by the least significant difference comparison by the Student's paired t-test and t-test probability limits of $p<0.05$ was used for two-sided testing in evaluation.

3. Results

Zeta potentials of electrospun samples in ethanol or in water were given in Table 1. All samples in ethanol had positive zeta potential values, whereas all samples in water, except sample 3 containing gelatin, had negative zeta potential values. The zeta potentials of sample 1 and sample 2 in water were closer to -25 mV compared to the zeta potential values of other samples in water. The zeta potentials lower than -25 mV or higher than +25 mV indicate stability for a given suspension [29]. The samples with PVA or PVA-alginate had the most stable suspensions in water compared to other samples. The zeta potential values of the rest of electrospun samples were not different from each other.

Table 1. Zeta potentials of electrospun samples in ethanol or in water

Sample no	Electrospun Sample	Samples in ethanol (E) or in water (W)	Zeta potential (mV)*	Diffusion Coefficient ($\mu\text{m}^2/\text{s}$)**	Calculated electrophoretic mobility, u_e ($\text{m}^2/\text{V}\cdot\text{s}$) via Smoluchowski equation	Calculated electrophoretic mobility, u_e ($\text{m}^2/\text{V}\cdot\text{s}$) via Henry's equation
1	PVA + Limonene	E	+2.71±0.07a	0.15±0.01bcd	+1.4x10⁻⁸	+61
		W	-12.60±2.32b	1.37±0.03a	-1.0x10 ⁻⁸	-1008
2	PVA + Alginate + Limonene	E	+1.18±0.26a	0.49±0.01bc	+0.6x10⁻⁸	+27
		W	-10.4±0.9b	1.91±0.04a	-0.8x10 ⁻⁸	-832
3	Gelatin + Limonene	E	+1.86±0.39a	0.69±0.01b	+0.9x10⁻⁸	+42
		W	+1.31±0.05a	1.12±0.10ab	+0.1x10 ⁻⁸	+105
4	Gelatin + Alginate + Limonene	E	+3.57±0.07a	0.25±0.00bcd	+1.8x10⁻⁸	+81
		W	-6.38±0.49ab	1.02±0.07ab	-0.5x10 ⁻⁸	-510
5	Gelatin + Lactalbumin + Limonene	E	+6.35±0.41a	0.28±0.07bcd	+3.2x10⁻⁸	+144
		W	-0.27±0.07a	0.77±0.21b	-0.2x10 ⁻⁹	-22
6	Only Gelatin***	E	-0.52±0.47	0.02±0.00	-0.3x10⁻⁸	-12
7	Gelatin Nanofiber 2***	E	+3.79±0.75	0.31±0.41	1.9x10⁻⁸	+86
8	Gelatin Nanofiber 7***	E	+21.90±0.10	1.19±0.08	10.9x10⁻⁸	+496

*Means±SD (n=3); values within each group followed by the same letter (in column, sample number and samples in ethanol or water) are not significantly different ($p\leq 0.05$)

**Means±SD (n=3); values within each group followed by the same letter (in column, sample number and samples in ethanol or water) are not significantly different ($p\leq 0.05$) and Reference: Dede and Altay, [8].

***Reference: Okutan et al. [27].

In this study, zeta potential values were used for calculating electrophoretic mobilities of electrospun nanofibers via Smoluchowski and Henry's equations (Table 1). While calculated electrophoretic mobility values of all samples in ethanol via Smoluchowski equation were founded positive, all samples except sample 3 (containing gelatin) in water was negative as similar as zeta potential values of samples. The same trend was true for the results of Henry's equation. In addition, the results of electrophoretic mobility calculations via Henry's for samples in water were founded 9.9×10^{-12} times to those samples calculation of Smoluchowski equation, the results of Henry's equation for samples in ethanol were founded as 2.2×10^{-10} times to that samples' calculated via Smoluchowski equation. Furthermore, zeta potentials of electrospun samples in ethanol were higher than samples in water except sample 4 (containing gelatin and alginate). Gao et al. [30] reported that the zeta potential values were directly proportional with ethanol proportion in the solvent. Delgado et al. [23] revealed that positive electrophoretic mobility values were consequences of positive zeta potential values.

Okutan et al. [27] determined zeta potentials of electrospun gelatin nanofibers in ethanol to characterize them and found the values between 3.79 ± 0.75 and 21.90 ± 0.10 as consequences of applied voltage (28-35kV), concentration of gelatin (7-20%, w/v) and feed rate (0.1-1mL/h). Calculating the electrophoretic mobility of electrospun gelatin nanofibers in ethanol result as between $+1.9 \times 10^{-8}$ and $+1.1 \times 10^{-7}$ m²/V.s for Smoluchowski equation and between +85.75 and +495.50 m²/V.s for Henry's equation. They also determined the zeta potential of only gelatin in ethanol and found it as -0.52 ± 0.47 [27] which its electrophoretic mobility results as -2.6×10^{-9} m²/V.s for Smoluchowski equation and -11.77 m²/V.s for Henry's equation. When compared to our gelatin containing samples (3, 4 and 5) to those electrospun gelatin nanofibers from Okutan et al. [27], our zeta potential values and electrophoretic mobility values were lower than those of Okutan et al. [27]. Besides all electrospun gelatin nanofibers from Okutan et al. [27] values were positive as ours. However, both zeta potential [27] and electrophoretic mobility values of gelatin in ethanol were negative. Gelatin electrospun nanofibers charged positively resulting in the zeta potentials and the mobilities as positive because of applied voltage during electrospinning. After all, sample 3 in our study has the only positive values of both zeta potential and electrophoretic mobility in water. It's thought that the applied voltage charged the electrospun gelatin nanofibers positively if used as only one polymer (gelatin) in the jet.

Results showed that higher electrophoretic mobility and zeta potential values mean lower diffusibility. When the results obtained related to the diffusion coefficient values of same samples, on the one hand, diffusion coefficient of solely gelatin in ethanol was found 0.02 ± 0.00 , after gelatin electrospun as nanofiber charged positively, both zeta potential (-0.52 ± 0.47 to $+3.79 \pm 0.75$) and electrophoretic mobility (-2.6×10^{-9} to 1.9×10^{-8} for Smoluchowski equation and -11.77 to $+85.75$ for Henry's equation) values increased with diffusion coefficient (0.31 ± 0.41). When added limonene to the structure, zeta potential ($+3.79 \pm 0.75$ to $+1.86 \pm 0.39$) and electrophoretic mobility (1.9×10^{-8} to 9.3×10^{-9} for Smoluchowski equation and $+85.75$ to $+42.08$ for Henry's equation) values decreased, but diffusion coefficient increased (0.69 ± 0.01) due to the limonene's being highly unstable and hydrophobic, is difficult to incorporate in aqueous food, beverage, fragrance, and cosmetic systems [31]. Then gelatin was electrospun with other polymers (alginate or lactalbumin) zeta potential ($+1.86 \pm 0.39$ to $+3.57 \pm 0.07$) and electrophoretic mobility (9.3×10^{-9} to 1.8×10^{-8} for Smoluchowski equation and $+42.08$ to $+80.77$ for Henry's equation) values increased, while diffusion coefficients (0.25 for sample containing gelatin + alginate and 0.28 for sample containing gelatin + lactalbumin) decreased closely. These polymers (alginate and lactalbumin) were thought to both decrease zeta potential and electrophoretic mobility values and increase diffusion coefficient values (Table 1).

On the other hand, using alginate with PVA electrospun nanofibers in ethanol decreased both zeta potential ($+2.71 \pm 0.07$ to $+1.18 \pm 0.26$) and electrophoretic mobility (1.4×10^{-8} to 5.9×10^{-9} for Smoluchowski's equation and $+61.32$ to $+26.70$ for Henry's equation) values and increased diffusion coefficient value (0.15 ± 0.01 to 0.49 ± 0.01) as same as alginate did for the sample containing gelatin + alginate + limonene (Table 1).

Same results can be seen for the samples in water (Table 1). Using alginate with PVA electrospun nanofibers in water decreased both zeta potential (-12.60 ± 2.32 to -10.4 ± 0.9) and electrophoretic mobility (-1.0×10^{-8} to -8.2×10^{-9} for Smoluchowski equation and -1008 to -832 for Henry's equation) values and increased diffusion coefficient value (1.37 ± 0.03 to 1.91 ± 0.04) as same as alginate did for the sample containing gelatin + alginate + limonene (Table 1). Furthermore, lactalbumin added gelatin electrospun nanofiber sample in water gave opposite results for zeta potential (decreased from $+1.31 \pm 0.05$ to -0.27 ± 0.07), electrophoretic mobility (decreased from $+1.04 \times 10^{-9}$ to -5.1×10^{-9} for Smoluchowski equation and $+104.8$ to -510.4 for Henry's equation) and diffusion coefficient (1.12 ± 0.10 to 0.77 ± 0.21) (Table 1).

4. Conclusions

The electrophoretic mobility of nanofibers in ethanol or in water was calculated by using zeta potential values via the Smoluchowski equation and the Henry equation. Calculations via both equations showed similar charging characteristics as zeta potentials. The effects of the molecular structure, charging behavior, viscosity and the dielectric constants of the polymers are very important factors in the calculation of the electrophoretic mobility. Moreover, results showed that higher electrophoretic mobility and zeta potential values mean lower diffusibility and diffusion coefficient values.

Acknowledgement

Mr. Dede thanks Mrs. Okutan and Mrs. Bakır for their help on dynamic light scattering measurements at Dr. Altay's nanofiber characterization lab.

References

- [1] Sato Y, Kusaka Y, Kobayashi M. Charging and aggregation behavior of cellulose nanofibers in aqueous solution. *Langmuir*, 2017, 33: 12660-12669.
- [2] Agarwal S, Wendorff JH, Greiner A. Use of electrospinning technique for biomedical applications. *Polymer*, 2008, 49(26): 5603-5621.
- [3] Pérez-Masiá R, López-Rubio A, Lagarón JM. Development of zein-based heat-management structures for smart food packaging. *Food Hydrocolloids*, 2013, 30(1): 182–191.
- [4] Samanta A, Takkar S, Kulshreshtha R, Nandan B, Srivastava RK. Electrospun composite matrices of poly(ϵ -caprolactone)-montmorillonite made using tenside free Pickering emulsions. *Mater. Sci. Eng., C*, 2016, 69: 685–691.
- [5] Su Y-R, Yu S-H, Chao A-C, Wu J-Y, Lin Y-F, Lu K-Y, Mi F-L. Preparation and properties of pH-responsive, self-assembled colloidal nanoparticles from guanidine-containing polypeptide and chitosan for antibiotic delivery. *Colloids Surf., A*, 2016, 494: 9–20.
- [6] Bhardwaj N, Kundu SC. Electrospinning: a fascinating fiber fabrication technique. *Biotechnol. Adv.*, 2010, 28: 325-347.
- [7] Shen SC, Ng WK, Chow PS, Tan RBH. *Development and application of nanofiber materials* (1st ed.). New York: Nova Science Pub., Inc. 2010.
- [8] Dede S, Altay F. Biosensors from the first generation to nano-biosensors. *Int. Adv. Res. Eng. Technol. J.*, 2018, 2 (2): 200-207.
- [9] Raychoudhury T, Naja G, Ghoshal S. Assessment of transport of two polyelectrolyte-stabilized zero-valent iron nanoparticles in porous media. *J. Contam. Hydrol.*, 2010, 118: 143-151.
- [10] Iwamoto S, Yamamoto S, Lee SH, Endo T. Solid-state shear pulverization as effective treatment for dispersing lignocellulose nanofibers in polypropylene composites. *Cellulose*, 2014, 21: 1573-1580.
- [11] Kowalewski TA, Blonski S, Barral S. Experiments and Modeling of Electrospinning Process. *Bull. Pol. Acad. Sci. Tech. Sci.*, 2005, 53: 385–394.
- [12] Reneker DH, Yarin AL. Electrospinning Jets and Polymer Nanofibers. *Polymer*, 2008, 49: 2387–2425.
- [13] Předota M, Machesky LM, Wesolowski JD. Molecular Origins of the Zeta Potential. *Langmuir*, 2016, 32(40): 10189–10198.
- [14] Xue J, Xie J, Liu W, Xia Y. *Electrospun Nanofibers: New Concepts, Materials, and Applications*. *Acc. Chem. Res.*, 2017, 50(8): 1976-1987.
- [15] Monaghan BR, White HL. Effect of proteins on electrophoretic mobility and sedimentation velocity of red cells. *J. Gen. Physiol.*, 1936, 19(5): 715–726.
- [16] Kaledin LA, Tepper F, Kaledin TG. Long-range attractive forces extending from alumina nanofiber surface, *Int. J. Smart Nano Mater.*, 2014, 5:3, 133-151.
- [17] Drzymala J, Sadowski Z, Holysz L, Chibowski E. Ice/Water Interface: Zeta Potential, Point of Zero Charge, and Hydrophobicity. *J. Colloid Interface Sci*, 1999, 220: 229–234.
- [18] Cho D, Lee SG, Frey WM. Characterizing zeta potential of functional nanofibers in a microfluidic device. *J. Colloid Interface Sci*, 2012, 372: 252–260.
- [19] Skoglund S, Hedberg J, Yunda E, Godymchuk A, Blomberg E, Wallinder IO. Difficulties and flaws in performing accurate determinations of zeta potentials of metal nanoparticles in complex solutions—Four case studies. *PLoS One*, 2017, 12(7):e0181735.
- [20] Kobayashi M, Sasaki A. Electrophoretic mobility of latex spheres in mixture solutions containing mono and divalent counter ions. *Colloids Surf., A*, 2014, 440: 74-78.
- [21] Nishiya M, Sugimoto T, Kobayashi M. Electrophoretic mobility of carboxyl latex particles in the mixed solution of 1:1 and 2:1 electrolytes: experiments and modeling. *Colloids Surf., A*, 2016, 504: 219-227.

- [22] Chassagne C, Ibanez M. Electrophoretic mobility of latex nanospheres in electrolytes: experimental challenges. *Pure Appl. Chem.*, 2013, 85(1): 41-51.
- [23] Delgado AV, González-Caballero F, Hunter RJ, Koopal LK, Lyklema J. Measurement and interpretation of electrokinetic phenomena. *Pure Appl. Chem.*, 2005, 77: 1753–1805.
- [24] Smoluchowski M. *Handbuch der Electricität und des Magnetismus (Graetz)*, vol. II, p. 366. Leipzig, Germany: Barth., 1921.
- [25] Hunter RJ. *Introduction to Modern Colloid Science*. Oxford, UK: Oxford University Press, 1993.
- [26] Dede S, Lokumcu Altay F. Nanofiber encapsulation of limonene and modeling its release mechanisms. *Acta Alimentaria*, 2019, 48(1): 56–64.
- [27] Okutan N, Terzi P, Altay F. Affecting parameters on electrospinning process and characterization of electrospun gelatin nanofibers. *Food Hydrocolloids*, 2014, 39: 19-26.
- [28] *CRC Handbook of Chemistry and Physics*, 73rd Edition. Ed. David R. Lide. Boca Raton, FL, USA: CRC Press, 1992.
- [29] Srinivasan S, Barbhuiya S, Charan DS, Pandey SP. Characterising cement–superplasticizer interaction using zeta potential measurements. *Constr. Build. Mater.*, 2010, 24: 517–2521.
- [30] Gao J, Li Q, Chen W, Liu Y, Yu H. Self-Assembly of Nanocellulose and Indomethacin into Hierarchically Ordered Structures with High Encapsulation Efficiency for Sustained Release Applications. *ChemPlusChem*, 2014, 79: 725 – 731.
- [31] Li P-H, Lu W-C. Effects of storage conditions on the physical stability of D-limonene nanoemulsion. *Food Hydrocolloids*, 2015, 53: 218-224.

COPYRIGHT RELEASE FORM

TURKISH JOURNAL OF SCIENCE AND TECHNOLOGY (TJST) Published by Firat University

Firat University, Fen Bilimleri Enstitüsü Müdürlüğü
Turkish Journal of Science & Technology Editörlüğü
Elazığ-TURKEY,
Manuscript title:

Full names of all authors (in order to appear on manuscript):

Name, address etc. of corresponding author:

ID Number: Telephone:

E-mail: Mobile phone:

The author(s) warrant(s) that:

- a) the manuscript submitted is his/her/their own original work;
- b) all authors participated in the work in a substantive way and are prepared to take public responsibility for the work;
- c) all authors have seen and approved the manuscript as submitted;
- d) the manuscript has not been published and is not being submitted or considered for publication elsewhere;
- e) the text, illustrations, and any other materials included in the manuscript do not infringe upon any existing copyright or other rights of anyone. Notwithstanding the above, the Contributor(s) or, if applicable the Contributor's Employer, retain(s) all proprietary rights other than copyright, such as

a) patent rights;

b) to use, free of charge, all parts of this article for the author's future works in books, lectures, classroom teaching or oral presentations;

c) the right to reproduce the article for their own purposes provided the copies are not offered for sale.

However, reproduction, posting, transmission or other distribution or use of the article or any material contained therein, in any medium as permitted hereunder, requires a citation to the Journal and appropriate credit to Firat University as publisher, suitable in form and content as follows:

Title of article, author(s), journal title and volume/issue, Copyright© year.

All materials related to manuscripts, accepted or rejected, including photographs, original figures etc., will be kept by Turkish Journal of Science and Technology editority for one year following the editor's decision. These materials will then be destroyed. I/We indemnify Firat University and the Editors of the Journals, and hold them harmless from any loss, expense or damage occasioned by a claim or suit by a third party for copyright infringement, or any suit arising out of any breach of the foregoing warranties as a result of publication of my/our article. I/We also warrant that the article contains no libelous or unlawful statements and does not contain material or instructions that might cause harm or injury.

This copyright form must be signed by all authors. Separate copies of the form (completed in full) may be submitted by authors located at different institutions; however, all signatures must be original.

ID number: ID number:

Full name (block letters) Full name (block letters)

Signature Date Signature Date

ID number: ID number:

Full name (block letters) Full name (block letters)

Signature Date Signature Date

ID number: ID number:

Turkish authors must supply their ID card number; foreign authors must supply their passport number (if possible)